

Group Decisions Influence Emergence and Regulation of Leaders during Collective Migration of Epithelial Cells

THÈSE N° 7392 (2017)

PRÉSENTÉE LE 14 MARS 2017

À LA FACULTÉ DES SCIENCES DE LA VIE

PROGRAMME DOCTORAL EN BIOTECHNOLOGIE ET GÉNIE BIOLOGIQUE

ÉCOLE POLYTECHNIQUE FÉDÉRALE DE LAUSANNE

POUR L'OBTENTION DU GRADE DE DOCTEUR ÈS SCIENCES

PAR

Medhavi VISHWAKARMA

acceptée sur proposition du jury:

Prof. A. Radenovic, présidente du jury

Prof. J. A. Hubbell, Prof. J. Spatz, directeurs de thèse

Prof. . V. Vogel, rapporteuse

Prof. D. Müller, rapporteur

Prof. K. Johnsson, rapporteur



ÉCOLE POLYTECHNIQUE
FÉDÉRALE DE LAUSANNE

Suisse
2017

..He found connections everywhere. Nothing, not even the tiniest organism, was looked at on its own. 'In this great chain of causes and effects,' Humboldt said, 'no single fact can be considered in isolation.' With this insight, he invented the web of life, the concept of nature, as we know it today.

-Andrea Wulf, *The Invention of Nature*.

Abstract

Collective migration is a central event involving coordinated movement of several individuals. One of the critical events during collective migration is the emergence of leading individuals, who provide directional guidance for the group movement. While on the move, animals select their leaders by a collective decision making process, which require active participation of the followers. On the contrary, the prevalent view on collective cell migration, especially in the context of epithelial cells during wound healing, assumes a hierarchical leader-follower organization and belittles the contribution of follower cells in choosing or regulating the leaders. Furthermore, how the dynamics of cells located at the wound margin evolve as the wound heals, remains illusive. Here, we report and analyse distinct phases of collective migration during wound closure and demonstrate how cellular-level shared decision-making process and collective mechanical dynamics influence selection, regulation and kinematics of leader cells in these phases.

We found that in the preparatory phase, before the initiation of migration (Phase 0), the selection of leader cells at the epithelial wound margin depends on the pre-migratory dynamics of the follower cells situated immediately behind the future leaders. Long before the prospective leaders actually start displaying their phenotypic peculiarities, cells behind them manifest stochastic augmentations in the traction forces and monolayer stresses, and display large perimeter-to-area ratio indicating a local unjamming in the followers much before the leaders are selected. Further, introducing an unjammed or fluidic follower at the back stimulates leader cell formation at the margin thereby indicating the role of collective bulk dynamics in leader cell selection. Interestingly, the length upto which cells cooperatively join forces, corresponds very well with the distance between the two emerging leaders and this mechano-biological control remains preserved even in the presence of geometric bias or physiological levels of chemical cue at the interface.

Immediately after the initiation of migration (Phase 1), leaders show their distinct phenotypes and drive the cellular outgrowths. In this phase, pluricellular actin belt at the margin regulates the fraction of marginal leaders, which therefore remains unchanged, while the number of followers per leader increases with time. As the migration progresses, fraction of leader cells increases while the latter settles to a steady level set again by the length scale of cell-cell force transmission (Phase 2). Any perturbations in mechanical forces that modifies the force correlation lengths, invariably enforces a change in the number of followers per leader thereby modifying the time required to transit from one phase to the other. Furthermore, orientation of focal adhesions and persistence of cellular motions also display this phase specific behaviour. Together, these findings provide a novel system insight into collective cell migration and indicate integrative leader-follower interactions during wound closure.

Given the physiological and pathological importance of leader cell formation in epithelial wound healing, in organogenesis and in metastatic migration of cancer cells, the system-view that the results offer here is anticipated to have to a long-standing impact on the design and discovery of avant-garde therapeutic strategies in future.

Keywords

Collective cell migration, epithelial cells, wound healing, wound margin, leader cells, non-leader cells, follower cells, dynamic heterogeneity, force-correlation length, collective dynamics, jammed cells, unjammed cells, propensity of leaders, persistence of migration, mechano-transduction, focal-adhesions, micro-patterning, traction-force microscopy, monolayer-stress microscopy, reflection interference contrast microscopy

Zusammenfassung

Kollektive Migration ist ein allgemeiner Prozess der die koordinierte Bewegung mehrerer Individuen beschreibt. Eines der wichtigsten Ereignisse während der kollektiven Migration ist das Auftreten von führenden Individuen, die richtungsweisend für die Gruppenbewegung sind. Während Tiere wandern, bestimmen sie ihr Alphanimal durch eine demokratische Entscheidung, welche das aktive Agieren der nachfolgenden Tiere erfordert. Im Gegensatz dazu ist die vorherrschende Meinung bei kollektiver Zellmigration, dass eine hierarchische Organisation zwischen den anführenden Zellen und den nachfolgenden Zellen existiert. Damit wird, vor allem in Bezug auf Epithelzellen während der Wundheilung, ein eventueller Einfluss der nachfolgenden Zellen auf die Auswahl und die Regulation der Anführer vernachlässigt. Darüber hinaus ist die Dynamik der Zellen am Wundrand während der Heilung noch ungeklärt. In dieser Arbeit werden daher spezifische Phasen der kollektiven Migration während der Wundheilung analysiert, um zu untersuchen, wie demokratische Entscheidungsprozesse und kollektive mechanische Dynamik die Auswahl, Regulation und Kinematik von anführenden Zellen in diesen Phasen beeinflussen.

In der Vorbereitungsphase, vor Beginn der Migration (Phase 0), hängt die Auswahl der anführenden Zellen am Wundrand von der prä-migratorischen Dynamik der folgenden Zellen, die direkt hinter den zukünftigen Anführern lokalisiert sind, ab. Lange bevor die zukünftig anführenden Zellen ihren einzigartigen Phänotyp ausbilden, offenbaren sich stochastische Zunahmen der Zugkraft und des Druckes in der Zellschicht hinter den Anführern. Gleichzeitig zeigen diese Zellen ein großes Verhältnis zwischen Zellumfang zu Zellfläche, was auf eine lokale Enthemmung der nachfolgenden Zellen lange vor der Ausbildung von anführenden Zellen hinweist. Des Weiteren stimuliert eine enthemmte oder niedrig viskose Folgezelle die Bildung einer anführenden Zelle am Wundrand und bekräftigt damit die Rolle kollektiver Dynamik in der Auswahl von anführenden Zellen. Interessanter Weise entspricht die Distanz, über die Zellen kooperativ miteinander arbeiten können, sehr genau dem Abstand von zwei anführenden Zellen am Wundrand. Diese mechano-biologische Kontrolle bleibt auch in Anwesenheit von geometrischen Verzerrungen oder physiologischen Mengen an chemischen Signalmolekülen an der Oberfläche erhalten.

Direkt nach einsetzen der Migration (Phase 1), zeigen anführende Zellen ihren einzigartigen Phänotyp und treiben so die Zellbewegung voran. In dieser Phase reguliert ein plurizellulärer Aktgürtel am Wundrand die Anzahl an anführenden Zellen, die Ihrerseits von der „Wahrscheinlichkeit von anführenden Zellen“ definiert ist. Diese Anzahl an anführenden Zellen bleibt während der Wundheilung konstant, während die Anzahl an folgenden Zellen pro Anführer mit der Zeit zunimmt. Mit fortschreitendem Migrationsprozess, nimmt die Neigung zu anführenden Zellen zu,

während die Zahl dieser Zellen sich auf ein konstantes Level einpendelt, das wiederum durch die Längenskala der Zell-Zell Kraftübertragung bestimmt wird (Phase 2). Jegliche Störung der mechanischen Kräfte, welche die Kraftübertragungslänge modifizieren, führt zu einer Änderung der Anzahl an Folgezellen pro Anführer. Damit wird auch der Zeitrahmen für den Übergang von einer Phase zur nächsten verändert. Außerdem zeigen auch die Orientierung der Fokalkontakte und die Dauer von Zellbewegungen dieses phasenspezifische Verhalten. Zusammenfassend ermöglichen diese Beobachtungen eine neue Einsicht in kollektive Zellmigration und zeigen integrative Anführer-Folgezellen Interaktionen während der Wundheilung.

Schlüsselwörter

Kollektive Zell migration, Epithelzellen, Wundheilung, Wundrand, Anführende Zelle, Nicht-Anführende Zelle, Nachfolgerzellen, dynamische Heterogenität, Kraft-Korrelationslänge, kollektive Dynamik, gestaute Zellen, fluide Zellen, Verhaeltnis der Anführenden Zelle, Bestaendigkeit der Migration, Mechano-transduktion, fokale Adhäsionen, Mikrostrukturierung, Traktionskraftmikroskopie, Monolayer-Belastung-Mikroskopie, Reflexions-Interferenzkontrast-Mikroskopie

TABLE OF CONTENTS

| | |
|--|----|
| ABSTRACT | 5 |
| ZUSAMMENFASSUNG | 7 |
| LIST OF FIGURES | II |
| MOTIVATION | 13 |
| 1. INTRODUCTION..... | 15 |
| 1.1 ARCHITECTURE OF EUKARYOTIC CELL | 15 |
| 1.3 HOW CELLS MOVE | 16 |
| 1.4 FROM SINGLE CELL TO COLLECTIVE: INCREASING LEVEL OF COMPLEXITIES | 20 |
| 1.5 MODES AND MODELS TO STUDY COLLECTIVE MIGRATION | 21 |
| 1.6 ARCHITECTURE OF EPITHELIA..... | 25 |
| 1.7 EPITHELIAL WOUND HEALING | 26 |
| 1.8 COORDINATION AND DIRECTIONALITY IN EPITHELIAL CELLS..... | 30 |
| 1.9 VISUALIZING CELLULAR FORCES..... | 33 |
| 1.11 PREVALANT NOTIONS AND BLIND SPOTS | 38 |
| 2. AT THE ONSET OF MIGRATION: SELECTION OF LEADERS | 41 |
| 2.1 PREAMBLE | 41 |
| 2.2 UNJAMMING IN FOLLOWERS PRECEDE LEADER CELL FORMATION..... | 41 |
| 2.3 INTRODUCING FLUID FOLLOWER HELPS TO STIMULATE LEADER CELL FORMATION | 45 |
| 2.4 COLLECTIVE DYNAMICS OVERRIDES INTERFACIAL BIAS | 47 |
| 2.5 EFFECT OF CHEMOTACTIC SIGNALLING ON COLLECTIVE DYNAMICS | 49 |
| 2.6 OUTLOOK | 51 |
| 3. DYNAMIC TEMPORAL PHASES DURING EPITHELIAL WOUND HEALING | 53 |
| 3.1 PREAMBLE | 53 |
| 3.2 TWO DISTINCT PHASES OF CELLULAR DYNAMICS AT WOUND MARGIN | 54 |
| 3.3 MECHANOBIOLOGICAL CONTROL OF LEADER-FOLLOWER RATIO | 56 |
| 3.4 TIME-DEPENDENT REORIENTATIONS OF FOCAL ADHESIONS AT THE LEADING EDGE | 59 |
| 3.5 PHASE-DEPENDENT KINEMATIC DISTINCTION BETWEEN LEADER AND NON-LEADER CELLS..... | 61 |
| 3.6 OUTLOOK | 62 |
| 4. CONCLUDING REMARKS | 65 |
| 5. TO BE CONTINUED..... | 69 |
| 5.1 MOLECULAR MECHANISMS..... | 69 |
| 5.2 EFFECT OF MATRIX STIFFNESS | 71 |
| 6. MATERIALS AND METHODS | 73 |
| 6.1 CELL CULTURE AND MIGRATION EXPERIMENTS..... | 73 |
| 5.2 MICRO-PATTERNING..... | 74 |
| 5.3 VELOCIMETRY AND CELL TRACKING | 75 |
| 5.4 TRACTION FORCE AND MONOLAYER STRESS MICROSCOPY | 76 |
| 5.2 REFLECTION INTERFERENCE CONTRAST MICROSCOPY (RICM) | 79 |
| 5.5 AGAROSE SPOT ASSAY | 80 |
| 5.6 PLASMIDS, siRNAs, TRANSFECTION AND FRET | 81 |
| 5.7 INHIBITION STUDIES AND IMMUNOSTAININGS..... | 82 |
| 7. REFERENCES..... | 83 |
| ACKNOWLEDGEMENTS..... | 91 |
| CURRICULUM VITAE | 95 |
| DECLARATION OF AUTHORSHIP | 93 |

List of Figures

| | |
|--|----|
| Figure 1. Eukaryotic Cell. | 14 |
| Figure 2. Mechanisms of single cell migration. | 16 |
| Figure 3. Mechanisms for maintaining tensigrity in cells. | 18 |
| Figure 4. Collective cell migration in physiological events. | 20 |
| Figure 5. Mechanism of gastrulation during embryogenesis. | 21 |
| Figure 6. Morphogenic characteristics of epithelial and mesenchymal cells. | 22 |
| Figure 7. Organization of epithelial tissues. | 25 |
| Figure 8. Process of wound healing. | 28 |
| Figure 9. Mechanisms of epithelial wound closure. | 29 |
| Figure 10. Junctional integrity of epithelial cells. | 31 |
| Figure 11. Arp3-WAVE2 regulates E cadherin and actin dynamics at the zonula adherens. | 33 |
| Figure 12. Traction force microscopy. | 34 |
| Figure 13. Leader cells in epithelial wound healing. | 35 |
| Figure 14. Traction forces in migrating epithelia. | 36 |
| Figure 15. Monolayer stress microscopy. | 37 |
| Figure 16. Stress maps in epithelial cells. | 38 |
| Figure 17. Physical parameters of epithelial monolayer. | 42 |
| Figure 18. Elevated traction forces and monolayer stresses in followers. | 43 |
| Figure 19. Local unjamming in followers precede leader cell formation. | 44 |
| Figure 20. Merlin depleted cells exhibit unjammed state. | 45 |
| Figure 21. Introducing unjammed followers help to stimulate leader cell Formation. | 46 |
| Figure 22. Collective dynamics overrides the interfacial geometric bias. | 48 |
| Figure 23. Effect of chemotactic signalling on collective dynamic. | 49 |
| Figure 24. Effect of bulk EGF on monolayer stress profile. | 50 |
| Figure 25. Cartographic representation of a typical cellular outgrowth. | 53 |
| Figure 26. Distinct temporal phases of cellular dynamics at wound margin. | 54 |
| Figure 27. Perturbation of contractile forces modifies length scale of force transmission. | 56 |
| Figure 28. Propensity of leader cells upon modifications of cellular forces. | 57 |
| Figure 29. Force correlation length determines transition time between the two phases. | 58 |
| Figure 30. Detection of focal adhesions by RICM. | 59 |
| Figure 31. Orientation of focal adhesions in marginal cells. | 60 |

| | |
|---|----|
| Figure 32. Time dependent kinematic differences in marginal cells. | 61 |
| Figure 33. Molecular mechanisms involved in leader-follower organization. | 68 |
| Figure 34. Effect of matrix stiffness on leader cell propensity. | 69 |
| Figure 35. Collective cell migration in vitro. | 70 |
| Figure 36. Production of PDMS micro-stencils. | 72 |
| Figure 37. Snapshot of cell tracks obtained from FIJI MtrackJ. | 73 |
| Figure 38. Balance of forces considered in monolayer stress microscopy. | 76 |
| Figure 39. Reflection interference contrast microscopy. | 77 |

Motivation

Migration is ubiquitous among biological entities and can be observed at various levels of nature. In animal groups, it is usually triggered by an external stimulus such as change in weather conditions or availability of food. While some species prefer to move alone, others perform collective and cooperative movement, where members of the group directly or indirectly influence each other while migrating. In such cases, spectacular arrangements of collective movements can be observed; for example, synchronized taking off and landing events in birds, schooling of fishes and wagging of honeybees. It is intriguing how precisely the cooperation, guidance and information transfer is controlled and consensus to unidirectional migration is quickly achieved in these animal groups. In most species, the mechanisms orchestrating group movement depend upon how members of the group interact with each other. Consequently, collective behaviour can either be dominated by an autocratic leader where decisions made by a few dictate the behaviour of the entire group¹⁻³, or may emerge from a shared democratic process where each individual sense the directional cues and play critical role in cooperative group movement⁴. To avoid the costs of indecision and for the benefits of group living, some studies suggest that, democracy in which individuals interact and resolve conflicts before reaching the consensus, is often less costly as compared to extreme autocracy⁵. For example, in honeybees, foragers announce their findings of food source or suitable nest sites by dancing or wagging, hence other bees are informed about the quality and the direction of their findings^{6,7}. The process of shared decision making also govern collective migration of big animal groups as shown by the GPS (global positioning system) tracking of wild baboons⁸. Achieving unanimity however is tricky where social bonds are more complicated and individual preferences are different such as in humans. Although, also in this case, history clearly states the benefits of shared democracy and leadership where leaders are selected by voting, each leader follow a set of rules and have a territory of guidance which has limitations either in terms of area or number of followers⁹.

Interestingly, the striking phenomena of collective migration can also be observed at scales going down up to several microns in case of biological tissues that comprise our body. Collective migration of cells is not only fascinating but also essential without which, the embryos won't develop, the organs won't form and the wound won't heal. While some cells such as those comprising our immune system move as single entities, many cell types move in diverse interconnected groups during events such as embryo development, organ development, cancer metastasis and wound healing. Depending upon the connections these cells experience with each other, a range of collective migratory behaviors can be observed. They can move as tightly connected two-dimensional sheets such as

epidermal cells during wound healing, as loosely connected mesenchymal cohorts during embryogenesis, as three-dimensional structures during organ development, or as poorly organized mass during cancer invasion. In all cases, cells need to sense and interpret precise guidance signals, which instruct them to their designated aims. Do all the cells in a group sense the guidance cues and respond individually or a few leader cells read the signal and instruct others to follow? In both cases, how do the cells cooperate with each other in space and in time? How are the leaders selected and regulated temporally and spatially during the migration event? These questions are intriguing and are also of great therapeutic interests because errors in cell-migration may lead to lethal physiological consequences such as immune dysfunction and tumour progression. In the past few decades, researchers have been studying biophysical and molecular mechanisms of collective cell migration using variety of *in-vitro* and *in-vivo* models. These studies revealed many interesting aspects and at the same time, opened broad prospects for further research in the field of collective migration.

This thesis is limited to the studies of two-dimensional sheet like migration of epithelial cells relevant to wound healing. In the first chapter, we would deal with the basic principles of cell migration and the available models used to study mechanisms in collective cell migration, especially in the context of wound healing. Further in the chapter, we would discuss what is known so far about the important aspects required to orchestrate collective epithelial migration. For example, how epithelial cells sense and interpret precise guidance signals, how they coordinate and correlate with their neighbours and with the underlying substrate and what are the open questions and blind spots that require attention. We would then go to the next chapters, trying to find answers to some of those questions. To this end, we exploit the *in-vitro* scratch-free, wound healing assay to study time-resolved epithelial wound healing and use various microscopic and force measurement techniques to draw force cartography of epithelial monolayer as the wound heals.

I. Introduction

I.I Architecture of Eukaryotic cell

The origin of Eukaryotic cell was a milestone in the evolution of life. The level of organizational complexity in eukaryotes has permitted the development of all the multicellular organisms. Eukaryotes are typically 10 to 100 micrometers across and about 10 times the size of a typical prokaryote or bacterial cell. They mainly differ from prokaryotes in that they have membrane bound organelles and their DNA is contained within a nucleus. The eukaryotic DNA contain genetic information on the organization and structure of the cell. The various organelles help the cell to maintain homeostasis, provide energy and maintain cell shape by providing mechanisms for spatiotemporally controlled protein synthesis. Cells are embedded in protein and polysaccharide rich extracellular matrix (ECM), which fills the space between individual cells and between the cell and the substrate. The inside of cell (cytoplasm) is spanned by the cytoskeleton, a mesh of protein filaments that defines the cell's shape.

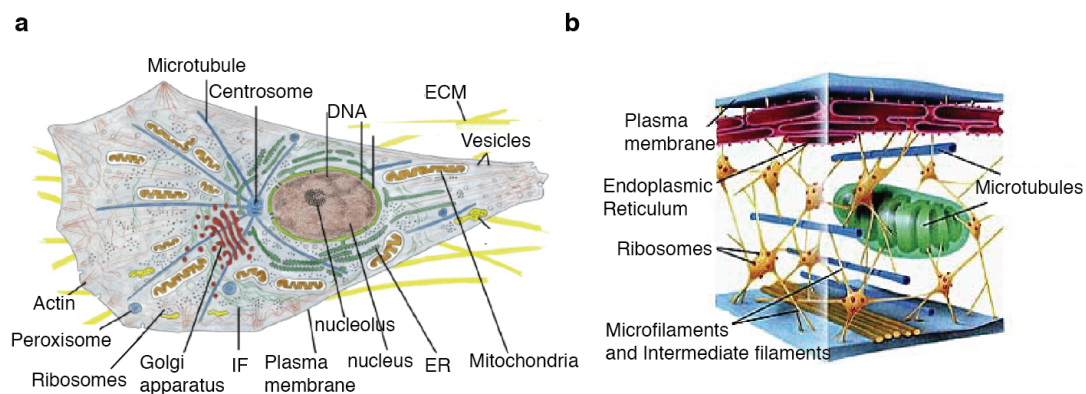


Figure 1. Eukaryotic cell. (a) Cartographic representation of major membrane bound organelles¹⁰. (b) Cytoskeleton of eukaryotic cells depicting importance of microtubules, microfilaments and intermediate filaments in maintaining the integrity of cells¹¹

The cytoskeleton consists of three main components, microtubules, actin filaments and intermediate filaments. All of them are helical structures that are self-assembled by subunits in an end-to-end and side-to-side fashion giving the three filaments their individual mechanical properties. While intermediate filaments are flexible rope-like structures, the microtubuli are built in a tube-like fashion made of tubulin polymers giving cell its rigidity. The actin filaments are the thinnest and the most fragile of the three but very precisely regulate cell contractility and cell motility¹⁰.

1.2 How cells move

Cell migration is a central phenomenon in the development and maintenance of multicellular organisms. Development of tissues, healing of wound and functioning of immune system, all require the orchestrated movement of cells in specific directions and locations, errors in which, might lead to lethal consequences. Understanding cell migration is therefore of great importance for development of novel therapeutic strategies and for controlling progression of diseases. In the past two decades, researchers have extensively studied migration at single cell level in response to external stimuli or a gradient. Due to the highly viscous extra cellular environment, cells are required to produce forces in order to move forward. While most prokaryotes protrude flagella that help them to propel forward, mechanisms involving migration of eukaryotic cells is far more complex. In this case, the initial response of a cell to a migration signal is to polarize and extend protrusions in the direction of migration. These protrusions are driven by actin polymerization and depending upon the actin polymerization machinery employed in forming these protrusions, they can be broad lamellipodia or spike-like filopodia. Both lamellipodia and filopodial protrusions contribute to migration depending upon the situation, for example lamellipodia can extend to long distances and pull cells along¹², while filopodia mainly explore the cell's surrounding, and contain receptors that detect diverse signals in the ECM^{13, 14}. Protrusions are further stabilized by adhering to the ECM via contact points mediated by proteins known as integrins and focal adhesions. These adhesions serve as traction sites for migration as the cell moves. Concurrently, adhesions are disassembled at the rear end, allowing the cell to detach from the back and move forward¹⁴ (Figure 2a). Each of these processes i.e. polarization, protrusion, attachment at front end and detachment at rear end; is complex at the molecular level and must also be synchronized with the others in both space and time.

Both Lamellipodia and filopodia are actin polymerization driven protrusions, which employ different machineries of actin regulating proteins to form branched or bundled actin filaments respectively¹⁴ (Figure 2b). Actin filaments in both cases are intrinsically polarized with fast-growing “barbed” ends and slow growing “pointed” ends, and this inherent polarity is used to drive membrane protrusion. Structure of lamellipodia was first reported in 1970 by Michael Abercrombie¹⁵ who used elegant electron microscopic images of fibroblasts and showed that lamellipodia contain actin microfilaments and not microtubules. Lamellipodia was then observed in many different cell types in vivo such as border cells in *Drosophila*, muscle precursors in chick embryos and neural crest cells in *Xenopus* and in Zebrafish^{12, 16}.

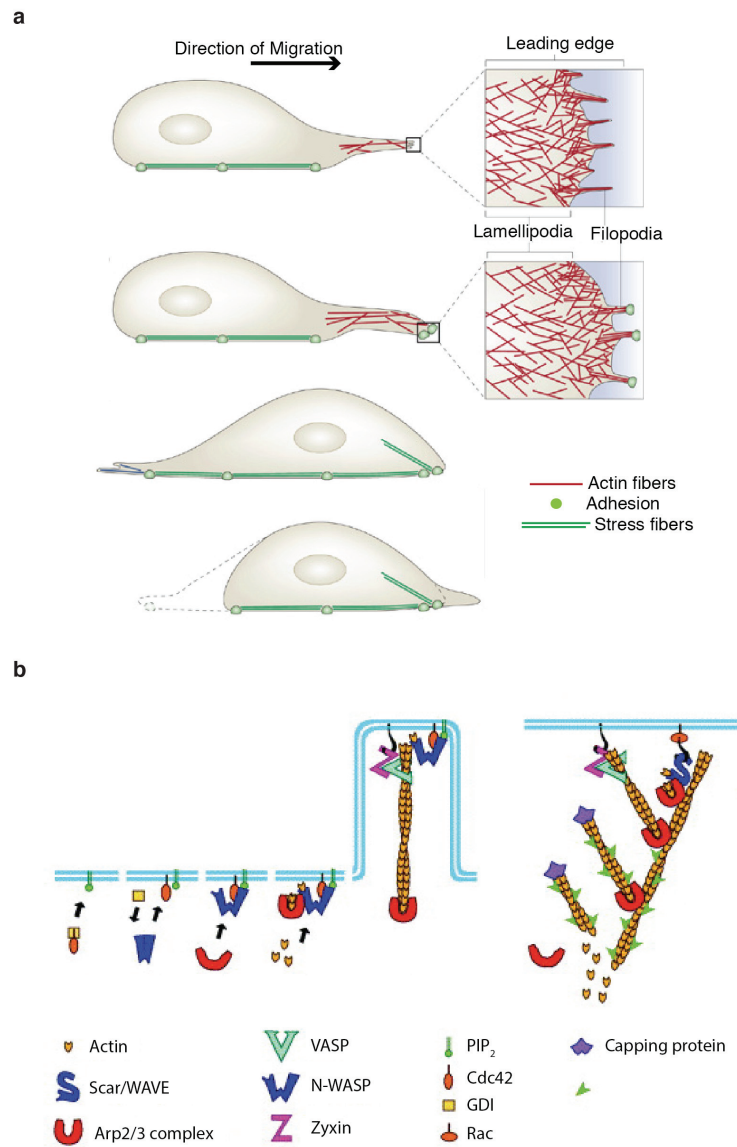


Figure 2. Mechanisms of single cell migration. (a) Schematic representation of the process of cell migration describing various stages of cell migration. Cells respond to the migration stimulus by developing membrane protrusion in the direction of migration. The protrusions are further stabilized by adhesion onto the matrix and the cell body move finally forward by disassembling adhesions at the rear end¹⁷ (b) formation of protrusive F-actin network at membrane¹⁸. Diagrammatic scheme of effector molecules involved in forming lamellipodial and filopodial protrusions

Cells respond to the migration signal via Rho GTPases such as Rac and cdc42, which gets activated by different guanine exchange factors GEFs at the leading edge. Activation of Rho GTPases is followed by activation of other downstream effector molecules, that work coordinately to form actin protrusion machinery, which finally lead to the formation of branched or bundled actin filaments. For instance, Activated Rac binds to PIR121 in the WAVE complex¹⁹ thereby inducing a structural rearrangement in the later to make the WAVE-WCA domain accessible for binding to Arp2/3 which nucleates branched

actin polymerization to form lamellipodial protrusions²⁰. The Rac target IRSp53 (Insulin Receptor tyrosine kinase substrate p53) contributes to lamellipodia extension by binding to Rac and WAVE2. Further, WAVEs can also be activated by tyrosine and serine/threonine phosphorylation, which induce the similar structural change required for binding of Arp2/3 to WCA domain²⁰. For filopodia formation, activated cdc42 binds to IRSp53, which thereby undergoes a structural change and bring together mDia2 and N-WASP. Activation of N-WASP in this way leaves its VCA domain accessible to the binding of Arp2/3 complex; filopodia assembly then emerges from the F actin network nucleated by Arp2/3^{13, 21}. Other actin nucleators have recently been found to contribute to filament extension and regulation, including cofilin and members of formins and spire family. Cofilin provide barbed ends for nucleation while Formins protect these barbed ends from capping thereby promoting filament elongation without branching. The role of formins is therefore more important during filament extension in filopodia. It is now known that filopodia can even be formed independent of N-WASP and Arp2/3 complex; formins, in particular mDia proteins can directly bundle filopodia from actin monomers²¹ (Figure 2b).

Next, for the migration to occur, these protrusions must be stabilized by integrins mediated attachments to the surroundings. Integrins are transmembrane receptors that link the cellular matrix with the cytoskeletal elements. They support cell migration by forming cellular adhesions onto the ECM as well as by linking these adhesions with actin filament network on the inside of the cell²². Two stages of matrix adhesions have been observed; first, formation of nascent focal adhesions and second, maturation to stable complexes (Figure 3a). Interactions between transmembrane integrins and extracellular matrix proteins trigger the dynamic accumulation of protein-dense structures that form the initial nascent focal adhesions connecting protrusions to the ECM as soon they form (Figure 3a, *left*), these nascent focal adhesion either rapidly turn over or develop into mature focal adhesions with increased size and strength owing to their anchorage to myosin-II mediated actin stress fibers²³ (Figure 3a, *right*). Therefore two kinetically, and molecularly distinct F-actin networks are present at the leading edge of migrating cells, one is highly dynamic branched or bundled network at the lamellipodial or filopodial protrusions which is continuously remodeled and is linked to the underlying substrate via dynamic, nascent focal adhesions; While the other F-actin network is more stable and involves myosin-II mediated actin polymerization at the lamella (right behind the lamellipodium) where contractile forces generated by extension or contraction of F-actin filaments are coupled to substrate attachments via mature focal adhesions²² (Figure 3b, 3c). These actin filaments are also referred to as stress fibers and are responsible for keeping cells into shape with the aid of molecular motors myosin. Polymers of F-actin serve as a scaffold for myosin II. Myosin- II filaments bind to two actin filaments and drive the translocation of bound filaments towards their fast growing barbed ends which results in their contraction or extension depending upon the location of myosin- II with respect to the filaments (Figure 3d). Myosin-2 activity is further regulated by myosin

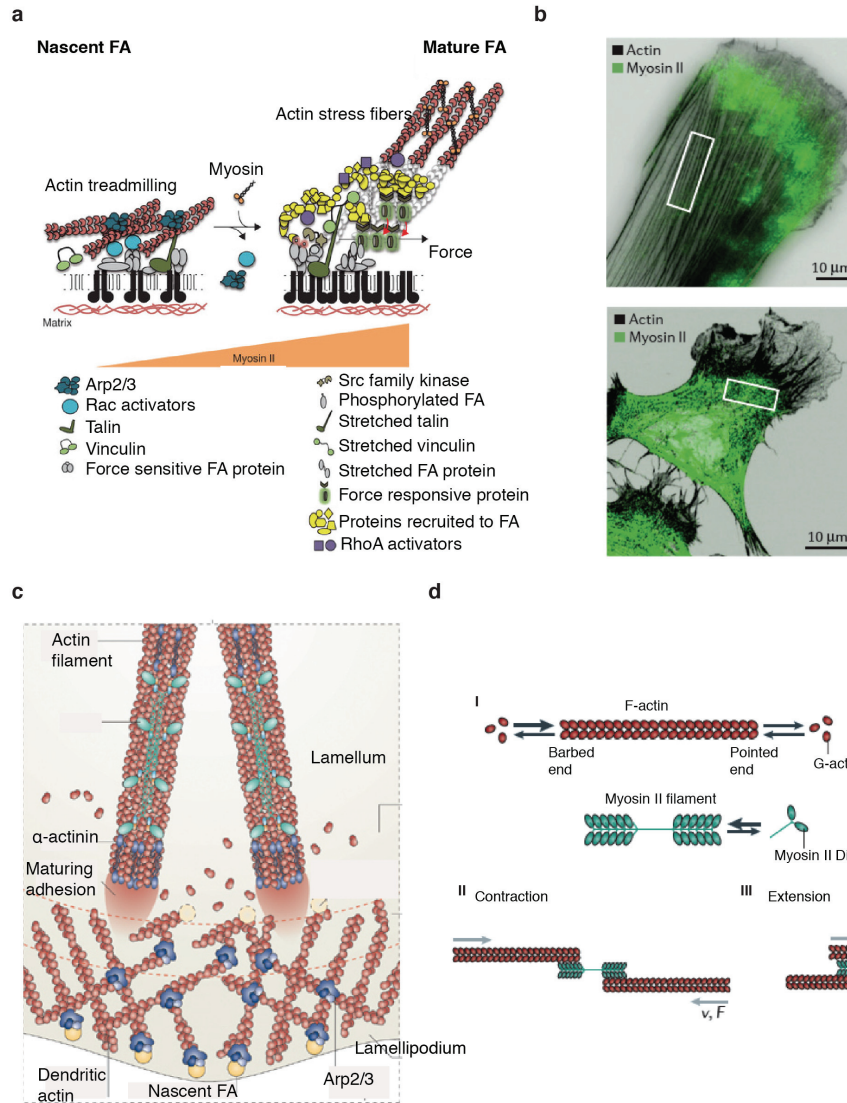


Figure 3. Mechanisms for maintaining tensegrity in cells (a) Formation of nascent and mature focal adhesions²⁴. Initial nascent focal adhesions are formed by first interactions of membrane protrusions with underlying matrix; these nascent adhesions connect with acto-myosin contractility and develop into mature adhesions. (b) Staining images show two distinct F-actin pools found in migrating cell²⁵. (c) Diagrammatic representation of the two actin pools showing fast growing branched actin pool at lamellipodia and slow growing bundled retrograde flow at lamella²⁶. (d) Schematic representation of mechanism involved in contraction and extension of actin stress fibers during actomyosin contractility²⁵

light chain phosphorylation, which is positively regulated by myosin light chain kinase or Rho kinase or negatively regulated by MLC phosphatase²⁷. Phosphorylation of myosin light chain activates myosin to generate more contractile forces while MLC phosphatase deactivates myosin to a relaxed state. Finally, in order for the cells to displace forward, adhesions must detach at the rear end of the cells, this can happen via various strategies for example mechanical disruption of adhesions by actomyosin

contractility, cytosolic disruption via various enzymes like phosphatases and/or kinases or extracellular disruption via metalloproteases²⁸.

1.3 From Single cell to collective: Increasing level of complexities

Although much is known about how cells see their surroundings, regulate tensegrity, and migrate as single entities, most of the tissue remodeling and regeneration events require coordinated migration of many cells in a group. In such cases, each member of the group not only need spatiotemporal synchronization of migration events within itself but also require precise orchestration of these events with other neighbouring cells.

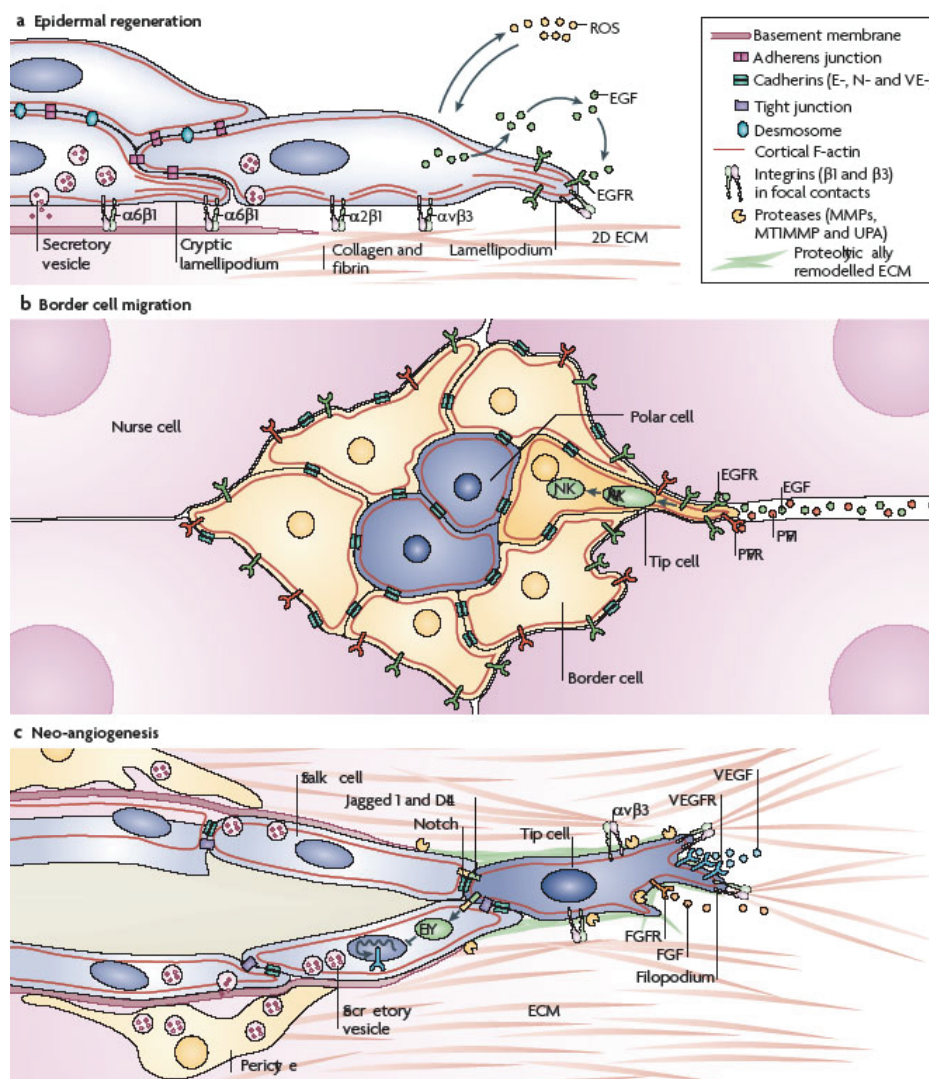


Figure 4. Collective cell migration in physiological events¹². Cartographic representation, (a) Two-dimensional sheet like migration of epithelial cells during wound healing. (b) Migration of border cells during oogenesis and (c) 3D sprouting and branching of epithelial cells during angiogenesis

Collective cell migration can be defined as the movement of cells in a group where individuals maintain either transient or stable cell-to-cell contacts, thereby influencing the migration of their neighbours while they move¹². Groups of cells migrate to complete their designated task, and depending upon their location, and the cell types, they exhibit different migratory behaviours. Some groups are loosely connected, with occasional contacts that come from single cells following the same track and guidance cue. The interactions here can be seldom such as in germ cells and immune cells²⁹ or frequent such as in neural crest cells. Other migrating groups are more tightly associated and maintain weak or strong cell-cell contacts all the time during migration, such as migration of primordial cells in zebrafish lateral line³⁰, migration and sprouting of epithelial cells during drosophila tracheal branching and angiogenesis^{31, 32}, migration of drosophila border cells during oogenesis^{33, 34} and migration of epidermal cells during wound closure^{35, 36} (Figure 4). In such cases, cells require precise synchronization of sensing and transmission of migration cues with their neighbours, in both space and time. The mechanisms that regulate this phenomenal coordination, however, remained elusive until last two decades when advances in live imaging and development of different model systems for studying collective migration have made it possible to visualize many group movements, some of them directly in their natural context^{12, 16}. Although, the available models have provided answers to many important fundamental questions in the field of collective cell migration, so far, we only have a fragmentary view of mechanisms that regulate collective cell migration in various scenarios with many riddles still unresolved.

1.4 Modes and Models to study collective migration

In recent years, the importance of collective migration in orchestrating complex morphogenic events has been realized. One of the major goals of developmental biology has been to define patterning principles that govern development of embryo and organs. Embryogenesis starts with fertilization of egg and sperm, resulting in the formation of zygote. This zygote then undergoes multiple cell division cycles to form blastula, which is a spherical layer of cells surrounding a fluid filled cavity or yolk. Blastula then develops and forms blastocyst characterized by an inner cell mass, which is distinct from the surrounding blastula. This is followed by gastrulation during which single-layered blastula is reorganized into a trilaminar structure known as the gastrula. During gastrulation, cells migrate to the interior of the blastula, forming germ layers. The germ layers are referred to as the ectoderm, mesoderm and endoderm. Each of these layers is responsible for development of different organs. Ectoderm gives rise to the neural crest and other tissues of nervous system. Mesoderm gives rise to muscles; the cartilage, blood vessels, bones, and connective tissue. Endoderm gives rise to the epithelium of the digestive system and respiratory system, and organs associated with the digestive system, such as the liver and pancreas (Figure 5).

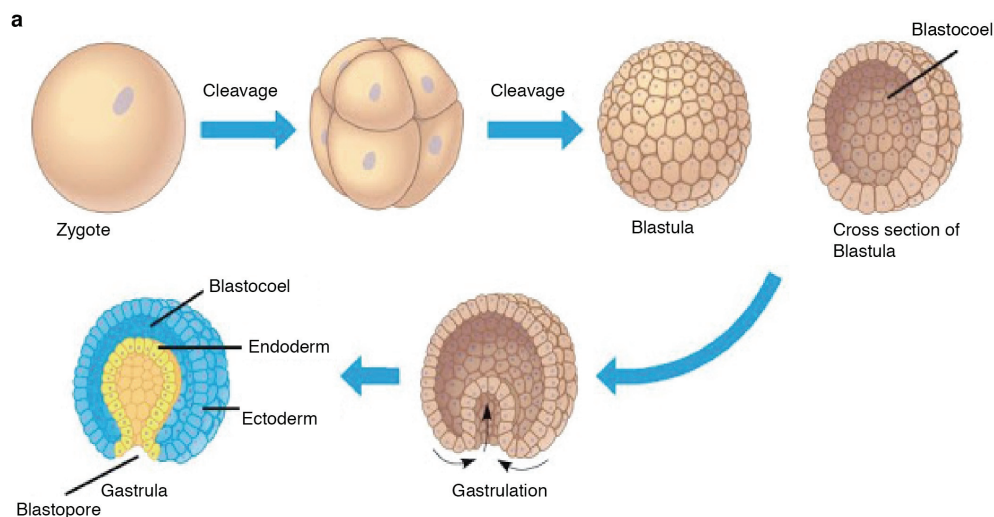


Figure 5. Mechanism of gastrulation during embryogenesis. A zygote undergoes multiple rounds of cleavage to form a blastula. Cells in a blastula migrate to form a trilaminar structure called gastrula, and the three layers of gastrula determine the different organ lineages (Figure courtesy: Pearson Education Inc.)

Structure of each of these organs is highly complex and three-dimensional and many comprise of branched tubular networks where branching pattern, size and shape of tubes are critical for the functioning of organ. How do the cells move and arrange themselves in these precise elaborate 3D structures? During the process, how do they sense the directional cues and coordinate with their neighbors? These questions are difficult to address in mammalian systems because of their complex organization and limited accessibility. During the past decades, studies in the area of developmental biology has led to the development of *in-vivo* as well as *in-vitro* model systems that can be used to various study mechanisms involved in orchestration of these complex biological events.

1.4.1 In-Vivo Models

Both vertebrate and invertebrate models have been used to study collective cell migration during embryogenesis and organogenesis. Typical examples include *Drosophila melanogaster*, a common fruit fly that is easy to keep, breeds quickly, and easily genetically modified; and Zebrafish, because of its suitability for genetics and transparent embryo. Study of *Drosophila* border cells during oogenesis, *Drosophila* tracheal cells during branching and sprouting morphogenesis, Zebrafish primordial cells and *Xenopus* neural crest cell, has emerged as a paradigm, and atleast begun to provide answers. These model organisms provide us an understanding of how collective migration is synchronized in various events during development. Cells involved in such events may exhibit two modes of migration; they can be tightly connected to each other and show epithelial like behaviour with cells retaining stable adherens junctions and apicobasal polarity (Figure 6a), or can be loosely connected to each other and

show mesenchymal like behaviour, with cells having transient adherens junctions^{16, 37}(Figure 6b). In both cases, cells influence each other and are associated strongly with the underlying substrate.

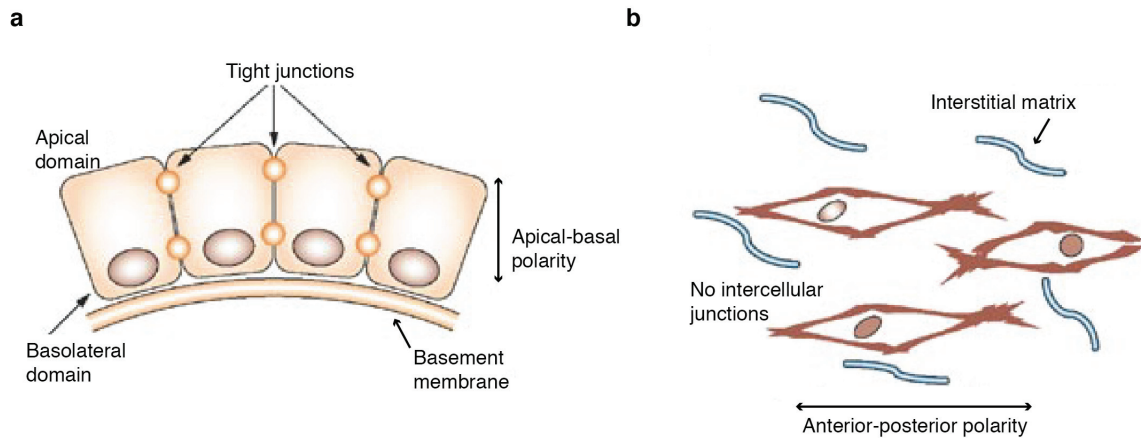


Figure 6. Morphogenic characteristics of epithelial and mesenchymal cells³⁷. (a) Epithelial cells are characterized by apical-basal polarity and strong cell-cell junctions while (b) Mesenchymal cells are connected to each other with transient cell-cell contacts.

During *Drosophila* oogenesis, cohesive border cells, which are essentially of epithelial nature, invade the germ-line cells and migrate between the giant nurse cells towards the oocyte. These cells migrate using other cells as substratum and retain their epithelial character with the apical membranes interacting with the germ-line cells via cadherin mediated contacts^{33, 38}. Interestingly, during migration, a leader cell at the front guides the cohort³⁹ and the leader-follower is dynamically rearranged and exchanged⁴⁰. Next, studying *Drosophila* tracheal branching reveals that tracheal cells respond to the ligand Bnl in the adjacent tissue via the receptor Btl and invaginate from epithelial placodes to form tracheal sacs⁴¹. Cells with highest levels of Btl signaling take leader positions by producing lamellipodial protrusions whereas others behave as followers^{42, 43}. Lamellipodia formation is inhibited in followers by Delta-Notch dependent lateral inhibition. Leader cells produce high levels of Delta, which activates Notch in neighboring cells thereby inhibiting protrusion formation⁴⁴. Similar mechanisms coordinate sprouting angiogenesis of vertebrate blood vessels as seen in mouse retinal cells⁴⁵. Further, in some cases cells undergo a transition from epithelial to mesenchymal mode of migration. Such a mode of migration in ‘streams’ or loosely adherent groups of cells is common during migration of neural crest cells or in mesoderm migration. In such cases, cells exhibit high protrusive behavior, rapidly exchange neighbors and position of leaders is only transient⁴⁶. While both epithelial and mesenchymal modes of migration require cell-cell coordination at different levels, it has been only recently realized that for efficient and collaborative movement of cells in different occasions, orchestration of events not only in space but also in time is important. For example, migration of *Drosophila* border cells during oogenesis reveal time related distinct phases; where polarized cell behavior dominates in phase-I and dynamic

collective behavior dominates the phase-2⁴⁰. Similarly Dynamic phases involving mitosis and migration also appear during self-organizing tissue migration in the Zebrafish lateral line⁴⁷.

1.4.2 *In-Vitro Models*

During embryo development there are numerous occasions when stationary epithelial cells undergo complete or partial transition to mesenchymal cells with high protrusive and migratory behavior. The fascinating phenomena of EMT, which is one of the central events during embryogenesis, become fatal when acquired by tumour cells, which invade the surrounding tissues with the help of these migratory cells. The apparent question here is, how does the collective migration behavior function during cancer invasion? Organotypic 3D cultures, developed to study cancer invasion⁴⁸ lead to interesting insights about molecular and biophysical mechanisms involved in collective invasion of cancer cells⁴⁸⁻⁵⁰. Invasion of carcinoma cells can be modeled in vitro by overlaying 3D scaffolds with cells, which then generate vertical invasions into the tissue matrix,⁵⁰ or by implanting multiple spheroids that generate horizontal invasions into 3D-ECM culture⁴⁹. However, role of collective migration is not only limited to embryogenesis, organogenesis and cancer metastasis but is also significant in maintenance and repair of organs upon damage caused, for instance, by a wound. Wounds can result not only from accident or surgery but also from pathological situations such as cancer or infection^{51, 52}. Abnormal wound repair may result in inflammation and fibrosis⁵³ or may even initiate tumor⁵⁴. Efficient self-repair is therefore necessary for maintaining tissues in their functional form.

Animal tissues are grouped into four basic types: Connective, muscle, nervous and epithelial. Connective tissues are fibrous tissues made up of cells separated by matrix that can be liquid or rigid. For example, blood contains plasma, as its matrix while bone's matrix is rigid. Connective tissue such as blood, bones, tendons, ligaments, adipose and areolar tissues give shape to organs and holds them in place. Muscle tissues function to produce force and motion and comprise of smooth muscle (found in inner linings of organs), skeletal muscle (attached to bones) and cardiac muscle (found in heart). Nervous tissues make up the brain and the spinal cord. Epithelial tissue comprise of cells that cover the organ surfaces such as the surface of the skin, reproductive tract, inner lining or digestive tract etc. Epithelial tissue provides a barrier between external environment and the organ it covers. In the event of trauma such as a wound, the protective barrier is broken and an orchestrated cascade of biochemical events is set into motion to repair the damage. This process of healing involves highly coordinated interplay among cells, soluble factors and extracellular matrix with a final aim of efficient wound closure via migration of epithelial cells atop the wound bed. In the past few decades, researchers have been studying aspects of migrating epithelial cells during wound healing in vitro by using a classical "wound healing" scratch assay in which a confluent monolayer is scratched with a sharp object such as a razor blade, so as to mechanically remove a strip of cells. Progression of remaining cells would mimic the

scenario of wound healing and can be observed under a microscope to study mechanisms involved in orchestrating collective migration of these cells. The scratching however not only destroys the removed cells but also is traumatic for the cells on the border. Destroyed cells release intracellular content into the medium thereby changing the local environment. Also, due to the trauma, border cells become more permeable to the influx of extracellular components, which might trigger the migration. To uncouple migration from cell damage and/or cell permeabilization a confinement release assay was developed where a virgin surface is presented to a confluent epithelium; It has been shown that this sudden release of confinement or availability of space is sufficient to trigger migration of epithelial cells⁵⁵. Depending upon the context and the problem in question, both scratch wound assay and confinement release assays are used to study various aspects of wound healing in epithelial tissues. Based upon the shape of the cells and complexity of layers comprising the tissue, epithelial tissues can be classified into different types. By shape of the cells, epithelia could be Squamous, cuboidal or columnar (Figure 7a). By layer, epithelial tissue can be simple (single layered) or stratified (multi layered) (Figure 7b). Depending on the function, different combinations of shape and size comprise epithelial tissues of different organs. For example, simple squamous epithelium can be found in lining of airways and heart, where the primary function is diffusion and filtration while stratified squamous epithelium can be found in linings of esophagus, and in female reproductive organs, where the primary function is to protect against abrasion⁵⁶.

1.5 Architecture of Epithelia

The level of complexity goes up in tissues such as skin, the outermost layer covering the human body. Skin is the primary organ that provides the first physical barrier to any invading microorganism or toxin⁵⁷. The skin has multiple layers of ectodermal tissue broadly classified into epidermis, dermis and hypodermis (figure 7c). Epidermis, the outermost layer, made up of stratified squamous epithelium, forms a waterproof protective wrap for the skin. Epidermis is divided into several layers, where cells are formed through mitosis in the innermost layer. The daughter cells move up to the outermost layer (strata) changing shape and composition as they die due to isolation from their blood source. This process is called keratinization. The keratinized layer is responsible for homeostasis and act as a barrier for pathogens. Layer beneath the epidermis is called dermis and is tightly connected to the epidermis by a basement membrane. Dermis contains lymphatic and blood vessels, which provide nourishment to the epidermis and also assist in waste removal. It also contains hair follicles, sweat glands and sebaceous glands along with many nerve endings that provide sense of heat and touch. Hypodermis connects the skin to the underlying tissue⁵⁸.

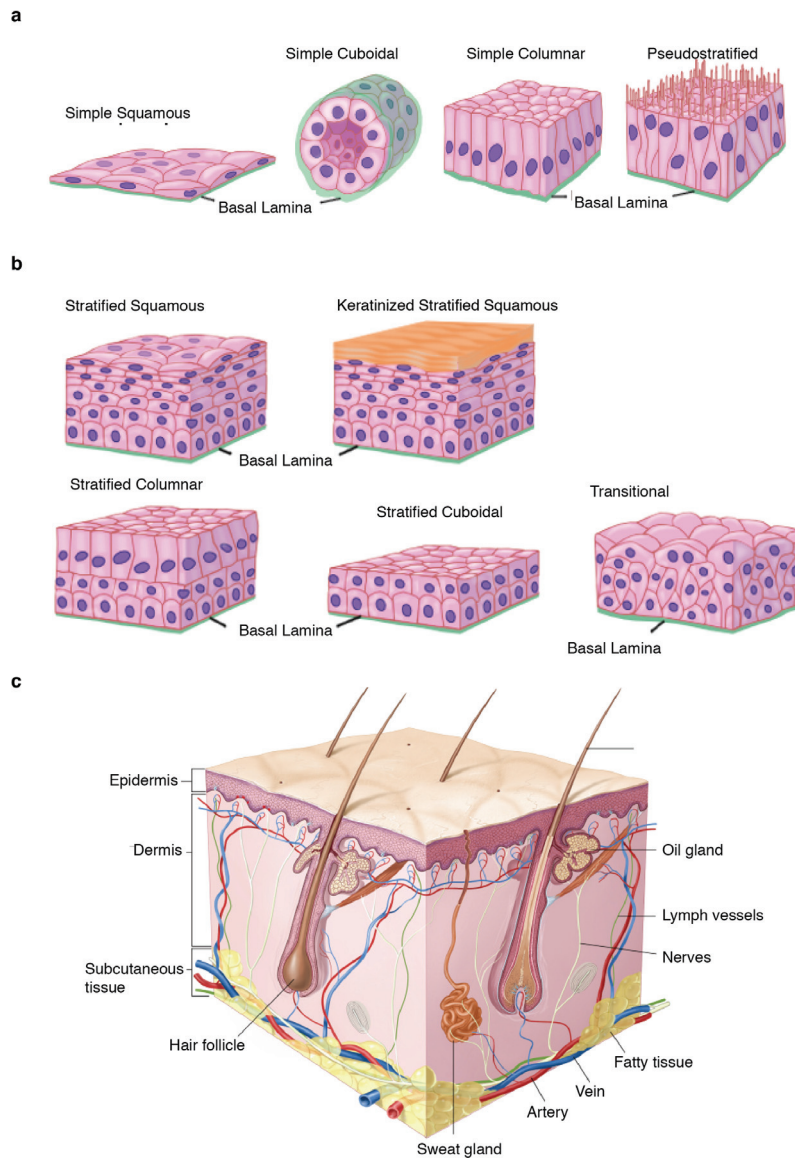


Figure 7. Organization of epithelial tissues. (a) Classification of epithelial tissues on the basis of shape of the cells. Epithelia can be Squamous (flat), cuboidal (aspect ratio between height and width is 1) or columnar (high height to width ratio). **(b)** Classification of epithelial tissue on the basis of complexity of layers⁵⁹. **(c)** structure of skin epithelia showing different layers of skin tissue (Figure adapted from NIH, pubmed)

1.6 Epithelial wound healing

Epithelial wound healing is a complex physiological process and comprises of dynamic wound closure, tissue remodelling, and immune response^{60, 61}. The whole process of healing can be divided into four distinct phases, homeostasis, inflammation, migration and proliferation, and finally tissue remodelling. For efficient wound closure, each phase must be precisely orchestrated with all the components put together to work in the exact order as required for the tissue to regain its original shape and integrity.

1.6.1 Process of healing

Homeostasis- Within the first few minutes of injury, damaged or Stressed cells activate stress signaling pathways, which lead to phosphorylation of a cascade of signalling molecules, that ultimately lead to changes such as alterations in gene expression. Most of these cells then release endogenous molecules DAMPs (Damage associated molecular patterns), which act as chemotactic, signal for activation of other cells in a similar way. Furthermore, hemorrhage of blood vessels is stopped by platelet activation and aggregation. Platelets aggregate to the injured site, gets activated, change into amorphous shape and release chemical signals for clotting. This results in activation of fibrin, which forms a mesh and acts as a glue to further bind the platelets together. This makes a clot, also called a platelet plug because it plugs the break in the blood vessels thereby preventing further bleeding^{36, 62} (Figure 8a).

Inflammation- Damaged blood vessels release leukocytes into the wound; this is followed by rapid activation of immune cells that are already present within the tissue. Activated T cells and Langerhans release a rapid pulse of chemokines and cytokines. These growth factors attract neutrophils and macrophages from the nearby vessels. Neutrophils kill the invading microbes by various strategies like burst of reactive oxygen species while macrophages, as professional phagocytes clear up matrix and cell debris⁶³ (Figure 8b).

Proliferation, contraction and wound closure- In this phase, new blood vessels are formed by angiogenesis. Network of these blood vessels provide nutrients and oxygen and aids in the formation of granulation tissue⁶⁴, which replaces the fibrin clot at the dermis and serve as a matrix onto which fibroblasts migrate and reconstitute the dermis. Fibroblasts then grow and form a new provisional extracellular matrix (ECM) by excreting collagen and fibronectin. Migrating fibroblasts form stress fibers, which enable connective tissue contraction. This contractility is further enhanced when fibroblasts are driven to differentiate into myofibroblasts by the action of growth factors, and mechanical stress. Together, fibroblasts and myofibroblasts help to close the wound and contribute to the synthesis, bundling and alignment of collagen fibers, the primary constituent of scar tissue^{65, 66}. Simultaneously, re-epithelialization of the epidermis occurs, in which epithelial cells proliferate and crawl on top of the provisional matrix thereby closing the wound⁶⁷ (Figure 8c).

Remodeling and Maturation- Remodeling is necessary for restoration of full functionality and a normal appearance of the injured tissue. Migrating and proliferating keratinocytes at the wound edge confront each other as the wound seals. Concurrently, the blood vessels within the scar are refined to form a functional network⁶⁸. The dense provisional ECM that was deposited during repair is remodeled⁶⁶, this happens by a delicate balance of collagen synthesis, bundling and degradation⁶⁶. Moreover, myofibroblasts, neutrophils and other unwanted immune cells undergo apoptosis at this stage⁶⁹ (Figure 8c).

1.6.2 Different modes of wound closure

Impaired wound healing leads to the various pathophysiological conditions, such as chronic inflammatory disorders, and autoimmune diseases and in some cases may even result in cancer development^{60, 70, 71}. One of the pivotal steps of a wound healing response is the collective migration of epidermal cells into the wounded area, which eventually culminates into wound closure⁷²⁻⁷⁶. In this respect, smaller wounds are usually sealed through a contraction-mediated ‘purse string’-like closure mediating formation of a supracellular actomyosin ring around the wound margin (Figure 9a). In such cases, healing require coordinated movement of all the cells at the edge due to ATP dependant constriction of actomyosin cable⁷⁷⁻⁸¹. Due to the supracellular coordination, purse string like closure is usually characterized by a very smooth edge. Closure of larger wounds, on the other hand, requires active migration of the surrounding cells into the wound bed^{55, 74, 75, 82-87} (Figure 9b).

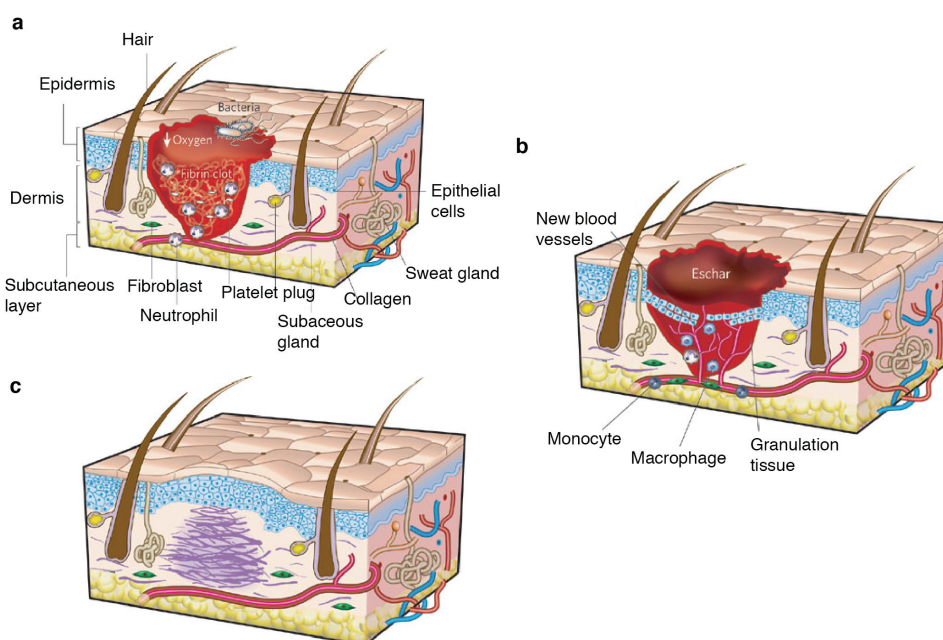


Figure 8. Process of wound healing ⁵². (a) Homeostasis; initial response of the stressed cells to stop bleeding lead to clotting, Inflammation and proliferation (b) Inflammation, proliferation and migration; Immune cells come into action and kills the invading microbes, new blood vessel form, fibroblasts migrate and produce a provisional matrix, finally epidermal cells proliferate and migrate to seal the gap. (c) Remodelling of the matrix and removal of unwanted molecules and cell debris accumulated in previous steps.

Accordingly, in the latter process, the cellular movement is initiated at the wound margin by the formation of a specialized cell type called leader cells⁸⁸⁻⁹⁰. These leaders are known to crawl upon the substrate with the aid of large lamellipodial protrusions, and contain the ability to pull along many cells while they migrate⁸⁷. Recent studies however reveal that both purse string and cell crawling mechanism

coexist and can mechanically influence each other⁸⁵. Cell movement at the gap relies on local curvature and actin organization. Negative curved regions show tangential alignment of both focal adhesions and traction forces and are dominated by actomyosin contractility mediated purse string closure while positive curved regions show high lamellipodial activity with focal adhesions and traction forces pointing perpendicular to the edge, these regions are therefore dominated mainly by cell crawling, guided by a motile leader cell (Figure 9c). In both cases, each cell is required to correlate its motion with that of its neighbors. Remarkably, while migrating, epithelial cells correlate over more than ten cell diameters in space^{91, 92}. To achieve this long-range correlation, it is intuitive that these cells should be able to connect with each other at the molecular level where each individual is able to correlate its polarization and motility with that of its neighbours. For example, moving cells should have the ability to coordinate polarized activation of Rho GTPases such as Rac1, Cdc42 and RhoA with their neighbors in both space and time^{50, 93}. In addition, cell contractility and polarization of cytoskeleton must also be synchronized in a similar way. In the last few years, researchers have been trying to put together, the knowledge obtained from aspects of single cell migration to study the molecular and biophysical aspects of coordination and directionality in epithelial cells.

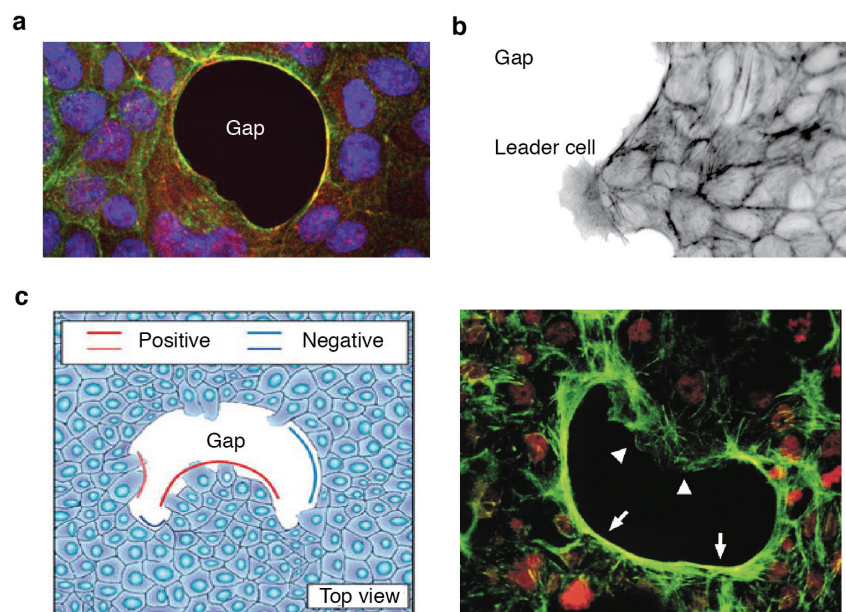


Figure 9. Mechanisms of epithelial wound closure. (a) Immunostaining image demonstrating purse string mechanism of wound closure⁹⁴. A smooth wound margin, showing constriction of supra-cellular acto-myosin cable and coordinated cell migration. (b) Actin staining image demonstrate cell crawling mediated by a leader cell. Cell crawling is characterized by a rough margin. Leader cell is seen at the tips of cellular outgrowths and is distinguished by large protruding lamellipodia (c) Diagrammatic representation (*left panel*) and staining image (*right panel*) showing combination of purse strings and cell crawling⁹⁵

1.7 Coordination and Directionality in epithelial cells

Epithelial cells not only adhere onto underlying substrate at the basal side through focal adhesions but also tightly connect with each other at the lateral side through cell-cell junctions⁹⁶ (Figure 10a). Any changes in cell-cell or cell-matrix adhesions during pathological situations lead to the initiation of migration in otherwise stationary epithelia⁹⁷. Therefore, both cell-cell and cell-substrate adhesions must play essential roles in maintaining the coordination required to achieve the long-range velocity correlation seen in epithelial cells⁵⁵.

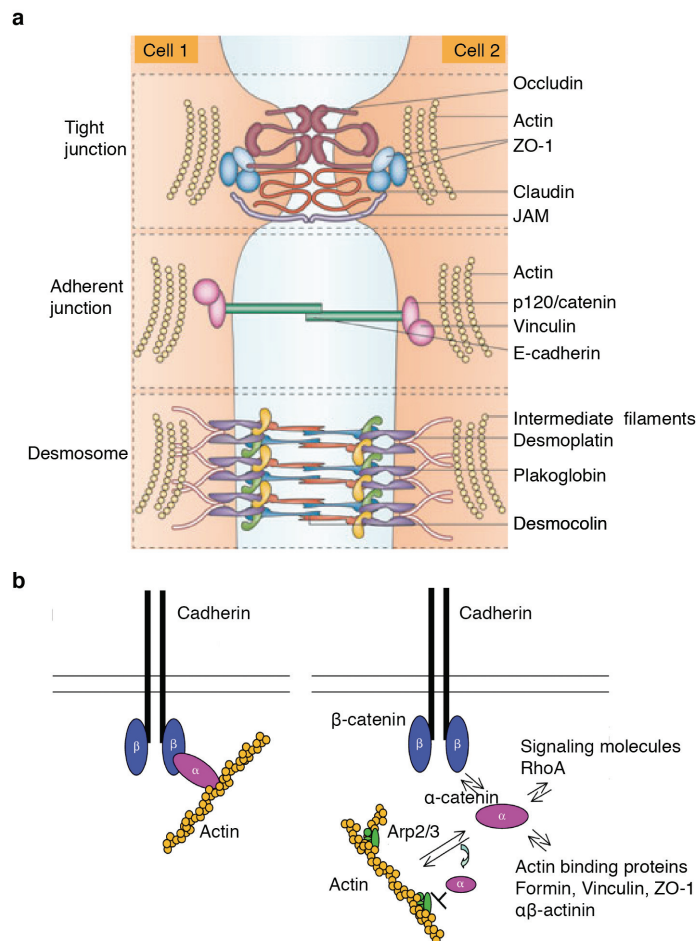


Figure 10. Junctional integrity of epithelial cells. (a) lateral cell-cell attachments. Cells connect with their neighbours by three types of junctional complexes: tight junctions, adherens junctions and desmosomes. **(b)** Linkage of cadherin junctions with actin cytoskeleton⁹⁸. E-cadherin is anchored to the cytosolic side of cell via β -catenin. This cadherin-catenin complex is connected to actin cytoskeleton via force sensing molecule α -catenin.

For cell-cell attachments, epithelial cells mainly contain three types of junctional complexes; tight junctions, desmosomes and adherens junctions. Tight junctions are the circumferential rings mainly at the apex of epithelial cells that seals adjacent cells together and function to regulate ion flux between the cells. Desmosomes anchor cells side to side and are coupled at the cytoplasmic side with intermediate

filaments. Adherens junctions involve calcium dependent transmembrane proteins called cadherins⁹⁹. Depending upon the tissue type, cadherins can be N-cadherin (neural cadherins), P-cadherin (placental cadherins) or E-cadherin (epithelial cadherins). In the context of wound healing, E cadherin is mainly responsible for gluing epithelial cells together. The N terminal domain of E-cadherin mediates binding to cadherins presented on the surface of neighbouring cells. Through their C terminal cytoplasmic tail, cadherins bind to cytoskeletal and signalling proteins, which allow their anchoring to microfilaments, this interaction is important for stabilizing the junctions and for regulating cell shape and polarity¹⁰⁰. The major binding partners of E cadherins at the cytoplasmic side are the catenins: β -catenin, α -catenin and p120 catenin. β -catenin binds directly at the distal end of cadherin cytoplasmic tail where it serves as an anchor for α -catenin¹⁰¹. Since α -catenin can also bind to actin filaments in vitro¹⁰², it was widely accepted that α -catenin bridges cadherin- β -catenin complex to actin cytoskeleton (Figure 10b). However, this model was challenged by biochemical analysis, which revealed that purified cadherin-catenin complex does not bind F-actin¹⁰³. Rather, α -catenin was found to exist in two conformations, as a monomer or as a homo-dimer. Monomeric α -catenin binds to E-cadherin- β -catenin whereas dimer preferentially binds to actin filaments. Interestingly, homodimeric α -catenin directly regulates actin filament organization by suppressing Arp2/3 mediated actin polymerization, likely by competing with Arp2/3 for binding to F-actin^{103, 104}. The weak affinity of α -catenin for β -catenin ($K_d = 1\mu\text{M}$)¹⁰⁵ and its ability of to suppress Arp2/3 mediated lamellipodia formation suggest that cadherins might just be intermediate diffusional traps to locally concentrate α -catenin in the perijunctional cytosol which then serve as an indirect mechanism to stabilize cell-cell junctions^{104, 106} (Figure 10b). Few years later it was shown that the purified cadherin-catenin complex do bind to F-actin, but only under force or mechanical tension¹⁰⁷. Notably, force exerted on cadherin-catenin complex also recruit vinculin, a major focal adhesion complex protein to cell-cell junctions^{108, 109}. Because vinculin accumulates at mature focal adhesions upon actomyosin-generated tension (Figure 3a) and also binds to α -catenin, it has been proposed that α -catenin functions in harmony with vinculin and play essential role in transduction of mechanical forces via cell-cell junctions¹¹⁰.

Further, in order to maintain junctional integrity, it is important to balance the mechanical forces that cells exert on each other by the contractile forces that are generated at the junctional cytoskeleton. Myosin-2 generate contractile forces by contraction and extension of actin filaments at the junctions^{25,26}. Notably, two pools of actin at adherens junctions have been observed, the apical rings that also labelled myosin-2 and cortical pools that marked the site for actin nucleation and also labelled actin polymerization machinery comprising Arp2/3 and WAVE2 complex. Surprisingly, it was later shown that WAVE-2-Arp2/3 is a major nucleator of actin assembly, also at zonula adherens and inhibition of either Arp2/3 or WAVE2 depleted both cortical and junctional actin pools, reduced junctional tension

and compromised the ability of cells to buffer cell-cell forces^{111, 112} (Figure 11). Since Arp2/3-WAVE2 complex is the major driver of lamellipodial protrusions, it is tempting to speculate that differential polarization of actin polymerizing machinery towards the front and towards the junctions is probably essential for leader cell mediated directional guidance during epithelial crawling.

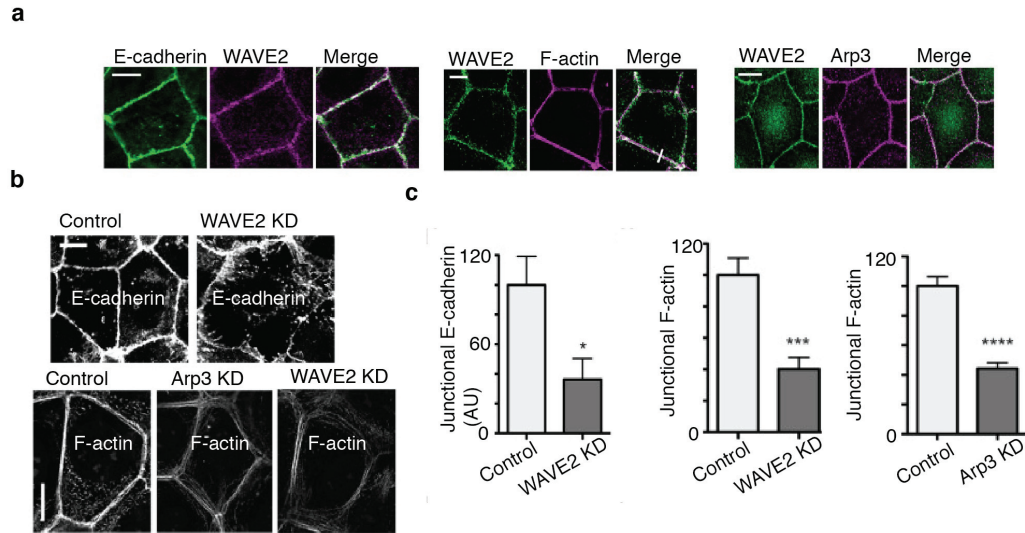


Figure 11. Arp3-WAVE2 regulates E-cadherin and actin dynamics at the zonula adherens¹¹¹. (a) Representative immunofluorescence images showing E-cadherin and WAVE2 (*left panel*), WAVE2 and F-actin (*middle panel*), and WAVE2 and Arp3 (*right panel*) colocalization at ZA (b) WAVE2 knock down (top) reduces apical concentration of E-cadherin into the ZA. Arp3 and WAVE2 knock down (bottom) reduces apical concentrations of F-actin in the ZA. (c) quantification of junctional E-cadherin and F-actin by line scan analysis.

In the past few years, considerable efforts have been made to decipher molecular mechanisms that control leader-follower organization in epithelial cells^{113, 114, 115}. Similar to mechanisms that coordinate directionality in “in-vivo” models such as sprouting angiogenesis in mouse retinal cells or tracheal branching in drosophila, it was found that in a migrating epithelium, leader-follower arrangement is also dynamically regulated via DII4 signaling through Notch-1; Leader cells display high DII4 levels, which acts upon the neighboring cells to activate Notch-1 in the later, Notch-1 in turn inhibits DII4 thereby preventing lamellipodia formation in followers. This information transmission from leader-to-follower takes place mechanically by cell-cell pulling forces; increasing mechanical stresses inhibits DII4 expression and leader cell formation while decreasing mechanical stresses dramatically increase the number of DII4 expressing cells and the number of leader cells¹¹⁴. Through different signaling pathways, several other studies also confirm that mechanism of information transfer between leader and followers is mediated via junctional sensing mediated by mechanical forces^{113, 115}. With these studies, it seemed certain that guidance mechanisms in collective migration is regulated in some way by a combined

influence of extrinsic cues, cell-cell signalling and local mechanical forces, the underlying physical picture that link biochemical events to physical forces remained unclear. Recent developments in force measuring techniques such as traction force and monolayer stress microscopy allowed us to map the cellular forces underlying migrating epithelial monolayer, and revealed many interesting, at the same time contradictory aspects of leader cell mediated guidance mechanisms^{87, 116}.

1.8 Visualizing cellular forces

In the context of cell adhesion and migration, the forces that are generated within the actin cytoskeleton are transmitted through integrin-based focal adhesions as traction forces onto the extracellular matrix (Figure 12a); these forces are essential for the cellular response to environmental cues during migration such as matrix stiffness, spatial distribution of ligands, contact inhibition etc. Forces that cells exert onto the underlying substrate were first visualized as visible wrinkles on a deformable silicone rubber substrate¹¹⁷. Since then several approaches have been used to measure cellular tractions forces.

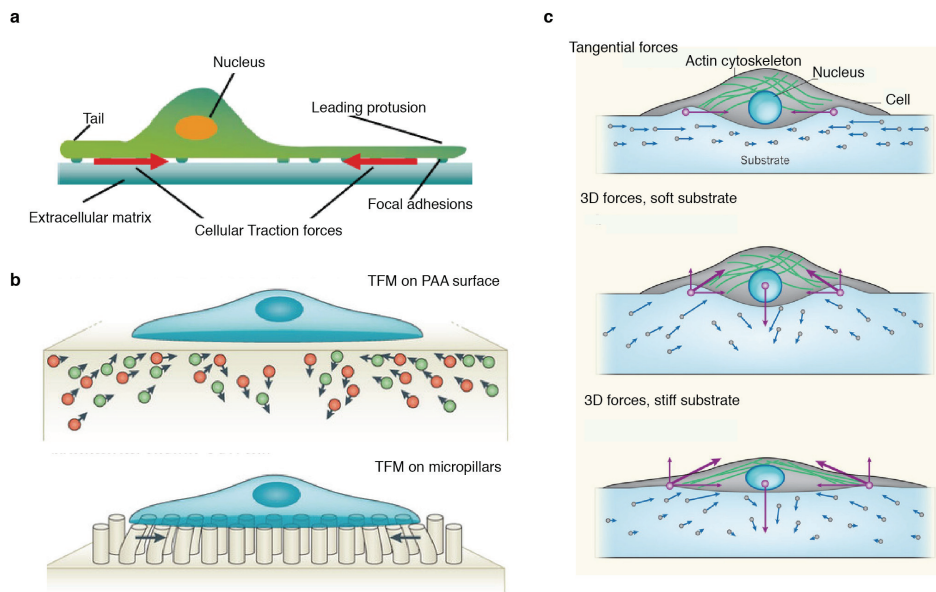


Figure 12. Traction force microscopy. (a) A cartoon showing cellular tractions due to adhesions and protrusion formation¹¹⁸. (b) Different strategies employed to measure cellular tractions, using beads incorporated in a soft PAA gel substrate or using PDMS micropillars¹¹⁹. Cell tractions can be calculated from displacement fields of beads or micropillars obtained by subtracting relaxed state positions from corresponding positions during migration. (c) 3D traction force microscopy¹²⁰.

In general, these force measurements techniques rely on measuring the displacement of a calibrated material when subjected to the force of interest. In the context of cell-matrix tractions, the standard experimental approach in the last two decades have been the use of soft elastic substrate, into which

calibrated fluorescent marker beads can be incorporated. Depending upon the elastic properties of the substrate, it can be deformed by the cells while they migrate thereby displacing the beads within, then by applying linear elastic theory, the displacements of these beads can be used to estimate traction force patterns^{118, 121, 122}. A slightly different approach is to use PDMS micropillars onto which cells are allowed to grow. Cells deflect the pillars while they move and by calculations similar to the previous, deflection of pillars can be used to get the traction force pattern of the cells^{119, 123} (Figure 12b). Although, measurements of cellular traction forces have led to a greater understanding of the processes that regulate cell-substrate interactions from molecular to multicellular level^{116, 124, 125}, these measurements only computed horizontal forces and assumed that component of forces perpendicular to the surface is negligible. However, migrating *Dictyostelium* cells on soft gel substrate showed that vertical forces in this case were of similar order as the tangential ones and therefore cannot be completely ignored. Newer 3D traction force techniques are therefore more precise since they also incorporate the z-force component by taking a 3D profile of the beads and tracking displacements of the beads in all directions¹²⁶ (Figure 12c). Mapping traction forces in a migrating epithelia revealed that traction forces in the monolayer are strongly heterogeneous and fluctuate both in space and time¹¹⁶. This heterogeneity in traction force was termed as dynamic heterogeneity, which mean that traction forces fluctuate dynamically and cannot be tied to any cell or region or time. Further, these fluctuations are governed by anomalous distribution implying that force hotspots occur with a high frequency region to region (Figure 13).

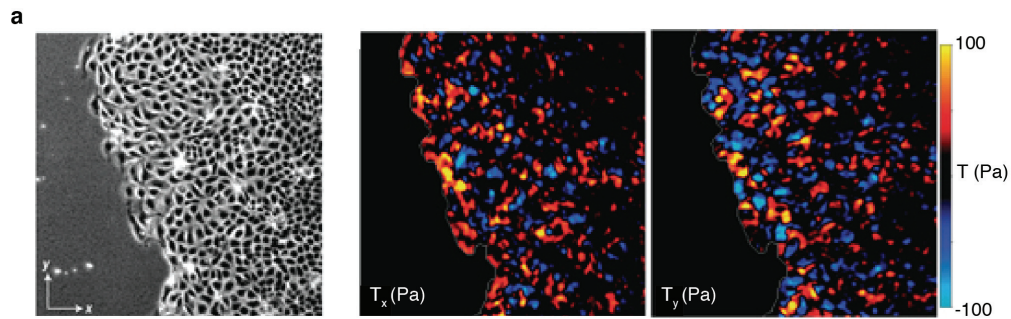


Figure 13. Traction forces in migrating epithelia¹¹⁶. Showing dynamic heterogeneity in cellular tractions in a migrating epithelial monolayer (*left*) i.e. traction forces fluctuate frequently in space and time and cells even several rows behind the leading edge can exhibit hot spots of high traction stresses (*middle and right panel* showing T_x and T_y respectively)

Maps of cellular traction forces in a migrating epithelial monolayer proclaimed conflicting physical pictures in the context of mechanisms that regulate collective guidance. For example, leader cells were shown to exhibit traction forces of high magnitude and are therefore known as the drivers that drag the monolayer along⁸⁷. Indeed, other observations support this idea, and suggest that leader cells display structural and biochemical differences from others, which are consistent with a role for pulling. For

instance, they produce prominent actin rich lamellipodial protrusions⁵⁵, which are supported by strong cellular adhesions¹²⁷ and display cytoskeletal polarity¹²⁸ (Figure 14). However, it was later argued that importance of leader cells might be overestimated and the high magnitude spots of traction forces observed in leaders are only a result of dynamic heterogeneity i.e. those hot spots are not limited there but extend to several rows behind the leading edge¹¹⁶ (Figure 13). This was supported by other morphological studies showing cells located many cells behind the leader extend cryptic lamellipodia¹²⁹. A completely different picture indicates that leading edge is not at all dragging the followers along but is being pushed by them. Each of these alternative and mutually exclusive physical pictures correspond to competing schools of thoughts, leaving the question, “how does the random traction fluctuations lead to cooperative cellular movement at defined length scales” unresolved.

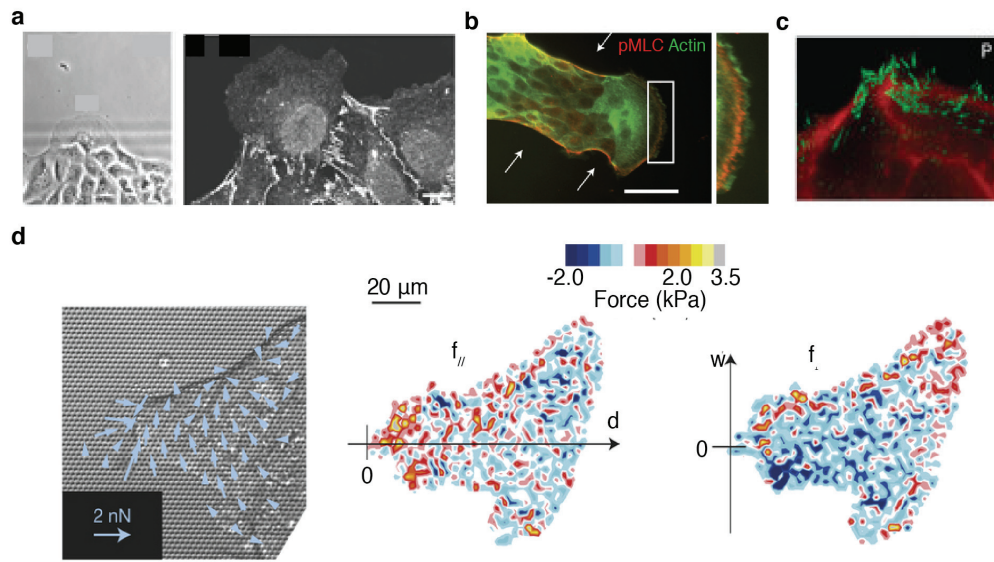


Figure 14. Leader cells in epithelial wound healing. (a) Representative phase contrast image showing leader cells with large lamellipodia appearing at the tips of migrating cellular outgrowths¹³⁰. (b) Immunostaining images showing actin filaments in lamellipodia. Follower cells are characterized by a thin actin cable that prevents them to form membrane protrusions⁸⁷. (c) Focal adhesions in the leader cells pointing in the direction of migration¹²⁷. (d) Traction forces from leading edge to the back show high traction forces in the leader cells⁸⁷

It was clear that in order to get a comprehensive view of cooperation at the level of cellular forces, knowledge of traction forces is not enough and mapping forces that cells exert on their adjacent neighbors is highly relevant¹³¹.

Monolayer stress microscopy

Defining comprehensively, the forces at work in a moving epithelia requires knowledge not only of the forces that cells exert on their substrate but also of the forces that they exert on their neighbors.

Measurement of forces at the cell-cell boundaries is termed as Monolayer stress microscopy (MSM). MSM starts with measuring the traction forces at the cell-substrate interface of a monolayer cell sheet and then uses a straightforward two-dimensional balance of forces to obtain the distribution of physical forces at every point within the monolayer.

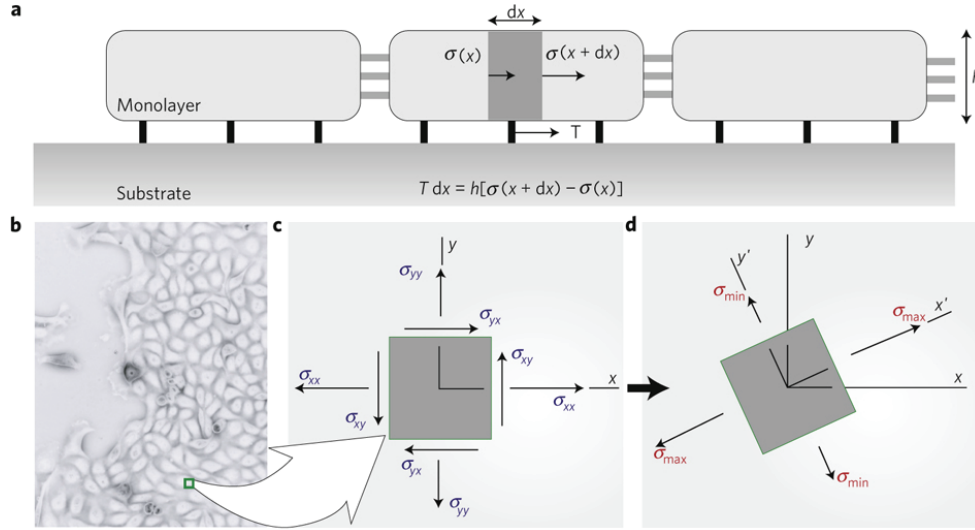


Figure 15. Monolayer stress microscopy. Sketch explaining the basic principle underlying monolayer stress microscopy (a) Monolayer of height h and length L where $L \gg h$ exert traction force (T) on the substrate. From Newton's law, Traction force at every point in the monolayer must be balanced by the corresponding stress at that point. (b) Representative image of a migrating epithelial monolayer where (c) stress at each point can be resolved into two components: normal stresses and shear stresses. (d) At each point, stress element can be rotated to an angle θ where shear stress vanishes and the normal stresses become principal normal stress (σ_{\max} and σ_{\min}). Stress ellipses drawn at the orientations of principal normal stress defines stress anisotropy at that point.

For calculus convenience, the technique works on a few assumptions. First, it assumes that the monolayer is thin and flat i.e. $L \gg h$; Second, vertical traction force components is negligible i.e. $T_z = 0$; third, monolayer is homogeneous and elastic i.e. two independent elastic constants, young's modulus (E) and Poisson ration (ν) are sufficient to describe the material properties of the monolayer and fourth, the region of interest is restricted to the optical field of view, and the entire monolayer is a repeatable unit of that region. Then as demanded by Newton's law, the traction forces applied by cells onto the substrate must be balanced by the forces that they exert on their neighbors, mechanical line forces were calculated everywhere in the monolayer. These line forces (force per unit length) were then converted to stresses (force per unit area) by using the average monolayer height, $h^{1/2}$ (Figure 15). Just like maps of traction forces beneath the cell sheet, the distribution of local normal stresses ($\bar{\sigma} = (\sigma_{\max} + \sigma_{\min}) / 2$) in migrating epithelial monolayer was also found to be severely heterogeneous both in space and time.

Mechanical stresses within a monolayer define a rugged stress landscape where normal stresses were found to be mostly tensile (positive) with values exceeding upto 300 Pa, these regions of high stresses alternate with regions of weak compressive (negative) stresses (Figure 16a).

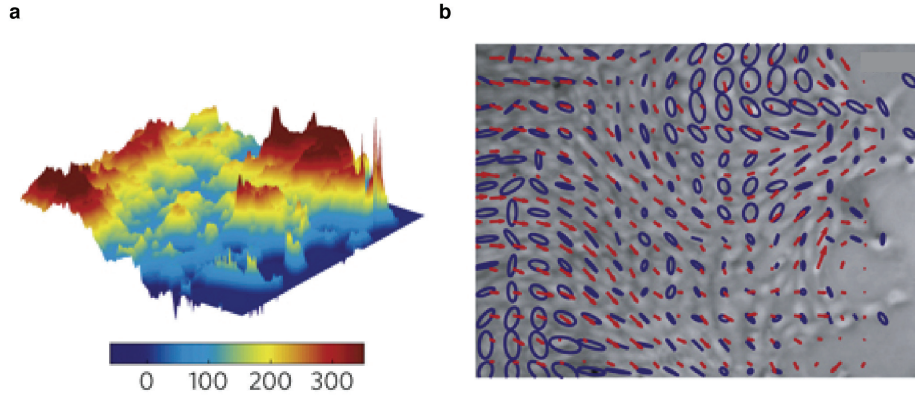


Figure 16. Stress maps in epithelial cells¹²⁴. (a) Representative stress profile in migrating epithelial monolayer showing a rugged stress landscape with peaks and basins extending upto multiple cell diameters. (b) Stress ellipses drawn over a phase contrast image of epithelial monolayer showing stress anisotropy. Ellipse size, shape and orientation vary from region to region in the monolayer but exhibit strong local correlations.

However, because intercellular stresses are essentially a spatial integral of underlying traction forces, the length scale of these fluctuations is longer and span tens of cells in area, also the time scale of these fluctuations are slower than the fluctuations of traction forces. Similar to the normal stresses, the distribution of local maximal shear stress was also characterized by a rugged landscape that evolves with time as the monolayer advances. Finally, the dependence of local stresses on orientation signifies stress anisotropy. To visualize this stress anisotropy, cell plane was rotated to find the orientations along which the local normal stress is maximum (σ_{max}) and minimum (σ_{min}) and shear stress (μ) is zero. The angle of rotation at each point is computed by the equation $(\sigma_{XX} - \sigma_{YY}) \tan 2\theta = 0$. Stress ellipses can then be drawn at these orientations where shear stress vanishes and normal stresses become principal normal stresses (σ_{max} and σ_{min}) (Figure 15). The eccentricity of the stress ellipses defines the preferred stress orientations. It was found that in epithelial monolayer, ellipse size, ellipse shape and ellipse orientation varied extensively from region to region, but with strong local correlations^{124, 131, 132} (Figure 16b).

It was also demonstrated that within this anisotropic stress field, there exist a strong tendency for epithelial cells to migrate preferentially along the orientation of local maximal principal stress. This preference however no longer exists if cell-cell junctions are disrupted; implying cell-cell junctions are remodeled actively so as to minimize shear stress. Moreover, correlation between orientation of maximal principal stress and cellular velocity is more in the regions where stress anisotropy is strongest. This collective tendency of cells to steer along the orientation of maximum principal stress is called

plithotaxis^{124, 131}. These findings therefore indicate, that mode of guidance is not a particular property of any one cell but is rather an emergent phenomenon of a collective system.

1.9 Prevalant notions and blind spots

Although the role of leader cells in collective epithelial guidance is debated and has not been shown explicitly, one cannot ignore their consistent appearance at the tips of migrating cellular outgrowths. These leaders are distinguished from the followers by their large forward protruding lamellipodia¹³⁰, their cytoskeletal polarity^{55, 127, 130}, and by the high traction forces that they exert⁸⁷. Further, it has been shown that an actin cable at the margin, regulated by myosin-mediated contractility, prevents the non-leader marginal cells to develop leader cell like properties and perturbation of this actin cable by laser locally increases cellular tractions and generate new leaders at the breaking points⁸⁷. Such photo-thermal ablation experiments were also performed to demonstrate the importance of leader cells by killing them, in such case, a dramatic decrease in the speed of the collective was observed and new leaders quickly emerged to rescue collectivity¹¹⁴. Owing to the importance, and the morphological and biophysical characteristics that leader cells possess, it is well accepted that leaders, if not globally, at least locally provide the directional guidance to the collective. Despite the importance of leaders cells during wound healing and other physiological relevant events, the biophysical and molecular mechanism(s) underlying the formation and regulation of leader cells remains poorly understood.

Prevalent view in the field of collective epithelial migration assumes a hierarchical leader-follower organization and deems the selection of leader to be an interfacial phenomena¹³³. This notion, however, stands on inadequate experimental evidences since most of the studies till now have focussed on properties of leader cells hours or even days after they were formed and the biophysical events before the selection of leader cells have never been captured. Further, previous investigations on collective cell migration shaping animal development have aptly highlighted the importance of distinct temporal phases that enable efficient collective guidance during oogenesis and during formation of zebrafist lateral line^{40, 134, 47}. However, the temporal evolution of the dynamics of epithelial cells during wound healing remains elusive. During the epithelial wound closure, remarkably only a fraction of cells in the wound margin, develop the leader cell like properties in the beginning, which then migrate at the tips of cellular outgrowths. These multicellular outgrowths, are known to be behaving as mechanical global entities or super-cells with single cell like force distribution⁸⁷. Given these facts, it is then natural to ask: How these super-cells evolve as the migrating front advances? Does the fraction of leader cells at the margin, remain constant as the migration progresses? What kind of characteristic difference do leaders and non-leaders show in their movements? Does that exhibit time dependence? In essence, despite our comprehensive knowledge of the morphological and kinematic qualities of the leader and non-leader

cells at the wound margin, we know very little about **how the leader cells are selected** and **how the dynamics of leader and non-leader cells evolve with time**, as the wound heals. In the following chapters, we would take help of the various microscopic and force measurement techniques to draw a time resolved biophysical cartography of epithelial wound healing in an attempt to address the aforementioned questions.

2. At the onset of migration: selection of leaders

2.1 Preamble

To understand the mechanisms underlying selection of leader cells in an epithelial wound margin, we attempted to go back in time and exploited force measurement and other biophysical techniques to examine the physical features of the monolayer much before the leaders actually emerged. We mimicked the process of re-epithelialization by using a well-established model wound assay that requires growing confluent monolayer of epithelial cells within confined areas and then, lifting off the confinement to trigger collective migration instead of actually injuring the tissue^{55, 113}. This method not only uncoupled migration from cell damage and/or cell permeabilization but also provided a smooth interface, which removed any geometrical interfacial bias. Interestingly, we found out that long before the leaders actually start displaying their phenotypic peculiarities, the followers behind them manifest stochastic augmentations in the traction forces and monolayer stresses and display large perimeter-to-area ratios, indicating a local unjamming³⁵. In fact, it is also possible to spatially bias the leader cell formation by introducing unjammed followers in the back. Furthermore, the length scale of dynamic fluctuations of cooperative forces within the monolayer corresponds very well with the separation distance between adjacent leader cells and this mechano-biological control of leader-cell formation also remains preserved in the presence interfacial bias provided by geometrical shape, or by physiological levels of chemical cues. These findings indicate the importance of collective dynamics and demonstrate how dynamic heterogeneity of cooperative forces in the bulk monolayer determines the fate of cells at the wound margin. Together, these results provide a novel system-insight into the process of leader cell selection during epithelial wound healing and challenge the hitherto believed notion, that assumed a hierarchal leader-follower selection and ignored the role of follower cell. Furthermore, this system view raises analogy to the process of selection of leaders in animal groups where shared decision making by followers determines the selection of leaders.

2.2 Unjamming in followers precede leader cell formation

We first hypothesized that formation of leader cells require preparatory structural rearrangement at the wound margin or within the monolayer. To test this hypothesis we examined the biophysical features exhibited by the cells within the monolayer much before the leaders were selected. Owing to the mechano-biological integrity of cytoskeletal elements at the multicellular levels, any structural changes in the monolayer would lead to changes in cell-matrix adhesions and hence would produce detectable

variations in the cell-matrix traction stresses. Therefore, elucidating cell matrix traction stress landscape with traction force microscopy would enable us to identify any zone going through high structural reorganization. To this end, we prepared soft polyacrylamide gel substrates containing fluorescent beads. We coated the gel with extracellular matrix protein fibronectin, and cultured Madin-Darby canine kidney (MDCK) epithelial cells within horizontally confined areas created by thin PDMS blocks on the gel (Figure 33c). When the cells attained confluency, we released the PDMS confinement, thereby providing a free matrix surface, and an unbiased monolayer interface for collective cell migration. Subsequently, we obtained time-lapse phase contrast images (for cells) and fluorescence images (for beads) during the migration. After two hours of migration, we trypsinized the cells and acquired the corresponding bead image in the relaxed state. We then used particle image velocimetry (PIV) analysis between two consecutive images to obtain the velocity fields and determined how far the cells correlate their motions by computing the correlation length of the lateral velocity component. Correlation length was determined as the point where the respective correlation function, $C(r)$, when expressed with the distance, r , became negligible in value (Figure 17a, *top*).

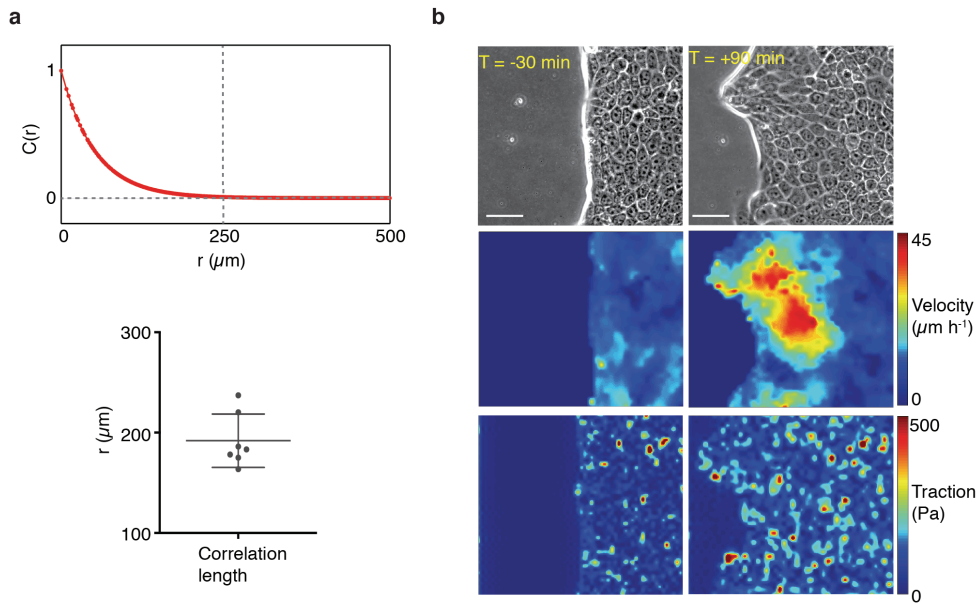


Figure 17. Physical parameters of epithelial monolayer. (a) Average velocity correlation length. Representative correlation function, $C(r)$, of average velocity as a function of the distance, r , for a migrating epithelial monolayer (*top* panel). Scattered dot plot showing statistical distribution of velocity correlation length averaged over 7 independent experiments. Line represents mean and error bars represent standard deviation. (b) Representative phase contrast images (*top*) immediately ($T = -30$ min, *left* panel) and two hours ($T = +90$ min, *right* panel) after confinement release, corresponding velocity (*middle*) and traction stress maps (*bottom*) showing very little or no migratory activity but adequate traction stresses in the followers immediately after confinement removal. Scale bars, 50 μm .

For a migrating epithelial monolayer, the average velocity correlation length was found to be around 180 μm (Figure 17a, *bottom*). Further, from the displacement of the beads at each time point, we obtained maps of cellular tractions. Interestingly, much before the cells exhibited any signs of noticeable migration (Figure 17b, *left panel*), we observed local increase in the cell-matrix traction forces (Figure 17b, *bottom left*). Here $T = 0$ is the time point when leader cell appear, and $T = -30$ represent the time point immediately after releasing the confinement.

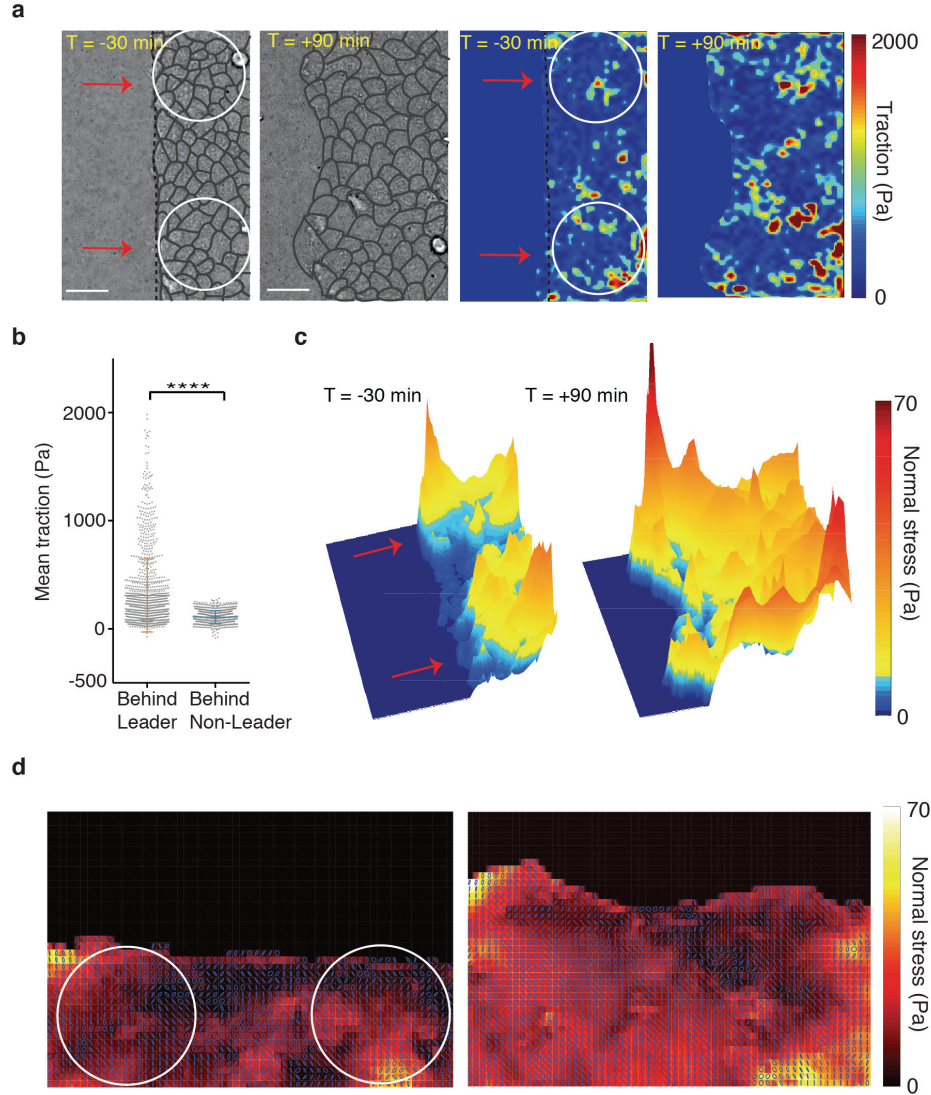


Figure 18. Elevated traction forces and monolayer stresses in the followers. (a) Representative phase contrast images with highlighted boundaries, corresponding traction force profiles and (c) corresponding landscape of average normal stress of the migrating collective at designated time points, $T = -30$ min and $T = +90$ min. Here $T = 0$ is the time point where leader cell appear. (b) Scattered dot plot showing statistical distribution of traction stresses in regions behind leader and non-leader cells respectively. Lines display mean and error bars represent standard deviation. Regions considered for calculating the distribution of traction stress are defined by velocity correlation length of cells. Scale bars, 50 μm .

We further noticed that the increased traction forces right after confinement removal were consistently more prevalent in the cells behind the future leaders (Figure 18a). For statistical analysis, we defined the region of computation by drawing a circle of diameter equal to the average velocity correlation length at that time point, and plotted the cellular tractions in the regions behind the future leaders and the non-leaders respectively. We found that, right after the confinement was removed, the augmentation in traction forces were more frequent in the followers within 2-6 cell layers behind the prospective leader cells than any other randomly chosen location of similar layer depth parallel to the wound margin (Figure 18b). Further, we applied a force balance algorithm to calculate average monolayer stresses from the corresponding cellular tractions. The monolayer stress maps revealed that the zones behind the future leaders also developed elevated tensile stresses (Figure 18c) and displayed high stress anisotropy much before the visible phenotype of leader cell developed (Figure 18d). Then, in order to examine the possible inference of the local increase in cellular tractions and tensile stresses on leader cell formation, we investigated microscopic structural traits of individual cells including cell shape and aspect ratio. It has been previously shown that, a confluent epithelial monolayer can exist in two distinct structural states: jammed (solid like) and unjammed (fluid like)¹³⁶. In the jammed or solid state, cells exhibit low velocities, move in large packs and rarely exchange neighbors; whereas in the unjammed or fluid like state, cells may display large movements or rearrangements and can also exchange neighbors¹³⁵. Moreover, as elucidated in normal and asthmatic bronchial epithelial cells, an unjammed monolayer correspond to considerably high cell-matrix traction and cell-cell tensile stresses as compared to a jammed one¹³⁵.

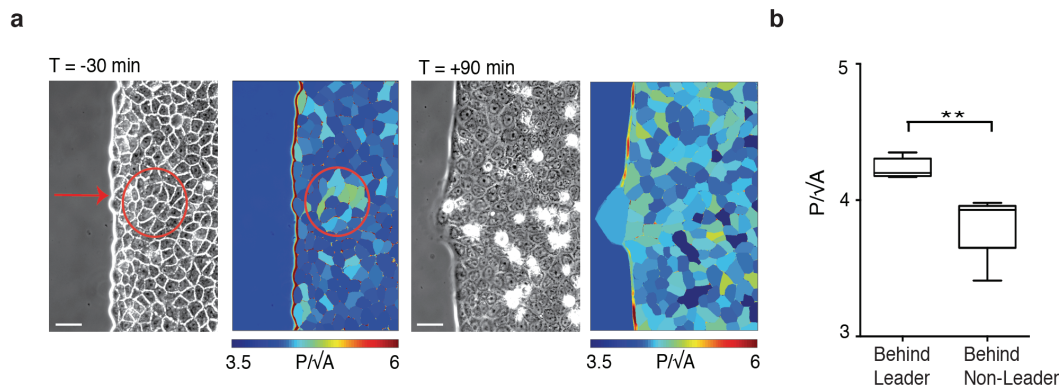


Figure 19. Local unjamming in followers precede leader cell formation. (a) Representative phase contrast images and corresponding maps of shape indices depicting cell shapes at fixed time points (T = -30 and T = +90 min). (b) Statistical distribution of shape indices in the regions behind leader and non-leader cells respectively. Box plots show median and quartiles. Whiskers are maximum and minimum data points. Regions considered for calculating the distribution of shape index are defined by velocity correlation length of cells. Scale bars, 50 μ m.

Taking this cue and the observed high tractions behind the perspective leaders, we explored the possibility of local unjamming within a pre-migratory monolayer. To capture the jammed or unjammed state of the monolayer, we exploited a non-dimensional shape index (p), which is computed by the ratio of cell perimeter to the square root of projected cross-sectional area ($p = P/\sqrt{A}$). Computation of shape indices of the individual cells in the monolayer revealed that follower cells behind the prospective leader cells display higher shape index than any other cells within the same depth (Figure 19a, 19b).

Taken together, these results revealed a development of augmented traction forces and tensile stresses in the followers behind the perspective leader attributed to a state of local unjamming in the pre-migratory monolayer. Since in an epithelial monolayer, the tensile stresses transmitted across the cell-cell junctions are balanced by the cell-cell adhesions, these results also implicated a local reinforcement in the adhesive stresses in the immediate followers.

2.3 Introducing fluid follower helps to stimulate leader cell formation

Next, we sought to investigate whether, the observed local increase in traction and tensile stresses, and the unjamming in the follower cells have any casual relationship with the cells ahead of them becoming the leader cells. Previous studies show that a tumour suppressor protein, merlin, supports collective cell migration by regulating the activity of Rac1 and thereby restricting the cell motility within the monolayer¹³. Furthermore, merlin knock down cells lose control over Rac1 activation, and exhibit low correlation lengths, and high lamellipodial activity¹³. Exploiting this property of merlin depletion, we knocked down merlin from the cells with a small interfering RNA (siRNA); and investigated the biophysical and morphological features of the cells. As expected, the resultant phenotype in the merlin knock-down cells (Figure 20, *top panel*), exhibited a typical unjammed behaviour and displayed high traction forces (*middle left panel*), high tensile stresses (*middle right panel*), and high shape indices (*right panel*), as compared to the control cells (Figure 20, *bottom panel*, Figure 21a). Taking advantage of unjammed property of merlin depleted cells; we then mixed fluorescently labelled merlin depleted cells with unlabelled wild-type cells in 1:10 ratio. Subsequently, we cultured the cells in confined areas using ibidi cell culture inserts until a confluent monolayer was obtained and then lifted off the confinement in order to trigger collective migration (Figure 33a). We then determined the probability of the emergence of a leader cell in front of any merlin depleted cell groups. The statistics took account of only those cases where the 2-6 layers behind the wound margin contained at-least two merlin-depleted cells but excluded any merlin depleted leader cells. For the control case, a scrambled siRNA replaced merlin siRNA while other conditions remained unchanged. Consequently, the results revealed that the presence of relatively unjammed merlin depleted cells within the diameter that span the average correlation length behind the edge, increases the probability of marginal cells in front of them to become leader cells (Figure 21c).

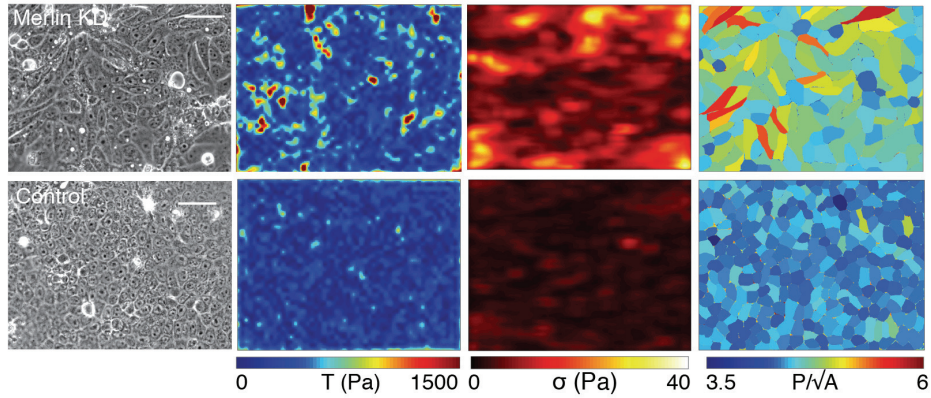


Figure 20. Merlin depleted cells exhibit unjammed state: Representative phase contrast images of merlin depleted (*top panel*) and wild-type (*bottom panel*) cells, corresponding traction stress landscapes, average normal stress landscapes and maps of cellular shape indices showing a state of high fluidity or unjamming in merlin depleted cells as compared to the control.

To further confirm this conclusion, we used an optogenic technique involving a photo-excitable form of RhoA (Cry2-RhoA) labelled with red fluorescent protein (mCherry) to transiently increase the cellular traction stresses¹³⁷.

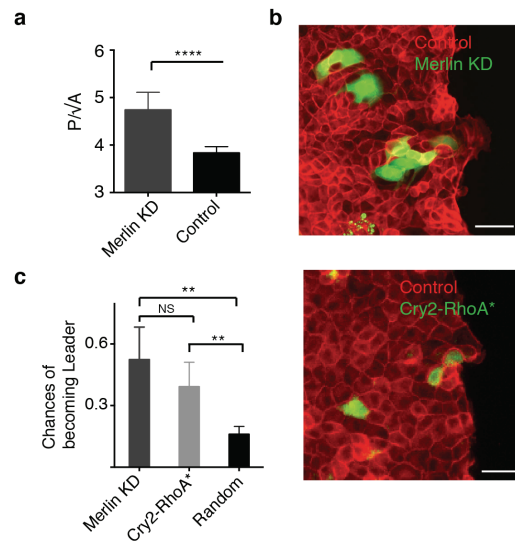


Figure 21. Introducing unjammed followers help to stimulate leader cell formation. (a) Bar graphs showing statistical distribution of shape indices from merlin depleted and control cells. **(b)** Merlin depleted cells were transfected with Lifeact-TagGFP2 plasmid (green) and co-cultured with wild-type MDCK cells (*top panel*). Wild type MDCK cells were transfected with photo-excitable Cry2-RhoA (*bottom panel*). Representative images show formation of leader cells triggered by unjammed followers behind them. Cells were fixed at $T = +90$ min and stained for actin (red). **(c)** Bar graphs showing statistical distribution of chances of leader cell formation in front of merlin depleted, Cry2-RhoA transfected and random follower. Scale bars, 50 μm . NS: not significant, $**P < 0.01$, student's T-test.

Upon excitation with blue light, Cry2-RhoA formed small aggregates, which increased the contractility and hence cellular tractions. Taking this cue, we transiently transfected MDCK cells with Cry2-RhoA plasmid by a forward transfection method using Lipofectamine. Owing to the low transfection efficiency of lipofectamine-mediated transfection (10%) in MDCK cells, we obtained small groups of cells in the monolayer, which were transfected with the plasmid. Subsequently, cells were imaged while being irradiated with a 400 μ s pulse of blue light at 40 seconds interval for 45 minutes. The irradiation did not cause any visible damage. Cells were then fixed and the probability of emergence of leaders in front of any Cry2-RhoA transfected cell was determined. Similar to the merlin depleted unjammed cells; we observed that within the diameter that spanned the average correlation length behind the margin, presence of Cry2-RhoA containing cells in the following layers also biased the leader cell formation in front of them (Figure 21c).

These results together revealed that local development of contractile stresses and unjamming in the followers stimulates the leader cell formation during collective migration of epithelial cells. While, previous reports suggest that a geometry based cue such as local variation of curvature at the monolayer interface is sufficient to trigger leader cell formation, and the effect scales up with the magnitude of the curvature; these results show that the factors influencing leader cell formation are much more complex than just interfacial bias and also consist of non-interfacial bulk components involving cells behind the leader. However, whether or not the collective mechanical dynamics in the cell monolayer, is able to compete with interfacial bias for the selection of leader cells remained unclear.

2.4 Collective dynamics overrides interfacial bias

A homogeneous epithelial monolayer, exhibit a rugged stress landscape which is characterized by stochastic appearance of peaks and basins, extending over several cell diameter (Figure 22a). This landscape also evolves with time describing a dynamic heterogeneity within the monolayer. Since the emergence of leader cells was preceded by appearance of high stress zones behind them, we assumed that the separation between adjacent leaders (Figure 22b) should closely match the separation between adjacent peaks (Figure 22a). As expected, the peak-to-peak separation distance in the stress landscapes correlated very well with the leader-to-leader separation distance (Figure 22c). This also validates back our hypothesis that mechano-biological stochasticity in the bulk monolayer determines the emergence of leader cells at the interface.

The next question we asked was; to what extent the contribution from collective dynamics can prevail when the monolayer interface is perturbed to bias the formation of leader cells? Previous studies showed that, monolayers containing beak-like interfacial shape exhibited high tractions at the beaks and formation of leader cells was always biased at these regions¹⁹⁸. Taking this cue, we generated monolayers

with curved beak-shaped regions using an adapted soft lithography based patterning technique³⁹. Black transparencies containing holes of desired shapes were used as masks to engrave about 50 μm thick positive reliefs of a negative photoresist onto silicon wafers when illuminated with UV light. Polydimethylsiloxane (PDMS) was pressed against the wafers at 65°C for 100 min to produce holes of the desired pattern in a thin PDMS membrane (Figure 34).

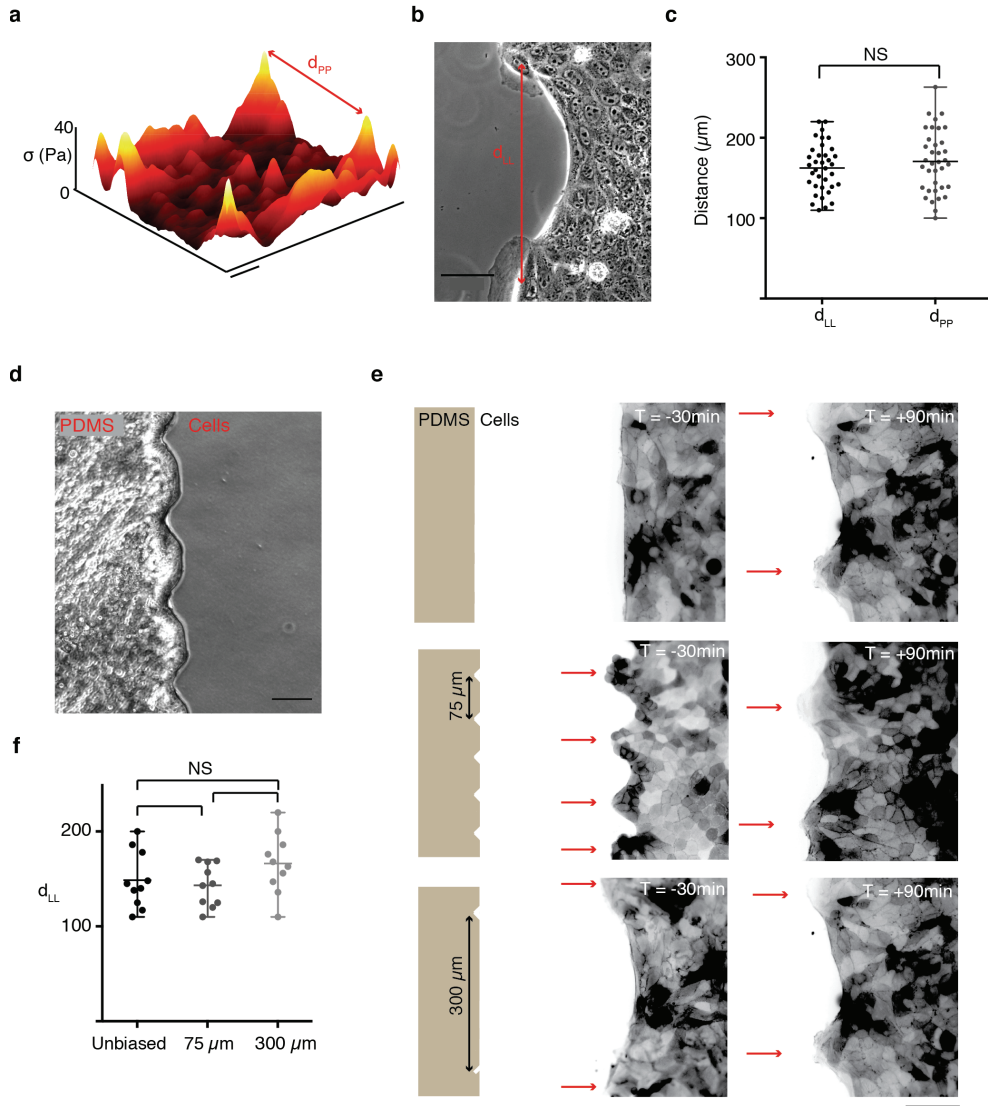


Figure 22. Collective dynamics overrides the interfacial geometric bias. (a) Characteristic landscape of average normal stress as measured in bulk monolayer, d_{PP} depicts peak-to-peak separation distance. (b) Representative phase contrast image of MDCK cells at $T = +90$ min where d_{LL} mark leader-to-leader separation distance. (c) Statistical distribution of d_{LL} and d_{PP} showing peak-to-peak and leader-to-leader separation distances. (d) Phase contrast image of a PDMS micro-stencil, demonstrating beak shape interfacial patterns to bias leader cell formation. (e) Representative images of migrating Lifeact-MDCK cells right after ($T = -30$ min) and two hours after ($T = +90$ min) confinement removal. (f) Statistical distribution of d_{LL} two hours after confinement removal ($T = +90$ min) for different micro-patterned and un-patterned (unbiased) monolayer. Scatter dot plots display maximum and minimum range as error bars. Scale bars, 50 μm .

MDCK cells were then seeded into these PDMS microstencils, which confine the cells in defined patterns in order to obtain monolayers with several beaks distributed at the interface (Figure 22d, 22e). By varying the spacing between two consecutive beaks, we controlled the length scale of interfacial bias in such a way that the beaks are either very close (75 μm separation distance) or farther apart (300 μm separation distance) from each other. The confinement was released after the confluent monolayer is formed and the cell migration was analyzed for two hours. If the interfacial bias were solely able to form leader cells at the beak-shaped curvatures, we would see leader cells appearing and sustaining at every beak-point in the patterned monolayers after two hours. On the contrary, we observed that in both cases, in spite of the interfacial bias, the final distribution of leader cell separation appeared to be very similar to that in the un-patterned monolayer (d_{LL} for unpatterned: $162 \pm 30.2 \mu\text{m}$; 75 μm pattern: $143 \pm 22.3 \mu\text{m}$; 300 μm pattern: $166.2 \pm 31.8 \mu\text{m}$, Figure 22e, 22f).

Together, these results established the importance of cellular dynamics within the epithelial monolayer in regulating the emergence of leader cells and demonstrated that the mechanical integrity of the cells can even over-ride any geometrical bias provided at the monolayer interface.

2.5 Effect of chemotactic signalling on collective dynamics

In *vivo*, the major driving factor for collective cell migration during wound healing is the release of chemo attractants such as growth factors and cytokines. Since the cells at the wound margin contain more free basolateral surfaces than the cells inside the monolayer, the chemical cues that are released during the process predominately affects the marginal cells imparting chemical perturbations to the interface. Consequently, we investigated the relative influence of this chemotactic signalling on leader cell formation and whether or not the afore-elucidated mechanobiological control overpowers the chemical cues. To this end, we designed a spot assay system where we generated a chemical gradient by entrapping growth factor (EGF) inside an agarose gel (Figure 23a). Previous studies showed that depending upon the concentration of chemoattractant trapped in the gel, the cells experience a relative gradient, which is a function of both distance and time. Steepness of this gradient depends on the concentration of chemo-attractant, the binding constant K_d of the chemoattractant-receptor bond, and on the diffusion coefficients of chemoattractant¹⁴⁰. Since all these parameters of EGF spot assay are well characterized¹⁴⁰, we simulated the spatiotemporal distribution of varying EGF concentrations to obtain the relevant concentrations required to perform the chemotaxis experiment. In general, eukaryotic cells require at least 1% relative chemoattractant gradient for the chemotactic migration¹⁴⁰. Respectively, the simulation results showed that, before the initiation of cell migration, the relative gradient remained much higher (5-10%) than the critical threshold. Further, the results also revealed that within the time frame of migration, on average, the marginal cells experienced approximately one-tenth of the loading

concentration (Figure 23b). Taking this cue, we prepared EGF loaded agarose gels (1.3 mm in radius) and kept them at a distance, 0.5 mm away from the monolayer edge (Figure 23a).

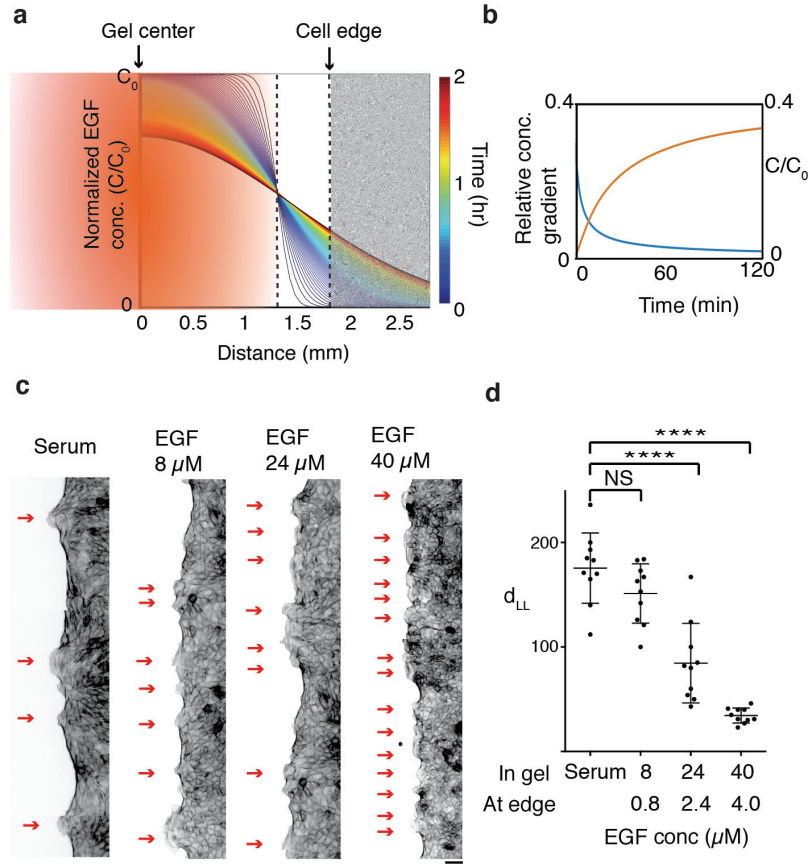


Figure 23. Effect of chemotactic signalling on collective dynamics. (a) Graphical representation of the experimental scheme showing how EGF diffuses out off the gel as a function of distance (x-axis) and time (colorbar). Gel center is at $x = 0$, radius of gel is approximately 1.3 mm and the gel is placed 0.5 mm away from the monolayer edge. (b) Relative concentration gradient (left y-axis) and normalized concentration of EGF (right y-axis) as a function of time. (c) Fixed images of cell monolayer at $T = +90$ min when presented to agarose gel containing 8 μ M and 24 μ M as compared to normal conditions (serum containing media) show different leader-cell separation distance at higher concentrations of EGF in the gel. (d) Statistical distribution of leader-cell separation distance in monolayers experiencing different concentrations of EGF at the edge as compared to control (5% serum containing cell culture medium where EGF is present in nM range). Lines represent mean and error bars represent standard deviation. Scale bars, 50 μ m. Data collected from atleast three independent experiments

We varied EGF concentrations in the gel (8, 24 and 40 μ M) to probe the effect of chemical gradient on leader cell formation. Interestingly, though presence of EGF in itself did not cause any significant change in the monolayer stress landscape in terms of peak-to-peak separation distance (Figure 24), increasing EGF concentration significantly decreased leader-to-leader separation distance. At higher concentrations of EGF (24 or 40 μ M), almost all the marginal cells presented to the gel protrude

lamellipodia (Figure 23c, 23d). Although, It is important to note that even at 8 μM EGF loading concentration, which correspond to an average of 0.8 μM EGF at the wound margin, and is already hundred to thousand times higher than the physiological relevant concentration for epithelial wound healing^{141, 142}, we observed only slight changes in the distribution of leader-to-leader separation (Figure 23c, 23d).

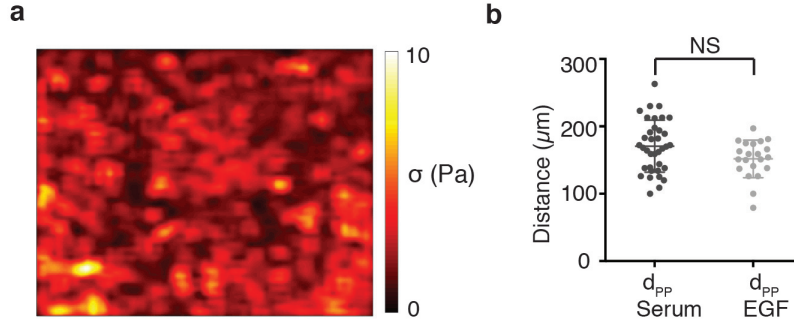


Figure 24. Effect of bulk EGF on monolayer stress profile. (a) Average normal stress map of a monolayer treated with 2.4 μM EGF in bulk solution showing stress profile similar to that of the control (Figure 2a). 2.4 μM is average concentration of EGF that the cells at monolayer edge experience when the gel is loaded with 24 μM EGF. **(b)** Dot plots showing statistical distribution of peak-to-peak separation distance (d_{pp}) in serum treated (medium containing 5% serum) and 2.4 μM EGF treated monolayers. Line represents mean and error bars represent standard deviation. NS: not significant.

These results indicate that extremely high chemical cues are required to overpower the mechanical integrity of the cells. In other words, similar to imposing interfacial cue, these findings clearly demonstrate the importance of non-interfacial mechano-biological control of leader cell formation over any imposed chemical cue. While relative concentration gradient of chemical attractants should provide the cue to directional guidance, the evolution of wound margin is ultimately governed by the inherent fluctuations of forces within the monolayer.

2.6 Outlook

Together, these results revealed a hitherto unknown mechanism underlying the emergence of leader cells during epithelial wound healing. The results demonstrate that selection of leader cells is largely governed by the collective dynamics of inner follower cells and the separation between the two leaders is determined by the length scale of this collective dynamics, also termed as dynamic heterogeneity, which is an inherent system property. Owing to the non-interfacial and mechano-biological nature of the process; this mechanism is fundamentally distinct from the previously accepted biochemical perspective of interfacial regulation of leader cell selection. Further, these results imply that, the collective

mechanical dynamics and, the ability of cells to join forces up-to a certain length scale might also influence events, even after the leaders are selected. How do the physical forces that underlie cellular cooperativity evolve with time? And how does this mechanical integrity of the system influence regulation of leader cells at the wound margin as the wound heals? In the following chapter, we would discuss the role of time-dependent phases in regulating efficient wound closure and study, how these phases are controlled at the level of cellular forces. We would further go on to understand the evolution of kinematic and biophysical properties of cells located at the wound margin.

3. Dynamic temporal phases during epithelial wound healing

3.1 Preamble

Effective wound closure requires coordinated migration of epithelial cells on top of the wound bed. While smaller wounds can be sealed through contraction-mediated purse-string like closure, healing of larger wounds requires active migration of surrounding cells mediated by cell crawling. Of special significance, in this context, are the active leader cells, which are present at the tips of cellular outgrowths that consist of non-leader marginal cells and passive follower cells. These leader cells exhibit morphological and biophysical features, which are consistent with their well-accepted role in collective guidance. In the previous chapter, we demonstrated how collective dynamics play crucial role in the selection of leader cells. These findings intrigued us to investigate how the aforementioned physical collectivity evolves with time as the wound heals, especially in the context of marginal leader and non-leader cells. To this end, we studied collective migration of epithelial monolayer using the similar scratch free wound-healing assay used before. We then tracked the temporal evolution of the leading edge and acquired diverse kinematic, mechanobiological, and structural information associated with marginal cells- both leaders and non-leaders- in a time dependent manner. With the help of biophysical techniques such as particle image velocimetry (PIV), traction force microscopy, monolayer stress microscopy, and reflection interference contrast microscopy, we uniquely characterized distinct temporal phases of cells located at the epithelial wound margin. The study reveals two distinct temporal phases of cellular dynamics at wound margin. Initially, the fraction of leader cells among the marginal cells remains unchanged while number of follower cells per leader increases with time (Phase 1). As the migration progresses, however, the leader cell fraction starts increasing while the latter settles to a steady level, set by the length-scale of cell-cell force transmission (Phase 2). Furthermore, orientation of the focal adhesion points and the persistence of cellular motions also display this phase-specific behaviour. Any perturbations in mechanical forces that modifies the force correlation lengths and upset the collective dynamics, invariably enforces a change in the number of followers per leader thereby modifying the time required to transit from one phase to the other. Collectively, these results uncover a unique time-dependent feature of the epithelial wound healing process and indicate the role of collective mechanical dynamics in regulating the interactions between leader, non-leader and the followers during healing.

3.2 Two distinct phases of cellular dynamics at wound margin

To study the spatiotemporal dynamics of epithelial wound healing, we mimicked the process of reepithelialization by using a well-established model wound assay that requires growing confluent monolayer of epithelial cells within confined areas and then lifting off the confinement to trigger collective migration instead of actually injuring the tissue^{55, 113} (Figure). We then monitored the expansion of monolayer in both space and time by using time-lapse phase contrast imaging where $T = 0$ is the time point right after removing the confinement. Approximately 30-45 minutes after the confinement release, leader cells with prominent lamellipodial protrusions emerged at the wound margin and as the migration progressed these leader cells occupied positions at the tips of migrating cohorts. With apparent hierarchy, the evolving outgrowth contained three distinct types of cells: a leader, the marginal followers (or non-leaders), and the bulk followers (Figure 25).

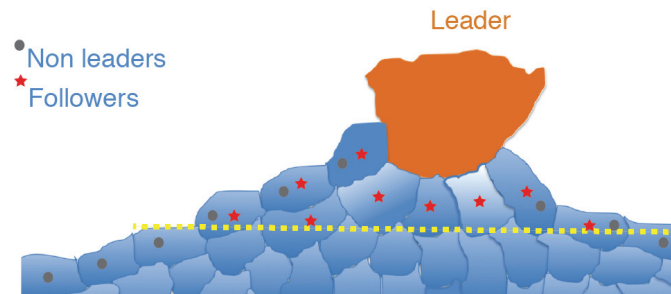


Figure 25: Cartographic representation of a typical cellular outgrowth consisting of a leader cell at the tip followed by marginal followers (non-leader) and bulk followers

Importantly, as mapped by PIV, the leader cells exhibited high instantaneous speeds than the non-leader follower as well as the bulk follower cells within the outgrowth (Figure 26a). Next, to determine the temporal dynamics of leader cell generation, ratio of leader cells to the total number of marginal cells was computed at defined time points. This ratio, also defined as the propensity of leader cell formation revealed a very interesting biphasic behavior in terms of emergence of leader cells (Figure 26b). During the first phase, which lasted for about three hours after migration initiation, the fraction of leader cells among the marginal cells remained constant. However, as soon as the monolayer entered phase-2, leader cell propensity started to gradually increase with time (Figure 26b). In addition to the quantitative difference demonstrated by the propensity of leader cells, the two phases were also distinct in qualitative cellular dynamics. In the first phase, each outgrowth comprised of one leader cell exclusively while the size of outgrowth increased with time (Figure 26a, *top panels* and Figure 26c). On the contrary, in the second phase, immediately after the transition point, new leaders started emerging besides the already existing ones (Figure 26a, *bottom panels*, Figure 26c) while the outgrowths continued to expand. Interestingly, the newly emerged leaders also showed high speed comparable to the initial leaders

(Figure 26a, *bottom panels*). Subsequently, counting the number of followers per leader within each outgrowth revealed another interesting trend. For a typical outgrowth, this quantity approached a stable value with time, getting offset by a fraction as a new leader emerged (Figure 26d).

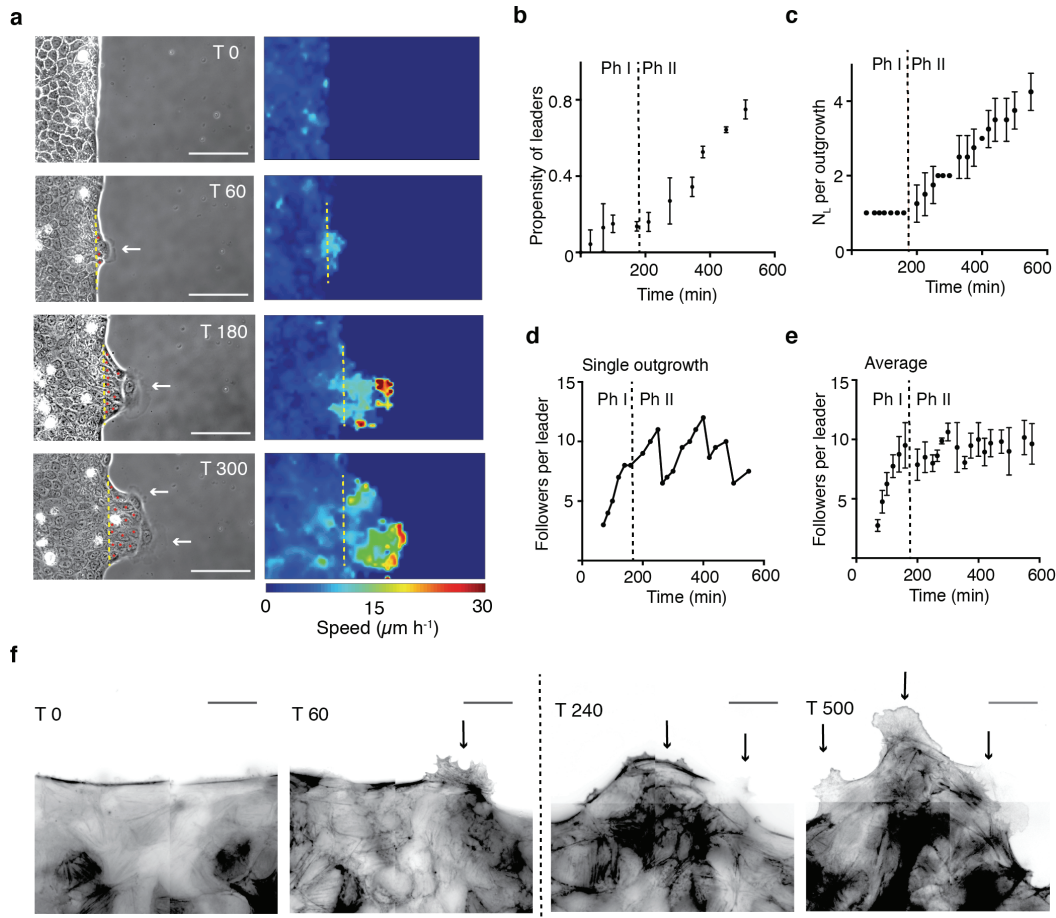


Figure 26. Distinct temporal phases of cellular dynamics at wound margin. (a) Representative phase contrast images (*left*) and velocity maps (*right*) of the migrating collective at four different time points (0, 60, 180 and 300 minutes) after the confinement removal. Arrows indicate the leaders while star mark the follower cells. Yellow lines demarcate the outgrowth boundary. Scale bars, 100 μm. (b) Changes in propensity of leaders with time reveals two dynamic phases, namely phase-I (Ph I) and phase-2 (Ph 2). (c) Number of leader cells (N_L) per outgrowth shows similar behavior as propensity. (d) Typical temporal variation in a single outgrowth and (e) statistical distribution of all the outgrowths, of the number of followers per leader. Statistically this quantity increases in phase-I but becomes stable in phase-2. (f) Emergence of new leaders with time as depicted by the staining of actin filaments. Arrows indicate leader cells. Scale bars, 25 μm.

On average, however, the resultant quantity, which is average number of followers per leader steadily increased in Phase-I but settled to a steady level in Phase-2 (Figure 26e). These results therefore, uniquely described a previously unknown feature of the temporal control of leader cell formation in the wound margin, in which the number of follower cells gradually increased to a target level, which then

become stable and nearly time invariant. Together, these results implied a systemic control of leader-follower interaction during collective migration analogous to the dynamic temporal phases observed during collective migration of *Drosophila* border cells⁴⁹ thereby indicating a broader applicability of the highlighted observations in collective migration of cells in general.

3.3 Mechanobiological control of leader-follower ratio

Leader cells formed during epithelial wound closure are known to generate high traction as well as cell-cell pulling forces mediated by actomyosin contractility⁸⁷. This force polarization then through the cell-cell junctions perturbs the cell behaviour deep within the monolayer, thereby influencing the movement of non-leaders and the immediate follower cells. The force landscape as determined by the monolayer stress microscopy presented a rugged landscape featuring many peaks and basins that extended over multiple cell diameters¹²⁴. This feature indicated the emergence of collective force transmission to a distance much larger than the individual cell diameter, this distance can be obtained by the characteristic length scale of the spatial autocorrelation function of the average normal stresses and is termed as the force correlation length¹⁴³ (Figure 27b).

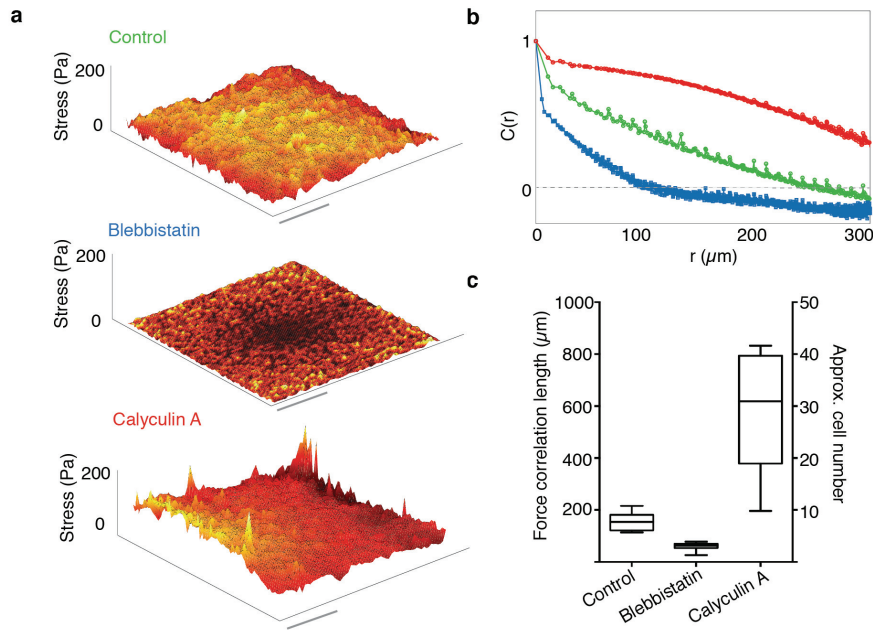


Figure 27. Perturbation of contractile forces modifies length scale of force transmission (a) Representative landscapes of average normal stress from control (top), blebbistatin-treated (middle) and calyculin A treated (bottom) collectives as measured in bulk. Scale bars, 200 μm . (b) Representative correlation function, $C(r)$, of the average normal stress as a function of distance, r , for control (green), blebbistatin (blue) and calyculin A (red)-treated collectives. (c) Force correlation length in terms of cell number from control, blebbistatin, and calyculin A-treated samples. In a box plot, central mark is the median, and the edges of the box are the 1st and 3rd quartiles.

Extending this notion further, this length also represent the average number of cells that can collectively integrate the forces through cell-cell junctions thereby giving rise to the observed ruggedness in the stress landscape (Figure 27a, *top panel*). Remarkably, the mean value of this length scale, when divided by the average cell diameter (20 μm) and thus expressed in terms of the number of cells, becomes identical to the steady level of average number of followers per leader (approximately 9 followers per leader, Figure 23c). This leader-follower ratio also represents the maximum allowable follower cells that can be recruited in a single outgrowth without requiring the emergence of additional leader and thus specifies the transition between Phase-1 and Phase-2 thereby indicating that the force correlation length might determine the average follower per leader in a migrating outgrowth.

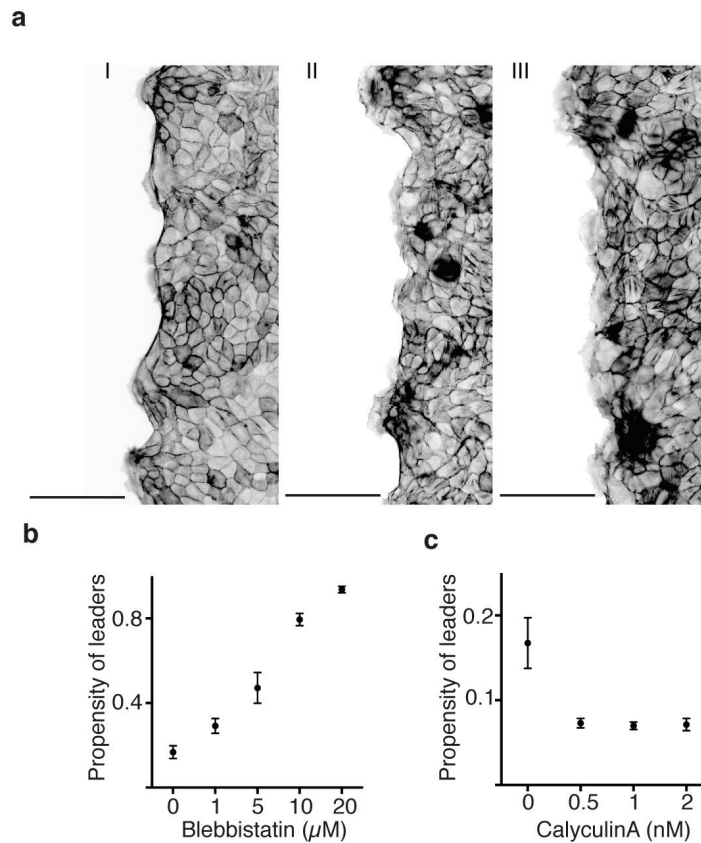


Figure 28. Propensity of leader cells upon modifications of cellular forces. (a) Representative images of collectives treated with varying concentrations of blebbistatin demonstrating increasing propensity of leader cells upon increasing drug concentrations. (b) and (c) Statistical distribution of propensity of leaders in collectives treated with increasing concentrations of blebbistatin and calyculin A

To test this hypothesis, we exploited the widely used pharmacological means of controlling the actomyosin contractility by treating the cells with drugs that perturb or enhance contractile forces in an attempt to tune force correlation length of the cells. For that, we treated the cells with non-muscle myosin-II inhibitor, blebbistatin, or a myosin-light chain phosphatase inhibitor, calyculin-A.

Blebbistatin reduced the contractile forces while calyculin-A increased it¹⁴⁴. As showed by previous studies, treatment of cells with high concentrations of blebbistatin reduced cellular contractility to an extent where all the cells produce lamellipodial protrusions and display leader-like characteristics¹⁴⁴. Conversely, treatment of cells with high concentrations of calyculin-A increased cellular contractility to an extent where cells can no longer maintain cell-cell junctions and start extruding out of the monolayer. To this end, We treated the cells with varying concentrations of these force modifying drugs and adjusted the drug concentration to a point where effect would be perceivable yet we would have measurable traction forces in case of blebbistatin and negligible cell extrusion in case of calyculin A treatment (Figure 28). As expected, blebbistatin treatment enhanced the ruggedness of the stress landscape (Figure 27a, *middle panel*) and lowered the force correlation length (Figure 27c) while calyculin treatment regularized the stress landscape (Figure 27a, *bottom panel*) and increased the force correlation length (Figure 27c). In each case, the force correlation in terms of cell number (Figure 27c)) matched the corresponding average number of followers per leader cells (Figure 29b) which agrees with our hypothesis that force correlation length determines the average follower per leader.

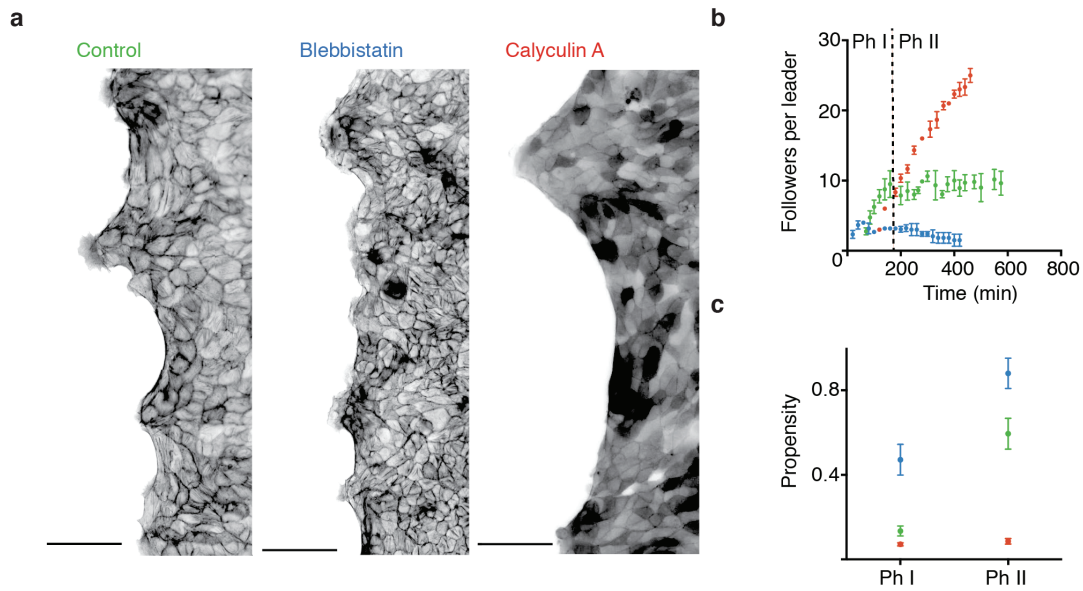


Figure 29. Force correlation length determines transition time between the two phases. (a) Representative images of control (left), blebbistatin- (middle) and calyculin A- treated collectives, as stained for actin shows different propensity of leader cells as well as different number of followers per leader cell. Scale bars, 100 μ m. **(b)** Number of followers per leader in control (green), blebbistatin (blue), and calyculin A (red)-treated collectives and **(c)** Propensity of leader cells in control (green), blebbustatin-(blue), and calyculin A (red)-treated collectives at two different time points, 120 and 300 minutes, marking phase I (Ph I) and phase 2 (Ph 2), respectively.

Moreover, extrapolating this notion further, the force correlation length should also determine the time required for the collective to undergo the transition between Ph-1 and Ph-2, which was indeed observed in our experiments. Blebbistatin treated cells required significantly less time and calyculin-A treated

cells required more time to transit from Ph-1 to Ph-2 as compared to the control case (Figure 29b). As expected, we also observed changes in propensity of leader cells in response to change in acto-myosin contractility i.e. blebbistatin and calyculin-A treated monolayers showed higher and lower propensity of leader cells, respectively, at the margin, than the control (Figure 29a, 29c).

Together, these results confirmed mechanobiological regulation of temporal phases of leader cell generation during collective migration of epithelial cells in wound closure. Single leader cells could sustain the extension of the outgrowth as long as the follower cell number remained lower than the typical range of stress propagation. However, crossing this limit promptly compelled emergence of new leaders in order to maintain the mechanical integrity of the outgrowth.

3.4 Time-dependent reorientations of focal adhesions at the leading edge

Effective cell migration crucially depends on the cellular ability to assemble and disassemble focal adhesions onto the underlying substrate. These focal adhesions function to transmit the forces generated within the actin cytoskeleton as traction forces on the matrix. For mechanical force mediated regulation of cell migration, precise control of these focal adhesion complexes in terms of their assembly, disassembly, size, shape and orientation is required¹⁴⁵⁻¹⁴⁸.

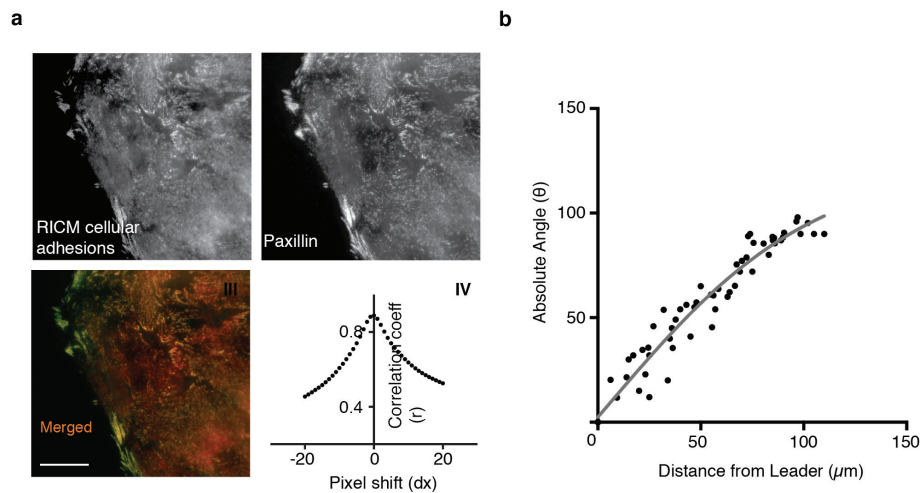


Figure 30. Detection of focal adhesions by RICM. (a) Representative phase contrast images showing overlap between RICM detected adhesion points (depicted in inverted color, *top left*) and paxillin (*top right*) localization. Scale bars, 25µm. Pearson correlation coefficient between two detection methods plotted as a function of pixel shift demonstrating excellent overlap. (b) Orientation of focal adhesion points along the wound margin with respect to average migration direction as a function of distance from the nearest leader cells shows focal adhesion points of non-leader cells pointing towards the nearest leader.

In this context, we attempted to study dynamic features of cellular adhesions with time. By conventional means, such a study would require stable expression of a fluorescent protein-tagged focal adhesion

protein such as paxillin or vinculin in all the cells. However, this manipulation might perturb the system and the inherent genetic noise would cause local variability in the expression level, further distorting the traction field. To avoid the effect of genetic modifications, we used a non-invasive optical technique called reflection interference contrast microscopy^{149, 150}, which present cell-substrate adhesion points as dark spots.

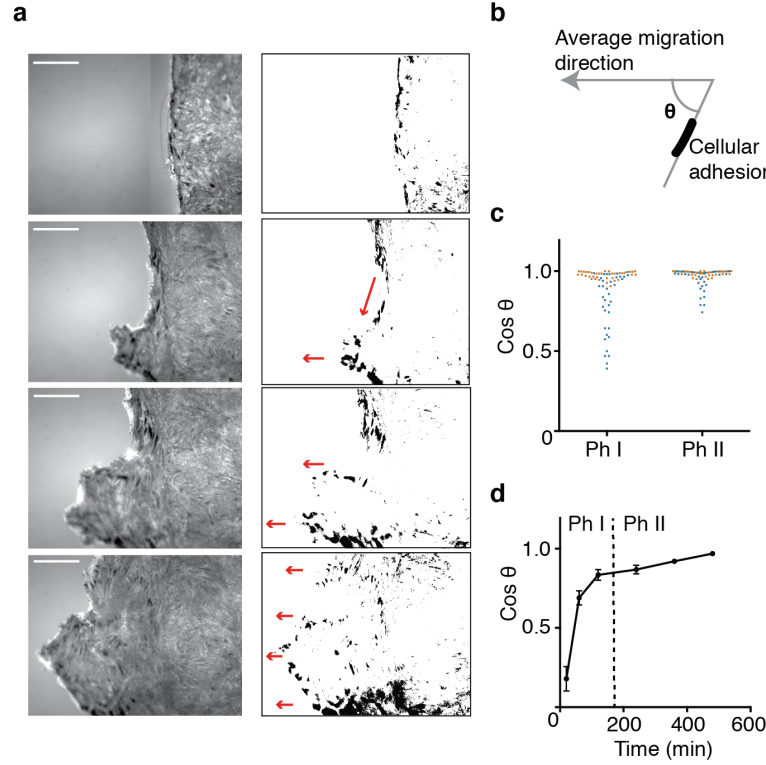


Figure 31. Orientation of focal adhesions in marginal cells. (a) Representative RICM images (left) and cell-substrate adhesion points after thresholding and background subtraction (Right) at four different time points (0, 60, 280 and 400 minutes) after the confinement removal. Scale bars, 20um (b) Orientation of cell-substrate adhesion points in marginal cells shown as the angle between the direction of migration and adhesion points. (c) Distribution of the orientation, as given as Cosine of angle, for leader (orange dots) and non-leader (blue dots) cells at two different time points, 120 and 300 minutes, marking phase 1 and 2 respectively. (d) Time evolution of average orientation of adhesion points accounting for all the marginal cells.

Monochromatic, polarized light was used to visualize the interference pattern of unstained live MDCK cells on a planer glass surface coated with fibronectin. The image consists of the interference pattern of light reflected from the surface of the glass and the interface of cells. Due to negative interference at the points of close contacts the cellular adhesions appeared darker than the background intensity. The average value of background intensity (I_b) and standard deviation (σ) was determined and all areas of at least 4×4 pixels with an intensity less than $(I_b - \sigma/2)$ were defined as adhesion points. To validate the fidelity of the RICM-based detection of focal adhesion points, marginal cells were fixed and stained with paxillin, an important component of focal adhesion complexes. Paxillin displayed excellent

correspondence and high correlation with RICM cellular adhesions (Figure 30). Next, on analysing the relative orientation of focal adhesions with respect to the migration direction of monolayer at any point of time (Figure 31b), we observed two important trends. First, the focal adhesions of the leader cells displayed a high bias in orientation towards the migration direction and this remained consistent in both the phases (Figure 31a, 31c). On the contrary, the remaining non-leader cells had their focal adhesions inclined towards the nearest leader (Figure 31a, *middle panel*) and hence, the relative angle showed much broader distribution as compared to the leader cells (Figure 31c). However, in the second phase, as propensity of leader cells increases, this distribution became narrower (Figure 31c) with average angular orientation of focal adhesions in marginal cells orienting towards the direction of migration (Figure 31d). Taken together, these results further elaborated the significance of dynamic temporal phases during wound healing and revealed an important time dependent distinction between the orientations of focal adhesions in the cells at the wound margin in the two phases.

3.5 Phase-dependent kinematic distinction between leader and non-leader cells

During the process of collective migration, forces operating through cell-cell junctions and focal adhesions ultimately functions to provide coordinated cellular movements. Although collective cell movements have been studied and modelled in past^{87, 114, 151}, how their movements evolve with time remains unknown. We therefore, looked into the kinematic distinction between leader and non-leader cells at the margin. We distinguished the leader cells from non-leaders by the broken actin belt and their forward protruding lamellipodia. To study the temporal evolution of kinematic parameters of the marginal cells, we individually marked and tracked the cells at the margin and followed their movements starting from the confinement removal ($T = 0$) until the wound is healed (Figure 32a). From the individual cell tracks, we obtained x,y coordinates at each time point, which we then used to compute individual cell speed and directional persistence of motion. For a given cell track, at a given instant of time, directional persistence is defined as the ratio of end-to-end distance and total accumulated distance of the track (Figure 32c). Remarkably, leader cells always acquired a higher speed than the non-leader cells (Figure 32b). Interestingly, non-leaders in phase-1 who would become leaders in the phase-2, migrated faster than the non-leaders which did not undergo this transition (Figure 32b). Considering that the former did not express any leader-like characteristics in phase-1, these results appeared very non-intuitive and suggested that the newly emerged leaders in phase-2 had already been primed in phase-1. Further, the difference in speed between leaders and non-leaders decreases in phase-2. Similarly, the leader cells always moved with higher directional persistence, than the non-leaders and this difference also decreases in phase-2 (Figure 32c).

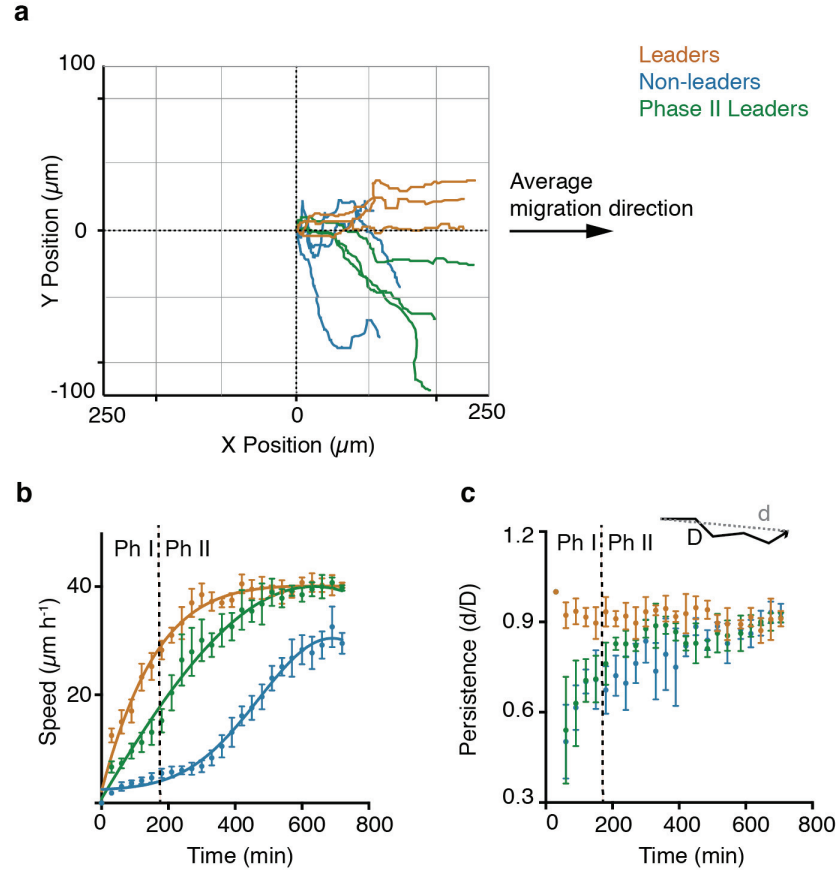


Figure 32. Time dependent kinematic differences among the marginal cells. Representative tracks of leaders (orange), non-leaders (blue), and phase-2 leader (green) cells over 10 hours after the confinement removal. Temporal variation in (b) instantaneous speed and (c) persistence of leaders (orange), non-leaders (blue), and phase-2 leader (green) cells. Persistence is ratio between the end-to-end displacement and the total distance migrated.

3.6 Outlook

Together, these results reveal existence of dynamic temporal phases during wound healing, and distinct mechanobiological and kinematic behaviours of leader and non-leader cells in each phase. Once the leaders are selected, they migrate at the tips of the cellular outgrowths that contain cells, which follow them. These cellular outgrowths behave as mechanical global entities and collective dynamics regulate the mechanics of the outgrowth. During Phase-I, the number of leader cells remain steady while the outgrowth continue to expand thereby recruiting more number of followers within. This goes on until a transition point (Phase-2) where another leader cell appear besides the existing one in the same outgrowth. This phenomena is controlled by the mechanical dynamics or the force correlation length, i.e. a single leader cell is able to sustain the extension of the outgrowth as long as the number of followers remain lower than the number of cells that cooperate to join forces together. Furthermore, the orientations of focal adhesions and kinematics of marginal cells also display this phase specific

behaviour. These results demonstrate how cellular level cooperativity is important in efficient wound healing mediated by cell crawling. While, these studies clearly draw the biophysical parameters that are of critical importance in controlling guidance mechanisms during wound healing, how this process is controlled at the bio-molecular level is still not clear.

4. Concluding remarks

The healing ability of epithelial tissue plays an important role in maintaining integrity of the organs. In this context, effective wound healing requires collective and cooperative migration of underlying cells to cover the denuded area. Depending upon the size and the shape of the wound, the mechanisms that regulate closure can be purse-string like i.e. mediated by the contraction of actomyosin cable that spans the wound edge, or can be active crawling like i.e. mediated by formation of large cellular outgrowths guided by leader cells. While purse string like closure usually operates in very small wounds; In this work, we focussed our attention on more common, larger wounds, that are mainly closed by the later mechanism, which involves crawling of several cells in outgrowths, guided by leader cells at the tips. We mimicked re-epithelialization by designing a custom-made, scratch-free wound-healing assay that uncoupled migration from other parameters such as cell damage and/or cell permeabilization. We then performed time-lapse studies and followed the entire process of healing. With the help of various microscopy and force measurement techniques, we obtained biophysical cartography of the monolayer during different time points in order to explain fundamentally relevant, yet unresolved riddles in wound healing such as, the mechanism(s) behind selection of leader cells and the temporal evolution of the wound margin.

Due to lack of experimental evidences, the mechanism underlying collective guidance in wound healing was in fact, misunderstood. The leaders were assumed to be selected autonomously, where geometry of the interface played critical role in biasing leader cell formation. In this study, we challenged this prevalent notion of leader-follower hierarchy and studied biophysical events in the monolayer much before the leaders were selected and until the wound is healed. We found out that efficient wound healing requires orchestration of cellular forces, from the very beginning, and that selection of leaders require local unjamming and pile up of cellular stresses in the followers right behind the prospective leader cells (Figure 18, Figure 19). This local increase in physical forces is a result of dynamic heterogeneity of the monolayer and the length scale of this dynamic heterogeneity determines the distance between the emerging leaders. We then competed the collective dynamics with interfacial bias by changing geometry of the interface in such a way that if interfacial bias were stronger than collective dynamics, the leaders would emerge much closer or much farther than the length scale of dynamic heterogeneity of the system. On the contrary, and as predicted, we observed that cellular dynamics overrode the interfacial bias and the distance between the two leaders closely matched the length scale of dynamic heterogeneity in both cases (Figure 22). Since most of the migration events in vivo are triggered by chemical cues sensed by the cells at the interface, we then placed a strong chemical gradient in front of the monolayer to determine if the collective dynamics can compete with increasing

relative steepness of the gradient. Interestingly, the distribution of leader cells at the margin did not change even in the presence of strong chemical gradient of EGF ($0.8 \mu\text{M}$ as sensed by the cells while the physiological concentrations of EGF is in the range of nanomolar). Only when the chemical gradient increased upto $2.4 \mu\text{M}$, we saw a change in the leader cell spacing (Figure 23). These findings confirmed that collective mechanical dynamics of inner follower cells is responsible for the selection of leader cells at the wound margin.

Next, we asked how does this collective dynamics influence events, after the leaders are selected? i.e. how do the physical forces that underlie cellular cooperativity regulate cells at the margin as the wound heals? And how does the cellular outgrowths, which are previously known to behave as independent mechanical global entities⁸⁷, evolve with time? In this context, we obtained time-lapse phase contrast images of the monolayer during the entire process of wound closure and then computed various physical parameters such as velocity profile, propensity of marginal leader cells, speed and persistence of migration, and dynamics of cellular adhesions. Interestingly, these results uncovered a unique time specific, biphasic behaviour of the cells at the wound margin. Furthermore, these temporal phases are regulated by the mechanical dynamics or the force correlation length of the cells and can be modified by modifying the length scale of force cooperativity.

During Phase-1, the propensity of leader cells remains steady, while the outgrowth continues to expand, hence recruiting more number of followers within i.e. the number of followers per leader increases in this phase. This goes on until a transition point (Phase-2) where another leader cell appear besides the existing one in the same outgrowth and hence the propensity of marginal leader cells starts to increase. Interestingly in this phase, the number of followers per leader settled to a steady level (Figure 26). Monolayer stress microscopy, together with pharmacological perturbation of the actomyosin contractility revealed that this level was remarkably identical to the typical number of cells that could join forces together, enabling long-ranged correlated force transmission (Figure 27, Figure 28). More importantly, the observation that a new leader emerges immediately after the number of followers per leader exceeds the mechanobiologically fixed threshold, indicates a mechanical integrity of the outgrowth as a super-cell, not only in terms of directionally consistent multicellular force polarization but also with respect to a presumably bidirectional systemic interaction between leader and follower cells.

Furthermore, the elucidated mechanical integrity of the outgrowths offer further plausible explanations for many previous observations such as emergence of a new leader cell after the ablation of an existing one and the existence of a typical length scale of auto-regulatory mechanism¹¹⁴. Our results also confirm many previously untested predictions of various theoretical endeavours that looked into the dynamics of the wound edge from the perspective of instability¹⁵¹. Both our experimental results and previous modelling suggest that the migration length scale at which new leaders emerge must depend on

the length scale of force transmission, and in higher force correlation length, it would take longer for the leaders to appear at the tips of cellular outgrowths¹⁵¹. However, none of the previous theories have predicted the priming of non-leader cells, which would become leaders in phase-2, as observed in our experiments. The non-leaders, which would undergo such a transition, displayed higher velocity and persistence as compared to the ones that did not (Figure 32). These temporal phases further raise analogy with the mode of collective guidance observed in, *in-vivo* studies such as during collective migration of *Drosophila* border cells, where two dynamically distinct phases of leader cell formation enable efficient information processing¹⁵².

Together, these findings provide a novel system insight into collective cell migration and indicate the importance of integrative cellular interactions during epithelial wound closure.

5. To be continued...

Although, our findings provide a comprehensive biophysical picture to the mechanism underlying collective guidance during epithelial wound healing, the physical forces are only a mode of information transfer from one cell to the other and the mechanism by which cells read these physical signals are much more complex. Epithelial cells communicate with each other through cell-cell junctions and with the underlying substrate through cell-substrate adhesions, which means any changes in cell-cell or cell-matrix adhesions should lead to detectable changes in the cell migratory behaviour. Further, owing to the long-range velocity correlation, observed in the epithelial cells, it is intuitive that each cell is able to correlate its polarization and motility with that of its neighbours. For example, they should be able to coordinate, cell contractility, as well as polarized activation of Rho GTPases and other downstream effector molecules with their neighbours, in both space and time. However, the understanding behind the molecular mechanisms that help the cells to respond to the physical forces during collective migration is very fragmentary. It is not clear, for example, how, at the molecular level, cells sense and transmit the operating physical forces to the neighbours in order to precisely regulate the leader-follower arrangement and the length scale of dynamic heterogeneity.

Furthermore, various studies suggest that the mechanical microenvironment of the substrate such as stiffness, also has a direct influence on the cellular migratory behavior and the information about matrix stiffness is transmitted to the cells through coupling of contractile forces between neighboring cells¹⁵³. However, how matrix stiffness regulates the length scale of cellular cooperativity, and influences the leader cells at the wound margin remain unclear.

5.1 Molecular Mechanisms

Previous studies show the importance of cell-cell junctions in mechano-transduction during collective migration and that disrupting cellular junctions by knocking down E-cadherin significantly reduced the collectivity and direction-sensing ability in *Drosophila* border cells¹¹⁵. Further, maintenance and remodeling of cell-cell junctions critically depends on the interaction of cadherin-catenin complex with the actomyosin contractility¹¹². Notably, two pools of actin at the adheren junctions have been observed, the apical rings that also labelled myosin-2 and the cortical pools that marked the site for actin nucleation and also labelled actin polymerization machinery comprising Arp2/3 and WAVE2 complex. Interestingly, it was shown by some studies that WAVE-2-Arp2/3 is a major nucleator of actin assembly, also at adheren junctions and inhibition of either Arp2/3 or WAVE2 depleted both cortical and junctional actin pools, reduced junctional tension and compromised the ability of cells to buffer cell-cell forces^{111, 112}. Since Arp2/3-WAVE2 complex is the major driver of lamellipodial protrusions, it is tempting

to speculate that differential polarization of actin polymerizing machinery towards the front and towards the junctions is probably essential for leader cell mediated directional guidance during epithelial crawling.

In order to test this hypothesis, we first looked into the localization of WAVE2. We allowed the cells to migrate for about two hours before fixing and staining them for WAVE2. Owing to its role in Arp2/3-mediated actin polymerization machinery, WAVE2 displayed clear localization in lamellipodia of the leading cell. Interestingly, in the non-leader cells, we observed WAVE2 localization in cell-cell junctions (Figure 33a), which indicate the role of WAVE-2-Arp2/3 in maintaining junctional integrity in non-leader cells. To ascertain the role of differential WAVE2 localization in leader and non-leader cells, and to determine if WAVE2-mediated actin nucleation occurs at the junctions, we studied dynamic incorporation of G-actin at the barbed ends of actin polymers in live cells¹⁵⁴. We used saponin-mediated cell-permeabilization assay that allows small molecules such as fluorescently tagged G-actin to cross the cell membrane while the cells are still active. We found high actin dynamics at the cell-cell junctions of non-leader cells (Figure 33b, *left*) and at the lamellipodia of the leader cells (Figure 33b, *right*). Furthermore, since lamellipodia formation starts with polarized activation of RhoGTPases, such as Rac1, we used a FRET sensor to study the activation of Rac1 in leader and non-leader cells. As expected, leader cells showed high Rac1 activation as compared to the non-leaders (Figure 33c, *bottom*).

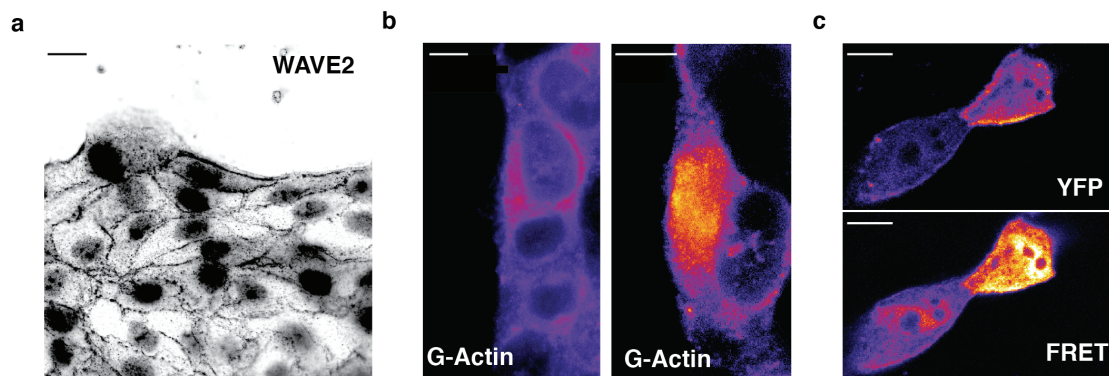


Figure 33. Molecular mechanisms involved in leader-follower organization. (a) Localization of WAVE2 in leader, non-leader and follower cells (b) Actin dynamics in non-leader (*left*) and leader (*right*) cells. (c) Rac1 activation dynamics by FRET sensor.

However, these findings does not confirm, but at least support our hypothesis that the cellular forces are transduced through differential polarization of Rac1 and actin polymerization machinery in leader and non-leader cells which finally dictate the leader-follower arrangement at the wound margin. Detailed molecular analysis by modulating each of the factors one by one with respect to the other is necessary to further validate the hypothesis.

5.2 Effect of Matrix Stiffness

Next, in order to determine the effect of matrix stiffness on the length scale of force cooperativity and hence the leader cell formation, we prepared polyacrylamide gels of varying stiffness (4 KPa, 11 KPa, 23 KPa, 35 KPa and 90 KPa), coated with 0.5 mg/ml fibronectin, and seeded cells under confined conditions, as before (Figure 35). After obtaining a confluent monolayer, the confinement was released to trigger collective cell migration. We then fixed the cells after 2 hours of migration and determined the propensity of leader cells at the wound margin.

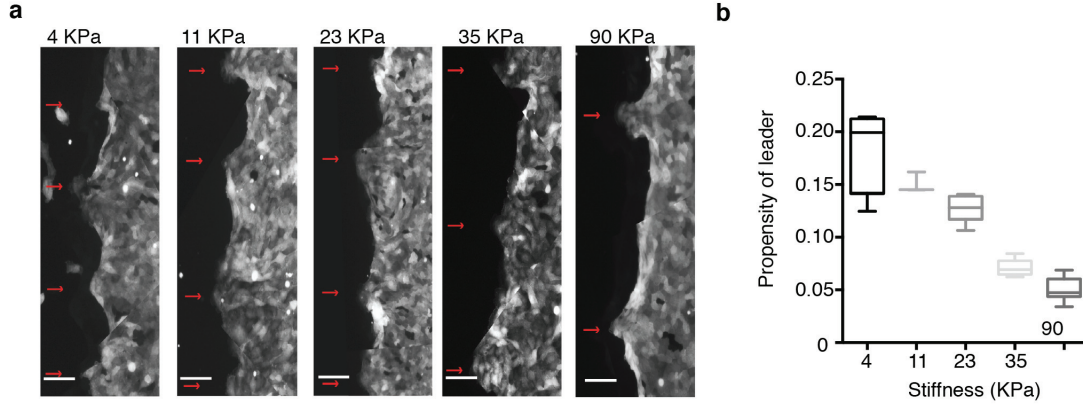


Figure 34. Effect of matrix stiffness on leader cell propensity. (a) Representative images of Life-Act MDCK cells on PAA gels of varying matrix stiffness. (b) Propensity of leader cells as a function of stiffness show decreasing number of leader cells with increasing stiffness (Performed by J.D. Russo)

Interestingly, decreasing stiffness decreased the leader cell separation distance (d_{LL}), and increasing stiffness increased the leader cell separation distance at the wound margin (Figure 34).

This implies, that with increasing matrix stiffness the length scale of force cooperation should also increase. Furthermore, the observation of similar length scale of leader cell separation distance (d_{LL}) on glass (highly stiff) and soft PAA gel substrate (11-23KPa) implies, either a different mode of cell-ECM talk, or a different mode of ECM binding, on glass and on PAA gel. These findings therefore open a multitude of questions that require thorough investigation.

6. Materials and Methods

6.1 Cell culture and migration experiments

Madin-Darby canine kidney cells (MDCKII, Health Protection Agency) were cultured in minimal essential medium (MEM, Sigma) supplemented with 2mM L-glutamine (Invitrogen), 10 U ml⁻¹ penicillin & 10 µg ml⁻¹ streptomycin (Pen Strep, Invitrogen) and 5% fetal bovine serum (FBS, Invitrogen). Cells were maintained in a standard cell-culture incubator at 37°C, 5% CO₂ environment and high humidity. Cells were passaged regularly when they reached 80-90% confluency.

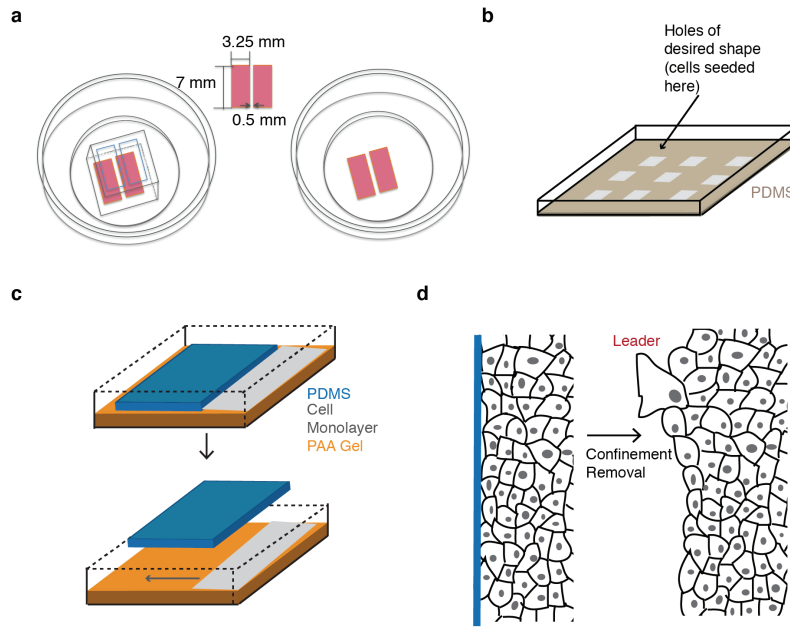


Figure 35. Collective cell migration in vitro. (a) Schematic diagram of commercially available Ibidi culture inserts for creating monolayers with unbiased interface (b) Customized PDMS micro-stencils for creating monolayers with defined patterns (c) Thin PDMS blocks for creating confined monolayers on PAA gel.

For performing collective cell migration, a confined space was created onto glass bottom dishes coated with 10 µg ml⁻¹ fibronectin using ibidi cell culture inserts (Ibidi, 80209, Figure 33a), or using custom-made PDMS micro-patterned stencils (Figure 33b). For traction force experiments, the confinement was created in a similar way onto polyacrylamide gel (PAA gel) coated with 0.5 mg ml⁻¹ fibronectin, by thin horizontal PDMS blocks (Figure 33c). Cells were then seeded into the dishes and incubated in a cell-culture incubator for 1 hour until they adhere onto the fibronectin coated substrate accessible through the holes of the micro-confinements. Any unattached cells were removed by replacing the media. The set up was incubated again overnight or until a confluent cell monolayer is obtained after which, the confinement was removed to trigger collective migration (Figure 33d)

6.2 Micro-patterning

Micro-patterning is a soft-lithography based technique that uses relief structures of photoresist as templates for a master Polydimethylsiloxane (PDMS) stamp to form desired patterns of cellular monolayers (Figure 36).

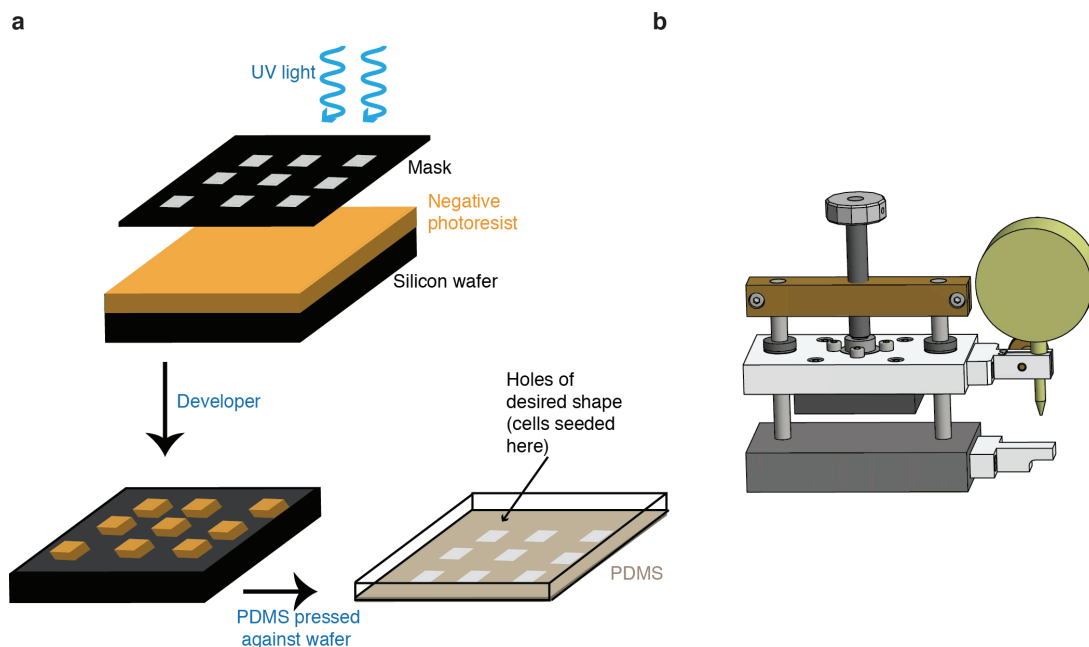


Figure 36. Production of PDMS micro-stencils. (a) Schematic representation demonstrating fabrication of patterned micro-stencils. Black transparencies containing holes of desired shapes are used as masks to engrave about 50 μm thick structures of a negative photoresist onto a silicon wafer when illuminated with UV light (top). A developer removes the unexposed photoresist from the wafer but retains the cured structures (bottom left). (b) PDMS pressed against the finished wafer in a customized mechanical press at 65°C for 100 min to produce holes of desired pattern in a thin PDMS membrane.

Step1: Creating photomasks. Desired shapes of monolayers were designed in a QCAD program (Figure 34a) and transferred on transparencies using a high-resolution printer (JD Phototools).

Step2: Preparing the template. In a clean room facility, SU-8/25 negative photoresist (MicroChem, Newton, MA, USA) was spin-coated on a 2" silicon wafer to a final thickness of about 50 μm . The wafer was then baked on a hot plate for 5 min at 65° C followed by a second baking for 15 min at 95° C. The transparencies containing, the "photographic negative" of the pattern to be transferred were used as masks to illuminate the wafer with UV light for 12 sec in Mask Aligner MBJ4 (Suess MicroTec Lithography, Munich, Germany). To remove the unexposed photoresist, wafers were immersed in SU-8 Developer mr-Dev600 (Microresist Technology, Berlin, Germany). The prepared wafers containing the desired geometric pattern were then treated with 1H,1H,2H,2H-Perfluorooctyl-trichlorosilane to reduce

surface adhesiveness.

Step3: Creating PDMS microstencils. Uncured PDMS and curing agent (10:1) were mixed well and degassed by centrifugation at 1.5 rpm for 10 minutes. A sandwich consisting of the patterned wafer, 0.5 mL of PDMS-catalyst mix, a piece of parafilm, a piece of paper and a glass slide was put into a custom made molding press to obtain uniform pressure distribution. PDMS was pressed against the wafer in a customized mechanical press (Figure 34b) at uniform pressure in order to create thin PDMS membrane containing holes of desired shapes. The assembly was put into a compartment dryer at 65°C for 100 min to allow PDMS polymerization. Subsequently, PDMS-catalyst mix was applied at the rims of the thin membrane and the set up was allowed to polymerize again at 65°C for 100 min to create micro-stencils with a depth, that is enough for cell culture and medium supply. To prevent cell adhesion, prepared stencil masks were incubated in a solution of Pluronic F-127 (Sigma Aldrich, 2% w/v in deionized water) for 30 minutes prior to use. These micro-stencils were then used to confine MDCK-II cells in the desired patterns onto glass surfaces coated with 10µg/ml fibronectin.

6.3 Velocimetry and Cell tracking

PIV is a widely used technique and gained importance from the field of hydrodynamics where it was used to map flow of a fluid¹⁵⁵. It soon became versatile and has been used recently for nonhydrodynamic problems such as motion of bacteria or cells⁹¹. Time-lapse images were obtained using an inverted phase contrast microscope. PIV analysis was carried out using the PIV algorithm from ImageJ¹⁵⁶. Briefly, the images were divided into sub-windows also known as interrogation windows and the correlation within each of these windows was calculated thereby yielding a displacement field between two successive images. From the displacement fields, velocity vectors and hence the velocity was calculated. The velocity field was expressed in micrometers per hour.

PIV analysis in this way, yielded two components of velocity at each center point (i, j), of the interrogation window, namely lateral component (U_{ij} , perpendicular to the direction of group movement) and axial component (V_{ij} , parallel to the direction of group movement). From these components, velocity fluctuations (u_{ij} , and v_{ij}) and hence respective correlation functions were determined¹¹³.

$$u_{ij} = U_{ij} - U_{mean} \quad (1)$$

$$v_{ij} = V_{ij} - V_{mean} \quad (2)$$

where U_{mean} and V_{mean} are the mean lateral and axial velocity components respectively. From the velocity fluctuations (Eq. 1 and Eq. 2), lateral and axial correlation functions were computed as

$$C(r)_l = C(r) = \{u(r') \times u(r'+r)\}_r / [\{u(r')^2\} \times \{u(r'+r)^2\}]^{1/2} \quad (3)$$

$$C(r)_a = \{v(r') \times v(r'+r)\}_r / [\{v(r')^2\} \times \{v(r'+r)^2\}]^{1/2} \quad (4)$$

Here {...} represents the average; r is the vector of coordinates (i,j). Correlation length was determined as the point where the respective correlation function becomes negligible. Velocity fluctuations (u_{ij} or v_{ij}) were preferred over absolute velocities to obtain the correct normalization of correlation functions⁹¹. Further because only lateral velocity components could distinguish between passive and active collective migration, only lateral correlation length was computed. For time dependent kinematic studies, nuclei of individual cells were tracked to obtain (x,y) coordinates at each time point using MtrackJ plugin of FIJI¹⁵⁷ (Figure 34). Instantaneous speed and directional persistence of each cell at each time point was then calculated from the respective cell tracks using Microsoft Excel. Directional persistence for a particular track was defined as the ratio of end-to-end distance to the total accumulated distance at that particular instance in time.

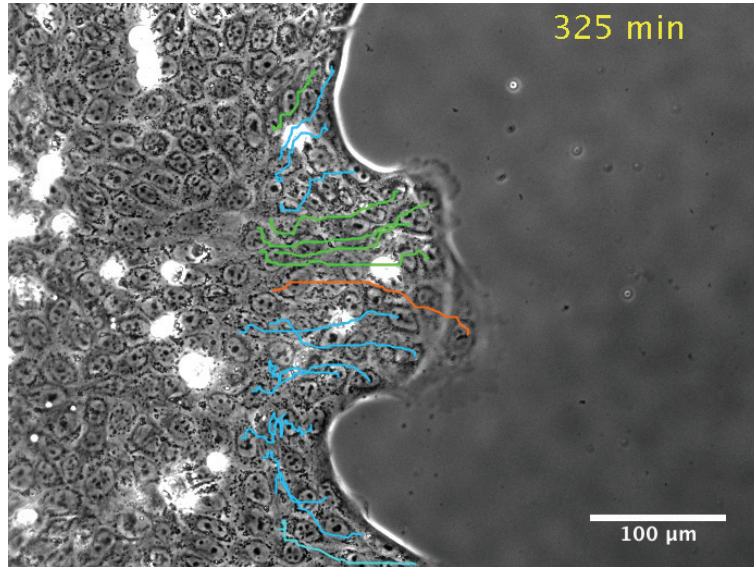


Figure 37. A snapshot of cell tracks obtained from FIJI MtrackJ tracking. Representative phase contrast image of epithelial monolayer and the corresponding cell tracks showing movements of cells in xy plane

6.4 Traction force and Monolayer stress microscopy

Traction force microscopy relies on measurement of local magnitude of substrate deformation induced by cellular movements. Briefly, cells are seeded on an optically transparent 3D substrate, embedded with fluorescent beads ranging from 0.2-1μm in size. A variety of hydrogels can be used as substrates, with a prerequisite that the mechanical behaviour of the hydrogel is characterized, and, that it is able to maintain cellular viability. The cells exert forces and deform the substrate as they move, thereby

displacing the underlying beads. Fluorescence microscopy is used to capture the positions of the beads as the cells migrate. Finally, the cells are trypsinized and the corresponding bead position in relaxed state is acquired. Bead displacement vectors can then be obtained by subtracting the bead positions in undeformed (relaxed) state with the corresponding deformed positions during cell migration. These displacement vectors were then used to compute the forces that cells exert on the substrate¹⁵⁸.

6.4.1 Preparation of traction force substrate

Glass bottom dishes (35 mm, MatTek) were treated with 0.1 M sodium hydroxide solution for 5 min, treated with 4% APTS (3-aminopropyl-triethoxysilane, Sigma Aldrich, Germany) in iso-propanol for 5 min and finally with 1% glutaraldehyde solution in water for 30 min. The dish was washed with deionized water three times and dried between each step. A second set (II) of cleaned glass coverslips (18 mm diameter) were dipped in RainX solution for 5 min, wiped with a laboratory cloth soaked with RainX and dried in a stream of nitrogen. Polyacrylamide gel was prepared from Acrylamide (40% in PBS), Bis-Acrylamide (2%) and PBS. Carboxylated polystyrene micro beads with 500nm diameter (2,65% solids in water) were added to the PAA mixture along with Tetramethylethylenediamine (TEMED) and Ammonium persulphate (APS) and immediately vortexed to allow complete mixing.

Table 5.4.1: Preparation of traction force substrates

| Total Solution (15 ml) | 11 kPa Stiffness | 23 kPa Stiffness |
|-------------------------|------------------|------------------|
| Water/ PBS | 10.63 ml | 9.937 ml |
| 40% Acrylamide | 3.75 ml | 2.812 ml |
| 2% BIS acrylamide | 525 μ l | 1.5 ml |
| Red beads (0.5 μ m) | 80 μ l | 300 μ l |
| APS | 50 μ l | 50 μ l |
| TEMED | 5 μ l | 5 μ l |

200 μ l of this mixture was pipetted onto the activated glass bottom dishes and a coverslip from the second set (II) was carefully placed on top with the rainX treated side facing towards the PAA. The set up was then inverted to allow the beads to settle at the surface while the gel polymerized. Gels with different stiffness can be prepared using different combinations of component mixtures.

6.4.2 Traction force microscopy

The gel surfaces were functionalized with 2mg/ml sulphosuccinimidyl-6-(4'-azido-2'-nitrophenylamino) hexanoate (Sulfo-SANPAH, Thermo Scientific) for 10 mins under UV light and then covalently coated with 0.5 mg ml⁻¹ fibronectin (Sigma) to ensure cell attachment. A horizontal confinement was created

on the functionalized PAA gels using thin PDMS blocks (Figure 33c). Cells were seeded in the confined areas and were then grown until a confluent monolayer is obtained. Subsequently, confinement was released by lifting off the PDMS block and images were acquired- in phase contrast channel for cells, and in red channel for beads- as the cells migrated. After experiment, cells were trypsinized and resulting bead positions were obtained. The bead position in relaxed state (after trypsinization) was then subtracted from the corresponding position recorded during migration to obtain bead displacement vectors. From these vectors, traction force vectors were calculated using an ImageJ plugin¹⁵⁶.

6.4.3 Monolayer stress microscopy

MSM starts with measuring the traction forces at the cell-substrate interface of a monolayer cell sheet and then uses a straightforward two-dimensional balance of forces to obtain the distribution of physical forces at every point within the monolayer. This algorithm was implemented in a set of functions written in MATLAB (MathWorks)¹¹³. The technique works on a few assumptions, first, monolayer is thin and flat i.e. lateral length that spans the monolayer (L) is much greater than the monolayer height (h). Second, stresses within the monolayer and traction forces at the cell-substrate interface are assumed to be planar with zero out-of-plane contribution ($\sigma_{zx} = \sigma_{zy} = \sigma_{zz} = T_z = 0$) Then applying the force balance assumption, we arrive at:

$$\frac{\delta\sigma_{xx}}{\delta x} + \frac{\delta\sigma_{xy}}{\delta x} = T_x, \frac{\delta\sigma_{yx}}{\delta y} + \frac{\delta\sigma_{yy}}{\delta y} = T_y \quad (1)$$

Where σ_{xx} and σ_{yy} are the components of average normal stresses and σ_{xy} and σ_{yx} are the components of shear stresses in the x and y directions respectively. Next, if monolayer is considered elastic and homogeneous then the two independent elastic constants, E (Young's modulus) and ν (Poisson's ratio) are able to describe the material properties and the stress strain relationship can be drawn as

$$\epsilon_{xx} = \frac{1}{E} (\sigma_{xx} - \nu\sigma_{yy}), \epsilon_{yy} = \frac{1}{E} (\sigma_{yy} - \nu\sigma_{xx}), \epsilon_{xy} = \frac{1}{E} (1 + \nu)\sigma_{xy} \quad (2)$$

Where $\epsilon_{xx}, \epsilon_{yy}, \epsilon_{xy}$ are strains in xy plane. To ensure that displacements can be integrated from strains, Saint-Venant's compatibility relation has to be satisfied. Then, from the force balance equation and the stress strain relationships, we obtain the Beltrami-Michell compatibility equation.

$$\left(\frac{\delta^2}{\delta x^2} + \frac{\delta^2}{\delta y^2} \right) (\sigma_{xx} + \sigma_{yy}) = (1 + \nu) \left(\frac{\delta T_x}{\delta x} + \frac{\delta T_y}{\delta y} \right) \quad (3)$$

For the boundary conditions, we assumed two kinds of boundary, namely the cell free boundary at the leading edge of the cell monolayer and optical edge boundaries at the other edges of the image. The cell free edge was specified by zero monolayer stresses whereas the optical edge was specified by

$$u_i n_i = 0 \text{ and } \sigma_{ij} n_j t_i = 0$$

where, u is the displacement, n and t are the normal and tangent unit vectors at the optical edge. Solving

the aforementioned equilibrium equations with respect to the boundary conditions, determine stresses everywhere within the monolayer.

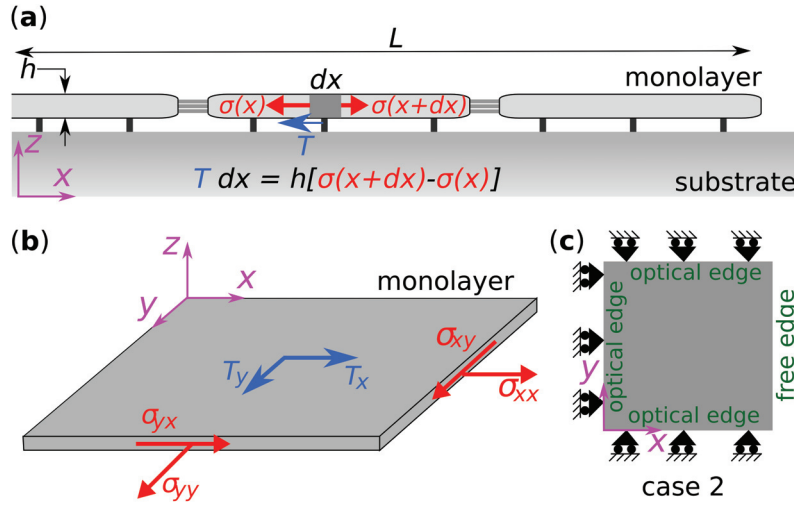


Figure 38. Balance of forces considered in monolayer stress microscopy¹³². (a) The cell monolayer is considered as a thin sheet where lateral length, L is much greater than height, h of the monolayer. Each cell exerts traction, T on the surface. These tractions are balanced by local monolayer stresses, s . (b) The force balance is ensured on xy plane and the out of plane contributions are neglected. (c) The optical field of view has three optical edges and a free edge. For boundary conditions, shear stresses at all the edges are zero and the normal stress at the free edge is zero. The monolayer is assumed to be containing a repeatable unit of this optical field of view.

6.5 Reflection interference contrast microscopy (RICM)

RICM works on the principal of interferometry and utilizes monochromatic polarized light to form image of an object on a glass surface. Intensity of the signal is a measure of proximity of the object to the surface. It was first used in the field of cell biology to study mechanisms of fibroblast adhesions on glass¹⁵⁹. The technique requires no genetic modifications and therefore is widely used for studying dynamic cell attachments^{149, 150}.

A monochromatic light is circularly polarized by a polarizer and is then reflected by a beam splitter towards the objective, which focuses the light onto the specimen (Figure 39a). Some of the light is reflected back from the glass surface while the rest travels into the cell and is reflected from the cell membrane. In this context, different situations can occur; first, when the cell membrane is too close, the light reflected from the membrane is shifted to half of a wavelength as compared to the light reflected from the glass thereby cancelling each other out and the interference between them would be negative (dark spot). When the membrane is not attached to the glass, the light reflected from the membrane will have a smaller phase shift as compared to the light reflected from the glass therefore they will not cancel each other and the interference is not negative (light grey spots) (Figure 39b). In this case the brightness of the spot depends upon the phase shift between the two reflected light rays.

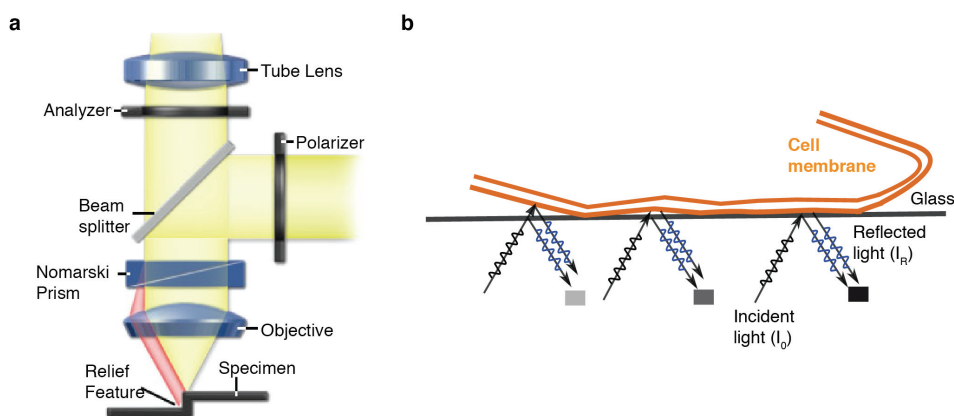


Figure 39. Reflection Interference contrast microscopy. (a) RICM setup, A monochromatic light is circularly polarized by a polarizer and is then reflected by a beam splitter to the specimen. **(b)** An interference between the light reflected back from the surface and the specimen is recorded to obtain an image that display cellular adhesions as negative interference or black spots on the image

When there is no specimen, only the light reflected from the glass is detected as bright spots¹⁵⁰. Time lapse imaging was carried out in both phase contrast and in RICM mode on an inverted microscope (Zeiss) equipped with an incubator capable of maintaining 37°C temperature, 95% relative humidity and 5% CO₂ concentration. An RICM filter cube, a beam splitter (50R/50T VIS), two polarization filters (AHF, Tübingen, Germany), and a LED light source (Zeiss, Gottingen, Germany) were used in order to produce coherent, monochromatic light. Images were taken with a defined focus option using a 63xPlan Neofluar Antiflex oil immersion objective (NA 1.25) (Zeiss, Gottingen, Germany). In order to obtain a large field of view, advanced tiles set up of the Zen software (Zen 2012) was used. For thresholding interference images, average value of background intensity (I_b) and standard deviation (σ) were determined and all areas of at least 4 × 4 pixels with an intensity less than ($I_b - \sigma/2$) were defined as adhesion points¹⁴⁹. The thresholding was done using MATLAB.

6.6 Agarose spot assay

Agarose spot assay is a simple technique used to perform chemotaxis or directed cell motion, it has recently been used¹⁶⁰ and intensively characterized¹⁴⁰ for chemotaxis of mammalian cells. This assay is inexpensive, simple to set up, and amenable to multiplexing, making it a valuable complement to more expensive and laborious methods such as microfluidic assays. It works by entrapping a chemoattractant inside a gel drop, which is then presented to the cells for directed migration.

MDCK-II cells were seeded in confined conditions using Ibidi cell-culture-inserts in MEM medium supplemented with 5% FBS, 2mM L-glutamine, 10 U ml⁻¹ penicillin & 10µg ml⁻¹ streptomycin and left to grow overnight to attain a confluent monolayer of cells. Subsequently, 0.5% Agarose solution in PBS was prepared, heated on a hot plate until boiling and swirled to facilitate complete dissolution.

When the temperature was cooled to 40°C, small volumes of agarose gel containing varying concentrations of chemo-attractant (EGF) was prepared. 10 µL spots of each of this gel solution containing EGF was pipetted rapidly, 0.5 mm away from the confined, confluent monolayer and were allowed to polymerize for 5 min at 4°C. The confinement was then released and media was replaced by MEM medium supplemented with 2mM L-glutamine, 10 U ml⁻¹ penicillin and 10 µg ml⁻¹ streptomycin but without serum. After 2 hours of migration, cells were fixed and permeabilized before adding Alexa fluor-488 labeled phalloidin (Thermo Fisher Scientific) for visualization of the actin cytoskeleton.

6.6.1 Calculation of relative chemo-attractant gradient

A major disadvantage to Agarose spot assay is that it can only sustain gradients that cells can sense for a limited duration. Additionally, the concentration profile is non-linear and varies over distance as well as time. Quantitative analysis of the agarose spot assay has therefore been done to clarify which concentrations of chemoattractant should be used and how far the gel should be placed from the cells so that the cells can sense the gradient in the required experimental time frame¹⁴⁰. For doing the numerical calculations, the spot was assumed to be large and volume of the dish was assumed to be 200 times larger than the spot. Then the concentration gradient can be formulated in a simple diffusion equation;

$$\frac{\delta c}{\delta t} = D \frac{\delta}{\delta r} \left[\frac{\delta c}{\delta x} \right] \quad (1)$$

Where c is the concentration of chemo-attractant, x is the distance from the centre of the spot, t is the time when the media was added or when the chemo-attractant is expected to start diffusing out of the gel and D is the diffusion coefficient. Since the pore size of the 0.5 % agarose gel (around 1 µm) is much larger than the size of the EGF, agarose is not expected to hinder the diffusion of EGF.

Further, a major determinant of chemiattractant response is the relative gradient, i.e. the steepness of the chemoattractant gradient normalized by the local concentration gradient. For a cell to sense and respond to chemotaxis, the relative gradient must be above a threshold value, which varies with the chemoattractant concentration and the K_d of the chemoattractant-receptor bond. In general, eukaryotic cells require at least 1% of the relative chemoattractant gradient for the chemotactic migration. Because there is no explicit solution of equation (1), finite element method was used and boundary values were applied to obtain the laplacian

$$\frac{\delta}{\delta r} \left[\frac{\delta c}{\delta x} \right]$$

By using the boundary conditions, such that when $x > (10 \times r)$, $c = 0$, we obtained the distribution of concentration gradient over the distance.

6.7 Plasmids, siRNAs, transfection and FRET

Transfection is a method of introducing negatively charged genetic material (e.g., phosphate backbones

of DNA and RNA) into cells through their negatively charged membrane. To overcome the electrostatic repulsion of the cell membrane, cationic liposome formulation such as lipofectamine is used. Lipofectamine contain cationic lipid head, which binds to the DNA to form liposomes, and a neutral co-lipid, which helps the DNA containing liposome to fuse with the plasma membrane thereby allowing the nucleic acid to cross into the cytoplasm and the genetic material to be available to the cell for replication or expression. Mammalian cells can be transfected by either a forward or a reverse transfection methods.

Plasmid pCry2PHR-mCh-RhoA was a gift from David Schaffer (Addgene plasmid # 42958)¹³⁷ and was purified with a Midiprep plasmid purification kit (Invitrogen). Merlin siRNA was purchased from Qiagen (catalog number). Plasmid and siRNA were transfected by the forward and reverse transfection methods, respectively, using Lipofectamine 2000 (Invitrogen), as instructed by the manufacturer. The scrambled siRNA was purchased from Qiagen.

Fluorescence resonance energy transfer (FRET), experiment was carried out in a Leica SP5 confocal laser scanning microscope using a 63x, 1.4-numerical-aperture oil immersion objective in a 37 and 5% CO₂ environment. MDCK cells were plated in eight-well glass Lab-Tek Chamber Slides (Nunc) and transfected as described above. After 24 h, cells were rinsed, and the old medium was replaced with fresh medium. Cells were then imaged with the confocal laser-scanning microscope. The exposure times for donor, acceptor and FRET channels were always kept constant. Each field yielded three 512×512 pixel images, representing the donor, acceptor and FRET channels.

6.8 Inhibition studies and Immunostainings

Blebbistatin, an inhibitor of myosin II, and calyculin A, a phosphatase inhibitor, were obtained from Sigma. Powders of these drugs were dissolved in DMSO (Sigma) to make the stock. Before removing the confinement, cells were treated with 1, 5, 10 and 20 μ M blebbistatin and 0.5, 1 and 2 nM calyculin A respectively in Opti-MEM reduced serum medium for 1h at 37°C in a 5% CO₂ humidified incubator. During migration, Opti-MEM was replaced by MEM containing 5% FBS, 2mM L-glutamine and the respective inhibitor. For actin stainings, cells were fixed and permeabilized before adding Alexa fluor-488 labeled phalloidin (Thermo Fisher Scientific) for visualization of the actin cytoskeleton. For studying dynamic G-actin incorporation, monolayers were permeabilized with saponin-media (0.2mg/ml saponin in permeabilization buffer, containing 138mM KCl, 4mM MgCl₂, 20mM HEPES, pH 7.4) for 7 min in the presence of 0.45 μ M Alexa-488-tagged-G-actin to favour barbed end incorporation. Cells were then fixed in 4% paraformaldehyde in cytoskeletal stabilization buffer containing 0.2% triton-X-100 in PBS and alexa-594-phalloidin (1:500).

7. References

1. King, A.J., Douglas, C.M., Huchard, E., Isaac, N.J. & Cowlshaw, G. Dominance and affiliation mediate despotism in a social primate. *Current biology : CB* **18**, 1833-1838 (2008).
2. Nagy, M., Akos, Z., Biro, D. & Vicsek, T. Hierarchical group dynamics in pigeon flocks. *Nature* **464**, 890-893 (2010).
3. Conradt, L., Krause, J., Couzin, I.D. & Roper, T.J. "Leading according to need" in self-organizing groups. *Am Nat* **173**, 304-312 (2009).
4. Iain D. Couzin, C.C.I., Naomi E. Leonard Uninformed Individuals Promote Democratic Consensus in Animal Groups. *Science* **334** (2011).
5. Conradt, L. Group Decision making in Animals. *Nature* (2003).
6. Seeley, T.D. *Honeybee democracy*. (Princeton University Press, Princeton, NJ; 2010).
7. Wray, M.K., Klein, B.A. & Seeley, T.D. Honey bees use social information in waggle dances more fully when foraging errors are more costly. *Behavioral Ecology* **23**, 125-131 (2011).
8. Strandburg-Peshkin, A., Farine, D.R., Couzin, I.D. & Crofoot, M.C. Shared decision-making drives collective movement in wild baboons. *Science* **348**, 1358-1361 (2015).
9. Buchanan, J.M. The Calculus of Consent: Logical Foundations of Constitutional Democracy. *The Online Library of Liberty* (1962).
10. Bruce Alberts, A.D.J., Julian Lewis, David Morgan Molecular biology of the cell. (1983).
11. Darling, D.J. The world of David Darling. (1999).
12. Friedl, P. & Gilmour, D. Collective cell migration in morphogenesis, regeneration and cancer. *Nature reviews. Molecular cell biology* **10**, 445-457 (2009).
13. Gupton, S.L. & Gertler, F.B. Filopodia: the fingers that do the walking. *Sci STKE* **2007**, re5 (2007).
14. Ridley, A.J. *et al.* Cell migration: integrating signals from front to back. *Science* **302**, 1704-1709 (2003).
15. Abercrombie The locomotion of fibroblasts in culture. *Experimental cell research* (1970).
16. Scarpa, E. & Mayor, R. Collective cell migration in development. *The Journal of cell biology* **212**, 143-155 (2016).
17. Mattila, P.K. & Lappalainen, P. Filopodia: molecular architecture and cellular functions. *Nature reviews. Molecular cell biology* **9**, 446-454 (2008).
18. Svitkina, T.M. Progress in protrusion: the tell-tale scar. *TIBS* (1999).
19. Takenawa, T. & Suetsugu, S. The WASP-WAVE protein network: connecting the membrane to the cytoskeleton. *Nature reviews. Molecular cell biology* **8**, 37-48 (2007).
20. Chen, Z. *et al.* Structure and control of the actin regulatory WAVE complex. *Nature* **468**, 533-538 (2010).
21. Ridley, A.J. Life at the leading edge. *Cell* **145**, 1012-1022 (2011).
22. Ponti, A. Two Distinct Actin Networks Drive the Protrusion of Migrating Cells. *Science*.
23. Gallegos, L., Ng, M.R. & Brugge, J.S. The myosin-II-responsive focal adhesion proteome: a tour de force? *Nature cell biology* **13**, 344-346 (2011).
24. Gallegos, L., Ng, M.R. & Brugge, J.S. The myosin-II-responsive focal adhesion proteome: a tour de force? *Nature cell biology* (2011).
25. Murrell, M., Oakes, P.W., Lenz, M. & Gardel, M.L. Forcing cells into shape: the mechanics of actomyosin contractility. *Nature reviews. Molecular cell biology* **16**, 486-498 (2015).
26. Vicente-Manzanares, M., Ma, X., Adelstein, R.S. & Horwitz, A.R. Non-muscle myosin II takes centre stage in cell adhesion and migration. *Nature Reviews Molecular Cell Biology* **10**, 778-790 (2009).
27. Riento, K. & Ridley, A.J. Rocks: multifunctional kinases in cell behaviour. *Nature reviews. Molecular cell biology* **4**, 446-456 (2003).

28. Kirfel, G. Cell migration: mechanisms of rear detachment and the formation of migration tracks. (2004).
29. Prabhat S. Kunwar, D.E.S., Ruth Lehmann In Vivo Migration: A Germ Cell Perspective. *Annu. Rev. Cell Dev. Biol.* **22**, 237-265 (2006).
30. Ghysen, A. & Dambly-Chaudiere, C. Development of the zebrafish lateral line. *Curr Opin Neurobiol* **14**, 67-73 (2004).
31. Ghabrial, A., Luschig, S., Metzstein, M.M. & Krasnow, M.A. Branching morphogenesis of the Drosophila tracheal system. *Annu Rev Cell Dev Biol* **19**, 623-647 (2003).
32. M, A. Genetic control of branching morphogenesis during Drosophila tracheal development. *Curr Opin Cell Biol.* (2000).
33. Rørth, P. Initiating and guiding migration: lessons from border cells. *TRENDS in Cell Biology Vol.12 No.7 July 2002* 325 (2002).
34. Montell, D.J. Border-cell migration: the race is on. *Nature reviews. Molecular cell biology* **4**, 13-24 (2003).
35. Sonnemann, K.J. & Bement, W.M. Wound repair: toward understanding and integration of single-cell and multicellular wound responses. *Annu Rev Cell Dev Biol* **27**, 237-263 (2011).
36. Shaw, T.J. & Martin, P. Wound repair at a glance. *Journal of cell science* **122**, 3209-3213 (2009).
37. Turley, E.A., Veiseh, M., Radisky, D.C. & Bissell, M.J. Mechanisms of disease: epithelial-mesenchymal transition--does cellular plasticity fuel neoplastic progression? *Nat Clin Pract Oncol* **5**, 280-290 (2008).
38. Niewiadomska, P., Godt, D. & Tepass, U. DE-Cadherin is required for intercellular motility during Drosophila oogenesis. *The Journal of cell biology* **144**, 533-547 (1999).
39. Prasad, M. & Montell, D.J. Cellular and molecular mechanisms of border cell migration analyzed using time-lapse live-cell imaging. *Developmental cell* **12**, 997-1005 (2007).
40. Bianco, A. *et al.* Two distinct modes of guidance signalling during collective migration of border cells. *Nature* **448**, 362-365 (2007).
41. Sutherland, D., Samakovlis, C. & Krasnow, M.A. branchless encodes a Drosophila FGF homolog that controls tracheal cell migration and the pattern of branching. *Cell* **87**, 1091-1101 (1996).
42. Caussinus, E., Colombelli, J. & Affolter, M. Tip-cell migration controls stalk-cell intercalation during Drosophila tracheal tube elongation. *Current biology : CB* **18**, 1727-1734 (2008).
43. Lebreton, G. & Casanova, J. Specification of leading and trailing cell features during collective migration in the Drosophila trachea. *Journal of cell science* **127**, 465-474 (2014).
44. Ghabrial, A.S. & Krasnow, M.A. Social interactions among epithelial cells during tracheal branching morphogenesis. *Nature* **441**, 746-749 (2006).
45. Gerhardt, H. *et al.* VEGF guides angiogenic sprouting utilizing endothelial tip cell filopodia. *The Journal of cell biology* **161**, 1163-1177 (2003).
46. Kuriyama, S. *et al.* In vivo collective cell migration requires an LPAR2-dependent increase in tissue fluidity. *The Journal of cell biology* **206**, 113-127 (2014).
47. Laguerre, L., Ghysen, A. & Dambly-Chaudiere, C. Mitotic patterns in the migrating lateral line cells of zebrafish embryos. *Dev Dyn* **238**, 1042-1051 (2009).
48. Nystrom, M.L. *et al.* Development of a quantitative method to analyse tumour cell invasion in organotypic culture. *J Pathol* **205**, 468-475 (2005).
49. Wolf, K. *et al.* Multi-step pericellular proteolysis controls the transition from individual to collective cancer cell invasion. *Nature cell biology* **9**, 893-904 (2007).
50. Gaggioli, C. *et al.* Fibroblast-led collective invasion of carcinoma cells with differing roles for RhoGTPases in leading and following cells. *Nature cell biology* **9**, 1392-1400 (2007).
51. Crosby, L.M. & Waters, C.M. Epithelial repair mechanisms in the lung. *Am J Physiol Lung Cell Mol Physiol* **298**, L715-731 (2010).
52. Gurtner, G.C., Werner, S., Barrandon, Y. & Longaker, M.T. Wound repair and regeneration. *Nature* **453**, 314-321 (2008).
53. Furie, B. & Furie, B.C. Mechanisms of thrombus formation. *N Engl J Med* **359**, 938-949 (2008).

54. Schuh, A.C., Keating, S.J., Monteclaro, F.S., Vogt, P.K. & Breitman, M.L. Obligatory wounding requirement for tumorigenesis in v-jun transgenic mice. *Nature* **346**, 756-760 (1990).
55. Poujade, M. *et al.* Collective migration of an epithelial monolayer in response to a model wound. *Proceedings of the National Academy of Sciences of the United States of America* **104**, 15988-15993 (2007).
56. Amerman, E.C. *Human anatomy & physiology*. (Pearson, Boston; 2016).
57. Peterson, L.W. & Artis, D. Intestinal epithelial cells: regulators of barrier function and immune homeostasis. *Nat Rev Immunol* **14**, 141-153 (2014).
58. Freshney, R.I. & Freshney, M.G. *Culture of epithelial cells*, Edn. 2nd. (Wiley-Liss, New York; 2002).
59. Dept. of Functional Biology and Cell Sciences, F.O.B. Atlas of Plant and Animal Histology. University of Vigo.
60. Sonnemann, K.J. & Bement, W.M. Wound repair: toward understanding and integration of single-cell and multicellular wound responses. *Annu Rev Cell Dev Biol* **27**, 237-263 (2011).
61. Cordeiro, J.V. & Jacinto, A. The role of transcription-independent damage signals in the initiation of epithelial wound healing. *Nat Rev Mol Cell Bio* **14**, 249-262 (2013).
62. Versteeg, H.H., Heemskerk, J.W., Levi, M. & Reitsma, P.H. New fundamentals in hemostasis. *Physiol Rev* **93**, 327-358 (2013).
63. Eming, S.A., Krieg, T. & Davidson, J.M. Inflammation in wound repair: molecular and cellular mechanisms. *J Invest Dermatol* **127**, 514-525 (2007).
64. Tonnesen, M.G., Feng, X. & Clark, R.A. Angiogenesis in wound healing. *J Invest Dermatol Symp Proc* **5**, 40-46 (2000).
65. Midwood, K.S., Williams, L.V. & Schwarzbauer, J.E. Tissue repair and the dynamics of the extracellular matrix. *Int J Biochem Cell Biol* **36**, 1031-1037 (2004).
66. Hinz, B. Formation and function of the myofibroblast during tissue repair. *J Invest Dermatol* **127**, 526-537 (2007).
67. Martin, P. Wound healing--aiming for perfect skin regeneration. *Science* **276**, 75-81 (1997).
68. Adams, R.H. & Alitalo, K. Molecular regulation of angiogenesis and lymphangiogenesis. *Nature reviews. Molecular cell biology* **8**, 464-478 (2007).
69. Haslett, C. Resolution of acute inflammation and the role of apoptosis in the tissue fate of granulocytes. *Clin Sci (Lond)* **83**, 639-648 (1992).
70. Arwert, E.N., Hoste, E. & Watt, F.M. Epithelial stem cells, wound healing and cancer. *Nature Reviews Cancer* **12**, 170-180 (2012).
71. Schafer, M. & Werner, S. Cancer as an overhealing wound: an old hypothesis revisited. *Nat Rev Mol Cell Bio* **9**, 628-638 (2008).
72. Crosby, L.M. & Waters, C.M. Epithelial repair mechanisms in the lung. *Am J Physiol Lung Cell Mol Physiol* **298**, L715-731 (2010).
73. Palmyre, A. *et al.* Collective epithelial migration drives kidney repair after acute injury. *PloS one* **9**, e101304 (2014).
74. Brugues, A. *et al.* Forces driving epithelial wound healing. *Nat Phys* **10**, 683-690 (2014).
75. Vedula, S.R. *et al.* Mechanics of epithelial closure over non-adherent environments. *Nat Commun* **6**, 6111 (2015).
76. Guillot, C. & Lecuit, T. Mechanics of epithelial tissue homeostasis and morphogenesis. *Science* **340**, 1185-1189 (2013).
77. Bement, W.M., Mandato, C.A. & Kirsch, M.N. Wound-induced assembly and closure of an actomyosin purse string in *Xenopus* oocytes. *Current biology : CB* **9**, 579-587 (1999).
78. Klarlund, J.K. Dual modes of motility at the leading edge of migrating epithelial cell sheets. *Proceedings of the National Academy of Sciences of the United States of America* **109**, 15799-15804 (2012).
79. Tamada, M., Perez, T.D., Nelson, W.J. & Sheetz, M.P. Two distinct modes of myosin assembly and dynamics during epithelial wound closure. *The Journal of cell biology* **176**, 27-33 (2007).
80. Kim, J.H. *et al.* Propulsion and navigation within the advancing monolayer sheet. *Nat Mater* **12**, 856-863 (2013).

81. Vedula, S.R. *et al.* Mechanics of epithelial closure over non-adherent environments. *Nature communications* **6**, 6111 (2015).
82. Begnaud, S., Chen, T., Delacour, D., Mege, R.M. & Ladoux, B. Mechanics of epithelial tissues during gap closure. *Curr Opin Cell Biol* **42**, 52-62 (2016).
83. Anon, E. *et al.* Cell crawling mediates collective cell migration to close undamaged epithelial gaps. *P Natl Acad Sci USA* **109**, 10891-10896 (2012).
84. Klarlund, J.K. Dual modes of motility at the leading edge of migrating epithelial cell sheets. *P Natl Acad Sci USA* **109**, 15799-15804 (2012).
85. Ravasio, A. *et al.* Gap geometry dictates epithelial closure efficiency. *Nat Commun* **6** (2015).
86. Anon, E. *et al.* Cell crawling mediates collective cell migration to close undamaged epithelial gaps. *Proceedings of the National Academy of Sciences of the United States of America* **109**, 10891-10896 (2012).
87. Reffay, M. *et al.* Interplay of RhoA and mechanical forces in collective cell migration driven by leader cells. *Nature cell biology* **16**, 217-223 (2014).
88. Kabla, A.J. Collective cell migration: leadership, invasion and segregation. *J R Soc Interface* **9**, 3268-3278 (2012).
89. Khalil, A.A. & Friedl, P. Determinants of leader cells in collective cell migration. *Integr Biol (Camb)* **2**, 568-574 (2010).
90. Haeger, A., Wolf, K., Zegers, M.M. & Friedl, P. Collective cell migration: guidance principles and hierarchies. *Trends Cell Biol* **25**, 556-566 (2015).
91. Petitjean, L. *et al.* Velocity fields in a collectively migrating epithelium. *Biophysical journal* **98**, 1790-1800 (2010).
92. Angelini, T.E., Hannezo, E., Trepatt, X., Fredberg, J.J. & Weitz, D.A. Cell migration driven by cooperative substrate deformation patterns. *Phys Rev Lett* **104**, 168104 (2010).
93. Ramel, D., Wang, X., Laflamme, C., Montell, D.J. & Emery, G. Rabi11 regulates cell-cell communication during collective cell movements. *Nature cell biology* **15**, 317-324 (2013).
94. Nier, V. *et al.* Tissue fusion over nonadhering surfaces. *Proceedings of the National Academy of Sciences of the United States of America* **112**, 9546-9551 (2015).
95. Ravasio, A. *et al.* Gap geometry dictates epithelial closure efficiency. *Nature communications* **6**, 7683 (2015).
96. Jefferson, J.J., Leung, C.L. & Liem, R.K. Plakins: goliaths that link cell junctions and the cytoskeleton. *Nature reviews. Molecular cell biology* **5**, 542-553 (2004).
97. Thiery, J.P. & Sleeman, J.P. Complex networks orchestrate epithelial-mesenchymal transitions. *Nature reviews. Molecular cell biology* **7**, 131-142 (2006).
98. Scott, J.A. & Yap, A.S. Cinderella no longer: -catenin steps out of cadherin's shadow. *Journal of cell science* **119**, 4599-4605 (2006).
99. Dejana, E. Endothelial cell-cell junctions: happy together. *Nature reviews. Molecular cell biology* **5**, 261-270 (2004).
100. Nishimura, T. & Takeichi, M. Remodeling of the adherens junctions during morphogenesis. *Curr Top Dev Biol* **89**, 33-54 (2009).
101. Niessen, C.M., Leckband, D. & Yap, A.S. Tissue Organization by Cadherin Adhesion Molecules: Dynamic Molecular and Cellular Mechanisms of Morphogenetic Regulation. *Physiological Reviews* **91**, 691-731 (2011).
102. Pokutta, S., Drees, F., Takai, Y., Nelson, W.J. & Weis, W.I. Biochemical and structural definition of the 1-afadin- and actin-binding sites of alpha-catenin. *The Journal of biological chemistry* **277**, 18868-18874 (2002).
103. Drees, F., Pokutta, S., Yamada, S., Nelson, W.J. & Weis, W.I. Alpha-catenin is a molecular switch that binds E-cadherin-beta-catenin and regulates actin-filament assembly. *Cell* **123**, 903-915 (2005).
104. Han, S.P. & Yap, A.S. An alpha-catenin deja vu. *Nature cell biology* **15**, 238-239 (2013).
105. Yamada, S., Pokutta, S., Drees, F., Weis, W.I. & Nelson, W.J. Deconstructing the cadherin-catenin-actin complex. *Cell* **123**, 889-901 (2005).

106. Benjamin, J.M. *et al.* AlphaE-catenin regulates actin dynamics independently of cadherin-mediated cell-cell adhesion. *The Journal of cell biology* **189**, 339-352 (2010).
107. Buckley, C.D. *et al.* Cell adhesion. The minimal cadherin-catenin complex binds to actin filaments under force. *Science* **346**, 1254211 (2014).
108. Huveneers, S. *et al.* Vinculin associates with endothelial VE-cadherin junctions to control force-dependent remodeling. *The Journal of cell biology* **196**, 641-652 (2012).
109. le Duc, Q. *et al.* Vinculin potentiates E-cadherin mechanosensing and is recruited to actin-anchored sites within adherens junctions in a myosin II-dependent manner. *The Journal of cell biology* **189**, 1107-1115 (2010).
110. Yao, M. *et al.* Force-dependent conformational switch of alpha-catenin controls vinculin binding. *Nature communications* **5**, 4525 (2014).
111. Verma, S. *et al.* A WAVE2-Arp2/3 actin nucleator apparatus supports junctional tension at the epithelial zonula adherens. *Molecular biology of the cell* **23**, 4601-4610 (2012).
112. Taha, A.A., Taha, M., Seebach, J. & Schnittler, H.J. ARP2/3-mediated junction-associated lamellipodia control VE-cadherin-based cell junction dynamics and maintain monolayer integrity. *Molecular biology of the cell* **25**, 245-256 (2013).
113. Das, T. *et al.* A molecular mechanotransduction pathway regulates collective migration of epithelial cells. *Nature cell biology* **17**, 276-287 (2015).
114. Riahi, R. *et al.* Notch1-Dll4 signalling and mechanical force regulate leader cell formation during collective cell migration. *Nature communications* **6**, 6556 (2015).
115. Cai, D. *et al.* Mechanical feedback through E-cadherin promotes direction sensing during collective cell migration. *Cell* **157**, 1146-1159 (2014).
116. Trepap, X. *et al.* Physical forces during collective cell migration. *Nature Physics* **5**, 426-430 (2009).
117. HARRIS, A.K. Silicon Rubber Substrata: A New Wrinkle in the Study of Cell Locomotion. *Science* (1980).
118. Gavin, R.H. Cytoskeleton: Methods and Protocols. (2009).
119. Iskratsch, T., Wolfenson, H. & Sheetz, M.P. Appreciating force and shape-the rise of mechanotransduction in cell biology. *Nature reviews. Molecular cell biology* **15**, 825-833 (2014).
120. LAdOUx, P.H.B.T. Push it, pull it. *Science* (2011).
121. Schwarz, U.S. & Gardel, M.L. United we stand: integrating the actin cytoskeleton and cell-matrix adhesions in cellular mechanotransduction. *Journal of cell science* **125**, 3051-3060 (2012).
122. Dembo, M. Stresses at the Cell-to-Substrate Interface during Locomotion of Fibroblasts. *Biophysical journal* (1999).
123. Tan, J.L. *et al.* Cells lying on a bed of microneedles: an approach to isolate mechanical force. *Proceedings of the National Academy of Sciences of the United States of America* **100**, 1484-1489 (2003).
124. Tambe, D.T. *et al.* Collective cell guidance by cooperative intercellular forces. *Nature Materials* **10**, 469-475 (2011).
125. Brugues, A. *et al.* Forces driving epithelial wound healing. *Nat Phys* **10**, 683-690 (2014).
126. Delanoe-Ayari, H., Rieu, J.P. & Sano, M. 4D traction force microscopy reveals asymmetric cortical forces in migrating Dictyostelium cells. *Phys Rev Lett* **105**, 248103 (2010).
127. Yang, Y. *et al.* Probing Leader Cells in Endothelial Collective Migration by Plasma Lithography Geometric Confinement. *Sci Rep* **6**, 22707 (2016).
128. Yamaguchi, N., Mizutani, T., Kawabata, K. & Haga, H. Leader cells regulate collective cell migration via Rac activation in the downstream signaling of integrin beta1 and PI3K. *Sci Rep* **5**, 7656 (2015).
129. Farooqui, R. & Fenteany, G. Multiple rows of cells behind an epithelial wound edge extend cryptic lamellipodia to collectively drive cell-sheet movement. *Journal of cell science* **118**, 51-63 (2005).
130. Omelchenko, T., Vasiliev, J.M., Gelfand, I.M., Feder, H.H. & Bonder, E.M. Rho-dependent formation of epithelial "leader" cells during wound healing. *Proceedings of the National Academy of Sciences of the United States of America* **100**, 10788-10793 (2003).

131. Trepap, X. & Fredberg, J.J. Plithotaxis and emergent dynamics in collective cellular migration. *Trends Cell Biol* **21**, 638-646 (2011).
132. Tambe, D.T. *et al.* Monolayer stress microscopy: limitations, artifacts, and accuracy of recovered intercellular stresses. *PloS one* **8**, e55172 (2013).
133. Haeger, A., Wolf, K., Zegers, M.M. & Friedl, P. Collective cell migration: guidance principles and hierarchies. *Trends Cell Biol* **25**, 556-566 (2015).
134. Montell, D.J., Yoon, W.H. & Starz-Gaiano, M. Group choreography: mechanisms orchestrating the collective movement of border cells. *Nat Rev Mol Cell Bio* **13**, 631-645 (2012).
135. Park, J.A. *et al.* Unjamming and cell shape in the asthmatic airway epithelium. *Nature Materials* **14**, 1040-+ (2015).
136. Bi, D., Lopez, J.H., Schwarz, J.M. & Manning, M.L. A density-independent rigidity transition in biological tissues. *Nature Physics* **11**, 1074-1079 (2015).
137. Bugaj, L.J., Choksi, A.T., Mesuda, C.K., Kane, R.S. & Schaffer, D.V. Optogenetic protein clustering and signaling activation in mammalian cells. *Nat Methods* **10**, 249-252 (2013).
138. Rausch, S. Polarizing cytoskeletal tension to induce leader cell formation during collective cell migration. *Biointerphases* (2013).
139. Duffy, D.C. Rapid Prototyping of Microfluidic Systems in Poly(dimethylsiloxane). (1998).
140. Szatmary, A.C., Stuelten, C.H. & Nossal, R. Improving the design of the agarose spot assay for eukaryotic cell chemotaxis. *RSC Adv* **4**, 57343-57349 (2014).
141. Kim, M.J. *et al.* Optimal concentration of human epidermal growth factor (hEGF) for epithelial healing in experimental corneal alkali wounds. *Curr Eye Res* **22**, 272-279 (2001).
142. Frey, M.R., Golovin, A. & Polk, D.B. Epidermal growth factor-stimulated intestinal epithelial cell migration requires Src family kinase-dependent p38 MAPK signaling. *The Journal of biological chemistry* **279**, 44513-44521 (2004).
143. Hardin, C. *et al.* Glassy dynamics, cell mechanics, and endothelial permeability. *J Phys Chem B* **117**, 12850-12856 (2013).
144. Kraning-Rush, C.M., Carey, S.P., Califano, J.P., Smith, B.N. & Reinhart-King, C.A. The role of the cytoskeleton in cellular force generation in 2D and 3D environments. *Phys Biol* **8**, 015009 (2011).
145. Kim, D.H. & Wirtz, D. Focal adhesion size uniquely predicts cell migration. *FASEB J* **27**, 1351-1361 (2013).
146. Geiger, B., Spatz, J.P. & Bershadsky, A.D. Environmental sensing through focal adhesions. *Nature reviews. Molecular cell biology* **10**, 21-33 (2009).
147. Mayor, R. & Etienne-Manneville, S. The front and rear of collective cell migration. *Nature reviews. Molecular cell biology* **17**, 97-109 (2016).
148. Ciobanaru, C., Faivre, B. & Le Clainche, C. Actin dynamics associated with focal adhesions. *Int J Cell Biol* **2012**, 941292 (2012).
149. Munding, T.A. *et al.* Investigating cell-ECM contact changes in response to hypoosmotic stimulation of hepatocytes in vivo with DW-RICM. *PloS one* **7**, e48100 (2012).
150. Limozin, L. & Sengupta, K. Quantitative reflection interference contrast microscopy (RICM) in soft matter and cell adhesion. *Chemphyschem* **10**, 2752-2768 (2009).
151. Mark, S. *et al.* Physical model of the dynamic instability in an expanding cell culture. *Biophysical journal* **98**, 361-370 (2010).
152. Montell, D.J., Yoon, W.H. & Starz-Gaiano, M. Group choreography: mechanisms orchestrating the collective movement of border cells. *Nature reviews. Molecular cell biology* **13**, 631-645 (2012).
153. Ng, M.R., Besser, A., Danuser, G. & Brugge, J.S. Substrate stiffness regulates cadherin-dependent collective migration through myosin-II contractility. *The Journal of cell biology* **199**, 545-563 (2012).
154. Kovacs, E.M. *et al.* N-WASP regulates the epithelial junctional actin cytoskeleton through a non-canonical post-nucleation pathway. *Nature cell biology* **13**, 934-943 (2011).
155. Raffel, M. Particle Image Velocimetry, A Practical Guide. *Springer Verlag* (1998).

- 156. Qingzong Tseng, E.D.P., Alexandre Deshieri Spatial organization of the extracellular matrix regulates cell-cell junction positioning. *PNAS* **109**, 1506-1511 (2012).
- 157. Meijering, E. Methods for cell and particle tracking. (2012).
- 158. Aratyn-Schaus, Y., Oakes, P.W., Stricker, J., Winter, S.P. & Gardel, M.L. Preparation of compliant matrices for quantifying cellular contraction. *Journal of visualized experiments : JoVE* (2010).
- 159. Curtis, A.S.G. The mechanism of adhesion of cell to glass: A study by Interference Reflection Microscopy. *The Journal of cell biology* (1964).
- 160. Wiggins, H. & Rappoport, J. An agarose spot assay for chemotactic invasion. *Biotechniques* **48**, 121-124 (2010).

Acknowledgements

I am so glad that I am calling this, ‘the beginning’ and not ‘the end’, and, a number of people have been instrumental in making sure that I get to this state of mind. It is indeed, my pleasure to acknowledge them for all the patience and support I received over the past many years.

It is needless to say that this thesis would not have been possible without the guidance of **Professor Joachim Spatz**. I feel privileged to have worked with you, because of the wonderful mentor and scientist you are. You gently guided the whole process from the very beginning, and have always offered a comforting motivation. I am amazed at your positive attitude and listening skills, and inspired by how little information you need to formulate critical, relevant and to the point questions. The tremendous efforts, the support and the trust you put in new ideas and young scientists, is incredible. It has been, and will always be a joy to have a discussion with you!

I would also like to thank **Professor Jeffrey Hubbell** for kindly accepting to be my thesis director, for putting a trust into this project and for the helpful discussions and, **Dr. Heike Boehm** for the intriguing discussions, for the critical suggestions and for being the mentor of my PhD program.

I would like to extend my heartiest gratitude to **Dr. Tamal Das**. I cannot imagine to have done what I did, if it wasn’t with you. You once told me, how lucky you feel to have met those certain people, who played that critical role in making you what you are today. I feel the same, for meeting you at that stage of my career. You are an amazing scientist and have inspired me each time with the depth of your knowledge. Thank you for being an inspiring teacher, for protecting me from negative distractions, for being critical when needed, yet, believing in me, and for talking me out when things were not working and I was falling apart. Without your patience and care, I would not have reached this stage.

I am extremely grateful to my thesis committee members, **Prof. Matthias Lutolf**, **Professor Kai Johnsson**, **Professor Viola Vogel**, **Professor Daniel Müller** and **Professor Aleksandra Radenovic** for reviewing my thesis, and for the exciting discussions during the candidacy and the oral exam.

I cherish the many discussions with my ex- and present co-workers, **Jacopo Di Russo**, **Patricia Hegger**, **Burcu Minsky**, **Tabea Mundinger**, **Christiane Antoni**, **Adria Sales**, **Johannes Hirte**, **Sabrina Rossberger**, and many others in department; scientific or non-scientific, and feel that they were essential for this work. In particular, the non-scientific and the gossipy ones, that kept me sane at critical times. Thanks to **Patricia** for translating, and **Christiane** for proofreading the German abstract. Special thanks to **Patricia** for the refreshing twenty-minutes walk, everyday after lunch.

Somewhere in between my crazy experiments, an years long friendship turned into promise of a life-long companionship. A thank you is not enough for my dear husband, **Bramha**, who listened to me every evening, talking on-and-on about my experiments, and handled all the variations of my moods

with such patience and love. Thank you for saying, 'I am proud of you' at times least expected. On the professional end, Thank you for helping me with MATLAB and for letting me take all the credit ☺

I would like to thank my friends, **SaiRam, Balaji, Jaya, Swati, Sudip, Swarna, Sreedhar, Geetika, Shradha, Vijay, Prashant** and **Poulomi** who are like my extended family, for keeping me alive in dull moments and for living with me in the bright ones.

Words are not enough for my family back in India who always backed my decisions and provided me the unconditional love and support. A special thanks to my mom, **Shobhna Nagpal** for always offering a listening ear, your simple solutions to the 'otherwise complex' problems, have always amazed me, and taught me how a slightly different perspective can sometimes make things so easy.

In the end, I would like to thank **Ms. Sonja Bodmer** and **Ms. Sanrda Roux** for being patient with my 'outside-EPFL-queries' and for being highly cooperative for the external courses and credits and, **Dr. Klaus Khunke**, for coordinating the MPS-EPFL PhD program. Finally, I would like to thank the administrative and the cleaning staff of the Max Planck Institute for being so cooperative and for maintaining a clean and healthy working environment.

I am extremely grateful to the Max Planck Society for the fellowship and to **Mr. Max Karl Ernst Ludwig Planck**, for the incredible work he did during one of the most difficult times of the history, without which; evidently, the world of science and technology would be lagging years behind from where it is today.

Declaration of Authorship

All the experiments included in this thesis are performed and analyzed by me under vigilant supervision of Prof. Joachim P. Spatz and Dr. Tamal Das, who conceived and designed the project together. Dr. Tamal Das developed computational tools for stress analysis. I acknowledge the support from Dr. Heike Boehm and Dr. Jacopo Di Russo in the interpretation and analysis of data.

I certify that, to the best of my knowledge, this thesis does not violate any proprietary rights and that any ideas, techniques, quotations or any other material from work of other people included in this thesis are fully acknowledged in accordance with standard referencing practices.

This thesis has not been accepted for any degree and is not concurrently submitted in candidature of any other degree.

Medhavi Vishwakarma

14th December 2016, Stuttgart

Curriculum Vitae

Medhavi Vishwakarma

Education and Experience

02/2013–Present: PhD (Biotechnology and Bioengineering)

Max planck Institute for Intelligent systems, École polytechnique fédérale de Lausanne (EPFL)

Thesis Supervisors: Prof. Joachim P. Spatz and Prof. Jeffrey Alan Hubbell

Group Decisions Regulate Emergence and Regulation of Leaders in Collective Migration of Epithelial Cells

07/2012–12/2012: Assistant Professor (Temporary)

Dr. B. R. Ambedkar National Institute of Technology, Jalandhar (India)

07/2010–06/2012: Masters' Technology (M.Tech) in Biotechnology and Biochemical engineering

Indian Institute of Technology, Kharagpur (India), University of Stuttgart, Germany

Thesis Supervisors: Prof. Robin Ghosh and Prof. Amit Kumar Das

07/2006–05/2010 Bachelors' Engineering in Biotechnology

University Institute of Engineering and Technology, Panjab University (India)

Digital competence

Well versed with windows 98/2000/xp operating systems, MS office, C Programming (Basics), MATLAB (Basics), LaTeX (Basics), QCAD (Advanced)

Awards and Scholarships

DAAD scholarship (Deutscher Akademischer Austausch Dienst) for Masters' Thesis in Stuttgart, Germany: September 2011 to May 2012

MHRD scholarship for Masters' in IIT Kharagpur by Ministry of Human Resource Development, Govt. of India: July 2010 to May 2012

All India GATE Rank 110 (out of 20000 appeared candidates) in Biotechnology (GATE: Graduate Aptitude test for Engineering, 2010)

Awarded in "My innovation" during Kshitij 2010 for "developing cheap and highly effective herbal cosmetics for utilization of Indian rural resources"

Awarded in Biotech fest'o8, Panjab University for "Presenting a working model on T4 bacteriophage infection"

Publications

Medhavi Vishwakarma, Tamal Das and Joachim P. Spatz*, "Group Decisions Regulate Emergence of Leaders during collective cell Migration," **Under Review, Nature**.

Medhavi Vishwakarma, Heike Boehm, Tamal Das* and Joachim P. Spatz*, "Mechanobiologically regulated temporal phases of leader cell generation during collective cell migration in Epithelial wound closure, " **Under Revision, Nature Communications**.

Vijay S. Vyas, Medhavi Vishwakarma, Igor Moudrakovski, Frederik Haase, Goekcen Savasci, Christian Ochsenfeld, Joachim P. Spatz and Bettina V. Lotsch, "An Imine-Covalent Organic Framework as smart drug-delivery vehicle for Quercetin transport," **Advanced Materials, July 2016**.

Félix Lussier, Thibault Brulé, Medhavi Vishwakarma, Tamal Das, Joachim P. Spatz, and Jean-François Masson, "Dynamic-SERS Optophysiology: A Nanosensor for Monitoring Cell Secretion Events, " **NanoLetters, May 2016**.

Conferences

Mechanobiology: from molecules to Tissues; June 2016, Quy Nhon, Vietnam- Oral contribution: Group Decisions Influence Emergence and Regulation of Leaders in Collective Epithelial Migration, Medhavi Vishwakarma, Tamal Das* and Joachim P. Spatz*

Gordan Research Conference: Signaling by adhesion; June 2016, Lewiston, United States-Poster: Regulation of Leader Cell Mediated Guidance in Epithelial Collective Movement, Medhavi Vishwakarma, Jacopo Di Russo, Tamal Das* and Joachim P. Spatz*

Collective Migration Symposium; July 2015, Heidelberg, Germany- Poster: Mechanotransductional regulation of leader cell formation during collective migration of epithelial cells, Medhavi Vishwakarma, Tamal Das, Heike Boehm and Joachim P. Spatz*

Summer School: MPI-EPFL Center for Molecular Nanoscience and Technology; July 2015, Ringberg, Germany- Poster: Mechanotransductional regulation of leader cell formation during collective migration of epithelial cells, Medhavi Vishwakarma, Tamal Das, Heike Boehm and Joachim P. Spatz*

Summer School: MPI-EPFL Center for Molecular Nanoscience and Technology; March 2014, Ascona, Switzerland- Poster: Understanding the genesis and dynamics of leader cells in collective migration, Medhavi Vishwakarma, Tamal Das, Heike Boehm and Joachim P. Spatz*

“If one advances in the direction of his dreams with perseverance, and make simple endeavours to live the life, the way he has imagined, he will meet serendipities, unexpectedly, and in common hours, that would each time, take him another step closer to his dream.”

-Adapted: Henry David Thoreau; *Life in the Woods*